CP2015

5th International Workshop on Computational Human Phantoms

19 - 22 July 2015 in Seoul, Korea

Welcome!

We are pleased to invite you to the 5th International Workshop on Computational Human Phantoms (CP2015), which will be held at Hotel President in Seoul, Korea on July 19 - 22, 2015.

Since the introduction of the first-generation phantoms in 1960s, the computational human phantoms have been essential tools in radiation protection, medical imaging, radiation treatment, and nonionizing radiation area. The rapid expansion of research and development in this topic led to the first international workshop on computational human phantoms held at National Radiological Protection Board (NRPB), U.K, in 1995, and since the first workshop, there have been significant efforts by many distinguished researchers on phantom technology. The continuation of the workshops organized by Oak Ridge National Laboratory, U.S.A (2000), Tsinghua University, China (2011), and IT'IS Foundation, Switzerland (2013) have played a key role in facilitating rapid research and development in computational human phantom technology.

The momentum of research on this important issue continues, and recent research and development started to address the emerging needs to simulate posture changes, cardiac and respiratory motions, as well as anatomical variability associated with gender, age, and obesity. The introduction of non-uniform rational B-spline (NURBS) and polygonal mesh phantoms offer the flexibility to deform shape and size, while maintaining a high level of anatomical realism. We sincerely hope that the CP2015 workshop will be the continuation of the success in research and development in this important topic. We hope that the CP2015 will be a great place for all attendees to share, exchange, and discuss their achievements and ideas, but also a great place to build friendship among the colleagues.

Seoul, which held the Olympic Games in 1988, is the metropolis with a population of about 10 million and the capital city of Korea. The venue, Hotel President, is located in the downtown of the city with a number of sightseeing spots, cherishing both the past and the present of Korea around it. Seoul is known for a well-developed system of public transportation (buses, subway, and taxes) at a good price and you can easily enjoy the sightseeing spots using the public transportation system. Seoul has been the capital city of Korea over 600 years, played a key role as a heart of Korean economy, and has been a microcosm of Korean society. Bring your family to see and enjoy old royal palaces, historical relics, traditional markets, modern style of shopping centers and streets, and a variety of exotic Korean traditional food, with most of them distributed around the hotel within the walking distance.

Again, we welcome you to the CP2015 workshop. We will do our best for the success of the workshop, hoping that all the attendees will be presented with the best chances of academic and scientific satisfaction and personal enjoyment. We are looking forward to seeing you in Seoul. Thank you!

CP2015
Seoul, Korea

Prof. Chan Hyeong Kim

CP2015 Workshop Chair

CONTENTS

MOST IMPORTANT INFORMATION

Emergency: 119
Police: 112

Seonghoon Kim: 0082 10 8205 7265
Min Cheol Han: 0082 10 2202 1944

Workshop E-mail: cp2015info@gmail.com
Workshop Website: www.cp2015.org

SCIENTIFIC PROGRAM

Keynote Presentation

July 19, Sunday

Registration

16:30-19:00	**Registration**

July 20, Monday

Welcome

08:00-09:00	**Registration**
09:00-09:10	**Welcome Address** *Chan Hyeong Kim* *CP2015 Chair*
09:10-09:20	**Congratulatory Address** *Jai Ki Lee,* *ICRP Main Commission Member / Past KARP President*

Session I - Development of Mesh-based Phantoms I

Session Chair: Dr. Maria Zankl and Prof. Tsi-Chian Chao

09:20-10:00	**The Past, Present, and Future of Computational Human Phantoms** *X. George Xu[1,2]* [1]School of Nuclear Science and Technology, University of Science and Technology of China, Hefei, China [2]Nuclear Engineering Program, Rensselaer Polytechnic Institute, Troy, New York, USA
10:00-10:20	**Construction of Pregnant Female Phantoms at Different Gestation Periods for Radiation Dosimetry** *Tianwu Xie[1], Habib Zaidi[1,2,*]* [1]Division of Nuclear Medicine and Molecular Imaging, Geneva University Hospital, Geneva, Switzerland [2]Department of Nuclear Medicine and Molecular Imaging, University Medical Center Groningen, Groningen, Netherlands
10:20-10:40	**The ACADEMY Project - A Computational Phantoms Working Group** *Marc Horner[1,*], Wolfgang Kainz[2], Kerim Genc[3], Paul Segars[4]* [1]Technical Support and Services, ANSYS, Inc. Evanston, IL, USA [2]Center for Devices and Radiologic Health, Food and Drug Administration, Silver Spring, MD, USA [3]Simpleware Inc., Herndon, VA, USA [4]Carl E. Ravin Advanced Imaging Laboratories, Duke University Medical Center, Durham, NC, USA
10:40-11:00	**Small Intestine Modeling Method for Use in Surface-based Computational Human Phantoms** *Yeon Soo Yeom[1], Han Sung Kim[1], Thang Tat Nguyen[1], Zhao Jun Wang[1], Min Cheol Han[1], Chan Hyeong Kim[1,*], Jai Ki Lee[1], Maria Zankl[2], Nina Petoussi-Henss[2], Wesley E. Bolch[3], Choonsik Lee[4], Beom Sun Chung[5]* [1]Department of Nuclear Engineering, Hanyang University, Seoul, Korea [2]Research Unit Medical Radiation Physics and Diagnostics, Helmholtz Zentrum München Deutsches Forschungszentrum für Gesundheit und Umwelt (GmbH), Neuherberg, Germany [3]J. Crayton Pruitt Family Department of Biomedical Engineering, University of Florida, Gainesville, Forida, USA [4]Division of Cancer Epidemiology & Genetics, National Cancer Institute, Bethesda, Maryland, USA [5]Department of Anatomy, Ajou University School of Medicine, Suwon, Korea
11:00-11:40	Group Photo & Coffee Break

Session II - Applications of Computational Phantoms in Radiation Protection

Session Chair: Prof. Xiaobin Xia and Mr. Wi-Ho Ha

11:40-12:00	**Application of Computational Human Phantom to Evaluate Annual Effective Dose by Usage of TENORM added Consumer Products** *Do Hyeon Yoo[1], Wook Geun Shin[1], Jae Gook Lee[2], Yeon Soo Yeom[3], Chan Hyeong Kim[3], Chul Hee Min[1,*]* [1]Department of Radiological Science, Yonsei University, Wonju, Republic of Korea [2]Korea Institute of Nuclear Safety, Daejeon, Republic of Korea [3]Department of Nuclear Engineering, Hanyang University, Seoul, Republic of Korea
12:00-12:20	**Application of Family Phantoms to Monte Carlo Calculations of Secondary Neutron Doses from Carbon Ion Therapy** *Mang Feng[1,*], Hongdong Liu[1], Zhi Chen[1], X. George Xu[1,2]* [1]School of Nuclear Science and Technology, University of Science and Technology of China, Hefei, China [2]Nuclear Engineering Program, Rensselaer Polytechnic Institute, Troy, New York, USA
12:20-12:40	**Application of Mesh-based Family Phantom for Radiation Dose Calculations Involving Interventional Radiology and Computed Tomography** *Wanli Huo[1,*], Yao Wang[1], Zhuang Xiong[2], Yifei Pi[1], Yiming Gao[3], Zhi Chen[1], X. George Xu[1,3]* [1]School of Nuclear Science and Technology, University of Science and Technology of China, Hefei, China [2]Department of Radiology, the First Hospital Affiliated to Anhui Medical University, Hefei, China [3]Nuclear Engineering Program, Rensselaer Polytechnic Institute: NES Building, Troy, New York, USA
12:40-13:00	**Application of Korean Voxel Model to The Efficiency Calibration of Whole Body Counter** *Jeong-In Kim[*], Seo-Kon Kang, Byoung-Il Lee* *Radiation Health Institute, KHNP, Seoul, Republic of Korea*
13:00-14:00	Lunch

Session III - Development of Mesh-based Phantoms II

Session Chair: Prof. Benjamin MW Tsui and Prof. Kwang Pyo Kim

14:00-14:20	**Construction of a Hybrid Computational Pediatric Phantom Library: Application to The Evaluation of The Effects of Body Habitus on Internal Radiation Dosimetry** *Tianwu Xie[1], Habib Zaidi[1,2,*]* [1]Division of Nuclear Medicine and Molecular Imaging, Geneva University Hospital, Geneva, Switzerland [2]Department of Nuclear Medicine and Molecular Imaging, University Medical Center Groningen, Groningen, Netherlands
14:20-14:40	**Continuously Deforming 4D Tetrahedral-mesh Phantom Based on Patient 4D CT Data** *Min Cheol Han[1], Yeon Soo Yeom[1], Chan Hyeong Kim[1,*], Seonghoon Kim[2], Jason W. Sohn[3]* [1]Department of Nuclear Engineering, Hanyang University, Seoul, Republic of Korea [2]Department of Radiation Oncology, College of Medicine, Hanyang University, Seoul, Republic of Korea [3]Department of Radiation Oncology, Case Western Reserve University, Cleveland, Ohio, USA
14:40-15:00	**Population of Whole-body Statistical Adult Phantoms and Assessing the Uncertainty of Organ Doses in Hyperthyroid Treatment with ^{131}I** *Elie Hoseinian Azghadi, Hashem Miri Hakimabad[*], Laleh Rafat Motavalli* Physics Department, Faculty of Sciences, Ferdowsi University of Mashhad, Mashhad, Iran

15:00-15:20	**Development of Mesh-based Age-dependent Family Phantoms** *Yifei Pi[1], Mang Feng[1], Wanli Huo[1], Lian Zhang[1], Tianyu Liu[2], Hui Lin[2], Lu Yang[1], Fang Zheng[1], Huayan Tan[1], Feng Pan[1], Zhi Chen[1], X. George Xu[1,2,*]* [1]School of Nuclear Science and Technology, University of Science and Technology of China, Hefei, China [2]Nuclear Engineering Program, Rensselaer Polytechnic Institute, Troy, New York, USA
15:20-15:40	**Development of a Male Adult Human Head Phantom Based on Polygon Mesh Surfaces** *Bintuan Zhang[1], Xiaobin Xia[1,*], Yinxiangzi Sheng[2], Yuhai Xu[1]* [1]Department of Radiation Safety, Shanghai Institute of Applied Physics, Chinese Academy of Sciences Shanghai, China [2]Shanghai Proton and Heavy Ion Center, Fudan University Shanghai Cancer Center, Shanghai, China
15:40-16:00	**Development of CT-based Mini-pig Physical and Computational Phantoms for Animal Dosimetry** *Sooyeun Park[1,3], Byeong Ryong Park[1], Sehwan Shim[2], Wi-Ho Ha[1,*], Sunhoo Park[2], Chan Hyeong Kim[3]* [1]Health Physics Team, National Radiation Emergency Medical Center, Korea Institute of Radiological & Medical Sciences, Seoul, Republic of Korea [2]Department of Nuclear Engineering, Hanyang University, Seoul, Republic of Korea [3]Laboratory of Radiation Exposure & Therapeutics, National Radiation Emergency Medical Center, Korea Institute of Radiological & Medical Sciences, Seoul, Republic of Korea
16:00-16:30	Coffee Break

Session IV - Computational Phantoms in Radiation Therapy and Medical Imaging

Session Chair: Prof. Niels Kuster and Dr. Sang Hyoun Choi

16:30-17:10	**Updates of The 4D XCAT Phantom Series for Biomedical Imaging and Radiation Dosimetry** *Benjamin M. W. Tsui[1,*], W. Paul Segars[2]* *[1]Department of Radiology, Johns Hopkins University, Baltimore, MD, USA* *[2]Department of Radiology, Duke University, Durham, NC, USA*
17:10-17:30	**Coronary Dose Calculations with Computational Phantoms After Radiotherapy** *David Broggio[1,*], Alexandra Moignier[1], Sylvie Derreumaux[2]* [1]IRSN/PRP-HOM/SDI/LEDI, Institut de Radioprotection et de Sûreté Nucléaire, Fontenay-aux-Roses, France [2]IRSN/PRP-HOM/SER/UEM, Institut de Radioprotection et de Sûreté Nucléaire, Fontenay-aux-Roses, France
17:30-17:50	**Evaluation of Motion Compensation Using Component Analysis in Nuclear Medicine Imaging: Phantom Simulation Study** *Kyeong Min Kim[*], Se Jong Oh* Korea Institute of Radiological & Medical Sciences, Seoul, Republic of Korea
17:50-18:10	**Simultaneous Algebraic Reconstruction Technique (SART) in Digital Breast Tomosynthesis Using Voxelized 3D Breast Phantom** *Sunghoon Choi[1], Ye-seul Kim[1], Haeng-Hwa Lee[1], Donghoon Lee[2], Shouchih Mu[2],Hee-Joung Kim[1,2,*]* *[1]Dept. of Radiological Science, Yonsei University, Wonju, Korea* *[2]Dept. of Radiation Convergence Engineering, Yonsei University, Wonju, Korea*
18:10-22:00	Reception

July 21, Tuesday

Session V - ICRP Reference Phantoms

Session Chair: Prof. Rui Qiu and Dr. Xianwu Xie

09:00-09:40	**ICRP Adult and Pediatric Reference Computational Phantoms** *Maria Zankl[1,*], Janine Becker[1], Choonsik Lee[2], Wesley E. Bolch[3], Yeon Soo Yeom[4], Chan Hyeong Kim[4]* [1]Research Unit Medical Radiation Physics and Diagnostics, Helmholtz Zentrum München – German Research Center for Environmental Health (GmbH), Neuherberg, Germany [2]Radiation Epidemiology Branch, National Cancer Institute, National Institutes of Health (NIH), Rockville, MD, U.S.A. [3]J. Crayton Pruitt Family Department of Biomedical Engineering, University of Florida, Gainesville, FL, U.S.A. [4]Department of Nuclear Engineering, Hanyang University, Seoul, Korea
09:40-10:00	**Development of Skeleton Model for Polygon-mesh Version of ICRP Reference Phantoms** *Zhao Jun Wang[1], Yeon Soo Yeom[1], Thang Tat Nguyen[1], Han Sung Kim[1], Min Cheol Han[1], Chan Hyeong Kim[1,*], Jai Ki Lee[1], Maria Zankl[2], Nina Petoussi-Henss[2], Wesley E. Bolch[3], Choonsik Lee[4], Beom Sun Chung[5]* [1]Department of Nuclear Engineering, Hanyang University, Seoul, Korea [2]Research Unit Medical Radiation Physics and Diagnostics, Helmholtz Zentrum München Deutsches Forschungszentrum für Gesundheit und Umwelt (GmbH), Neuherberg, Germany [3]J. Crayton Pruitt Family Department of Biomedical Engineering, University of Florida, Gainesville, Florida, USA [4]Division of Cancer Epidemiology & Genetics, National Cancer Institute, Bethesda, Maryland, USA [5]Department of Anatomy, Ajou University School of Medicine, Suwon, Korea
10:00-10:20	**Modeling Target Regions of Alimentary Tract in Polygon-mesh Version of ICRP Reference Phantoms** *Han Sung Kim[1], Yeon Soo Yeom[1], Thang Tat Nguyen[1], Zhao Jun Wang[1], Min Cheol Han[1], Chan Hyeong Kim[1,*], Jai Ki Lee[1], Maria Zankl[2], Nina Petoussi-Henss[2], Wesley E. Bolch[3], Choonsik Lee[4], and Beom Sun Chung[5]* [1]Department of Nuclear Engineering, Hanyang University, Seoul, Korea [2]Research Unit Medical Radiation Physics and Diagnostics, Helmholtz Zentrum München Deutsches Forschungszentrum für Gesundheit und Umwelt (GmbH), Neuherberg, Germany [3]J. Crayton Pruitt Family Department of Biomedical Engineering, University of Florida, Gainesville, Florida, USA [4]Division of Cancer Epidemiology & Genetics, National Cancer Institute, Bethesda, Maryland, USA [5]Department of Anatomy, Ajou University School of Medicine, Suwon, Korea
10:20-10:40	**Incorporation of Detailed Eye Model into Polygon-mesh Version of ICRP Reference Phantoms for Lens Dose Assessment** *Thang Tat Nguyen[1], Yeon Soo Yeom[1], Han Sung Kim[1], Zhao Jun Wang[1], Min Cheol Han[1], Chan Hyeong Kim[1,*], Jai Ki Lee[1], Maria Zankl[2], Nina Petoussi-Henss[2], Wesley E. Bolch[3], Choonsik Lee[4], and Beom Sun Chung[5]* [1]Department of Nuclear Engineering, Hanyang University, Seoul, Korea [2]Research Unit Medical Radiation Physics and Diagnostics, Helmholtz Zentrum München Deutsches Forschungszentrum für Gesundheit und Umwelt (GmbH), Neuherberg, Germany [3]J. Crayton Pruitt Family Department of Biomedical Engineering, University of Florida, Gainesville, Florida, USA [4]Division of Cancer Epidemiology & Genetics, National Cancer Institute, Bethesda, Maryland, USA [5]Department of Anatomy, Ajou University School of Medicine, Suwon, Korea
10:40-11:40	Poster & Coffee Break

Session VI - Monte Carlo Simulation and Dose Calculation Technique

Session Chair: Prof. Junli Li and Prof. Chul Hee Min

11:40-12:00	**CAD-and Image-based Monte Carlo Radiation Modeling Techniques and Its Application in Rad-HUMAN** *Yican Wu, Mengyun Cheng, Wen Wang, Ting Li, Jing Song, Lijuan Hao, Shengpeng Yu, Tao He, Shaoheng Zhou, Pengcheng Long, Liqin Hu, FDS Team* Key Laboratory of Neutronics and Radiation Safety, Institute of Nuclear Energy Safety Technology, Chinese Academy of Sciences, Hefei, China
12:00-12:20	**Real-time Radiation Dose Assessment Method Based on Voxel Phantom Using Parallel Technology** *Ting Li, Tao He, Liqin Hu, FDS Team* Key Laboratory of Neutronics and Radiation Safety, Institute of Nuclear Energy Safety Technology, Chinese Academy of Sciences, Hefei, China
12:20-12:40	**Near Real-time GPU and MIC-based Monte Carlo Code ARCHER for Radiation Dose Calculations in Voxelized and Mesh Phantoms** *Tianyu Liu[1], Noah Wolfe[2], Lin Su[1], Christopher D. Carothers[2], Bryan Bednarz[3], X. George Xu[1,*]* [1]Nuclear Engineering Program, Rensselaer Polytechnic Institute Troy, New York, USA [2]Computer Science Department, Rensselaer Polytechnic Institute Troy, New York, USA [3]Departments of Medical Physics and Human Oncology, University of Wisconsin-School of Medicine and Public Health Madison, Wisconsin, USA
12:40-13:00	**Cloud-based Software Methods for Managing a Large Phantom Database - Example of VirtualDose** *Mang Feng[1,*], Aiping Ding[2], Yiming Gao[2], Zhi Chen[1], X. George Xu[1,2]* [1]School of Nuclear Science and Technology, University of Science and Technology of China, Hefei, China, [2]Nuclear Engineering Program, Rensselaer Polytechnic Institute, Troy, New York, USA
13:00-14:00	Lunch

Session VII - Development of 3D and 4D Voxel Phantoms

Session Chair: Prof. X. George Xu and Mr. Jeong-In Kim

14:00-14:40	**The Combined Chinese reference Man/woman Voxel Phantom and the Construction of Multi-scale Dosimetry** *Junli Li, Rui Qiu, Chunyan Li, Zhen Wu* Department of engineering physics, Tsinghua University, Beijing, China
14:40-15:00	**The Development of Resolution Enhanced Chinese Reference Adult Female Voxel Phantom and Its Application on Organ Dose Calculation** *Tsi-Chian Chao[1,*], Yi-Chun Tsai[1], Pei-Shuan Lu[1], Chung-Chi Lee[1], Chuan-Jong Tung[1], Junli Li[2]* [1]Department of Medical Imaging and Radiological Sciences, College of Medicine, Chang Gung University, Taipei, Taiwan [2]Department of Engineering Physics, Tsinghua University, Beijing, China
15:00-15:20	**Monte Carlo Calculated Conversion Factors Based on a 3D Detailed Breast Model for the Estimation of Mean Glandular Dose in Mammography** *Wenjing Wang[1,2,3], Rui Qiu[1,2,3,*], Li Ren[1,2,3], Huan Liu[1,2,3], Chenxing Jiang[1,2,3], Junli Li[1,2,3]* [1]Department of Engineering Physics, Tsinghua University, Beijing, China [2]Key Laboratory of Particle & Radiation Imaging (Tsinghua University), Ministry of Education, Beijing, China [3]Key Laboratory of High Energy Radiation Imaging Fundamental Science for National Defense, Beijing, China
15:20-15:40	**Development of "4D Voxel Phantom" Reflecting Continuous Respiratory Motion of Patient** *Jeong Min Seo[1,2], Min Cheol Han[1], Se Hyung Lee[1,3], Seonghoon Kim[4], Chan Hyeong Kim[1,*], Yeon Soo Yeom[1]* [1]Department of Nuclear Engineering, Hanyang University, Seoul, Republic of Korea [2]Department of Radiologic Science, Daewon University College, Jecheon, Republic of Korea [3]Department of Radiation Oncology, Bundang Jesaeng General Hospital, Seongnam, Republic of Korea [4]Department of Radiation Oncology, College of Medicine, Hanyang University, Seoul, Republic of Korea
15:40-20:30	Technical Tour (+ Dinner)

July 22, Wednesday

Session VIII - Computational Phantoms in Non-ionizing Radiation Area and Special Issues

Session Chair: Dr. David Broggio and Dr. Marc Horner

09:00-09:40	**Development of the Functionalized Virtual Population based on Different Anatomies and Its Application to Implant Effectiveness and Safety Evaluations** *Niels Kuster[1,2,*]* [1]IT'IS Foundation, Zurich, Switzerland [2]ETHZ Zurich, Zurich, Switzerland
09:40-10:00	**Functionalized Anatomical Models for *In Silico* Investigation of EM-Neuronal Dynamics Interactions** *Esra Neufeld[1,*], Niels Kuster[1,2]* [1]IT'IS Foundation for Research on information Technologies in Society, Zurich, Switzerland [2]Swiss Federal Institute of Technology (ETHZ), Zurich, Switzerland
10:00-10:20	**Evaluation of MRI Exposure of Patients with Deep Brain Stimulator with Virtual Population 3.0 and 1.0 Anatomical Phantoms** *Aiping Yao[1,2,*], Earl Zastrow[1,2], Eugenia Cabot[1], Davnah Payne[1], Niels Kuster[1,2]* [1]IT'IS Foundation for Research on information Technologies in Society, Zurich, Switzerland [2]Swiss Federal Institute of Technology (ETHZ), Zurich, Switzerland
10:20-10:40	**Generating Useful Images for Medical Applications from the Visible Korean** *Min Suk Chung* Department of Anatomy, Ajou University School of Medicine, Suwon, Republic of Korea
10:40-11:00	**A Comprehensive Database of Physical Tissue Properties for Computational Simulations in Realistic Virtual Anatomies** *Christian Baumgartner[1,*], Esra Neufeld[1], Davnah Payne[1], and Niels Kuster[1,2]* [1]IT'IS Foundation, Zurich, Switzerland [2]ETH Zurich, Zurich, Switzerland
11:00-11:20	Coffee Break

Closing

11:20-11:40	**Awards**
11:40-12:00	**Closing** *X. George Xu* *CP Steering Committee Chair*

Poster Session

Poster 1	**Counting Efficiency Calibration of Stand-up Type Whole-body Counter Using BOMAB and ICRP Phantoms** *Jaeryong Yoo[1,2], Seyoung Park[1], Seokwon Yoon[1], Wi-Ho Ha[1], Seung-Sook Lee[1], Kwang Pyo Kim[2,*]* [1]National Radiation Emergency Medical Center, Korea Institute of Radiological and Medical Sciences, Seoul, Republic of Korea [2]Department of nuclear engineering, Kyung Hee University, Gyenggi-do, Republic of Korea
Poster 2	**Anatomically Realistic Computer Phantom Modeling of Human Fetuses at Various Stages of Pregnancy for Dosimetry Study** *Tomoaki Nagaoka[1,*], Tetsu Niwa[2],Soichi Watanabe[1]* [1]Electromagnetic Compatibility Laboratory, National Institute of Information and Communications Technology, Koganei, Japan [2]Department of Radiology, Tokai University School of Medicine Isehara, Japan
Poster 3	**RADAR Reference Adult and Pediatric Phantom Series - Nuclear Medicine and CT Dosimetry** *Michael G. Stabin[1], Diana E. Carver[1], Susan D. Kost[1], Nicholas D. Fraser[1], David R. Pickens[1], Ronald R. Price[1], W. Paul Segars[2]* [1]Vanderbilt University, Dept of Radiology and Radiological Sciences, Nashville, TN, USA [2]Carl E. Ravin Advanced Imaging Laboratories, Duke University, Durham, NC, USA

Oral Sessions

The Past, Present, and Future of Computational Human Phantoms

X. George Xu[1,2,*]

[1]School of Nuclear Science and Technology, University of Science and Technology of China, Hefei, China
[2]Nuclear Engineering Program, Rensselaer Polytechnic Institute, Troy, New York, USA

*Corresponding author: xug2@rpi.edu

Abstract **-** A recent review article identifies a clear progression of computational phantom complexity which can be denoted by three distinct generations [1]. The first generation of stylized phantoms, representing a grouping of less than dozen models, was initially developed in the 1960s at Oak Ridge National Laboratory to calculate internal doses from nuclear medicine procedures. Despite their anatomical simplicity, these computational phantoms were the best tools available at the time for internal/external dosimetry, image evaluation, and treatment dose evaluations. A second generation of a large number of voxelized phantoms arose rapidly in the late 1980s as a result of the increased availability of tomographic medical imaging and computers. Surprisingly, the last decade saw the emergence of the third generation of phantoms which are based on advanced geometries called boundary representation (BREP) in the form of Non-Uniform Rational B-Splines (NURBS) or polygonal meshes. This new class of phantoms now consists of over 287 models including those used for non-ionizing radiation applications. This review article aims to provide the reader with a general understanding of how the field of computational phantoms came about and the technical challenges it faced at different times. This goal is achieved by defining basic geometry modeling techniques and by analyzing selected phantoms in terms of geometrical features and dosimetric problems to be solved. Finally the author explains an unexpected finding during the course of preparing for this article that the phantoms from the past 50 years followed a pattern of exponential growth. The review ends on a brief discussion of future research needs.

REFERENCE

[1] X. George Xu, "An exponential growth of computational phantom research in radiation protection, imaging, and radiotherapy: a review of the fifty-year history," *Phys. Med. Biol.,* vol. 59, pp. R233–R302, 2014.

Construction of Pregnant Female Phantoms at Different Gestation Periods for Radiation Dosimetry

Tianwu Xie[1], Habib Zaidi[1,2,*]

[1]Division of Nuclear Medicine and Molecular Imaging, Geneva University Hospital, Geneva, Switzerland
[2]Department of Nuclear Medicine and Molecular Imaging, University Medical Center Groningen, Groningen, Netherlands

*Corresponding author: habib.zaidi@hcuge.ch

Abstract - Medical imaging procedures, including CT, PET, and SPECT, involving the use of ionizing radiation, are nowadays playing a pivotal role in clinical diagnosis, staging and restaging, and treatment monitoring of a number of diseases. Due to the high radiosensitivity of the embryo/fetus, the concerns of possible radiation-induced cancers from medical and non-medical exposures of the pregnant female continue to grow, thus stimulating the need for accurate fetal radiation dose estimation at the organ level from common nuclear medical procedures. Methods: To obtain realistic biological and physical representations of the pregnant female body and embedded fetus, we constructed a series of hybrid computational pregnant female phantoms including the fetus at 8, 10, 15, 20, 25, 30, 35 and 38 weeks post-conception ages. We evaluate the S-values of F-18 as well as the absorbed dose and effective dose for six F-18 labeled radiotracers using realistic anthropomorphic computational phantoms at 8 different gestation periods, and the most recent biokinetic data available. The Monte Carlo N-Particle eXtended (MCNPX) general purpose Monte Carlo code was used for radiation transport simulation. Results: The masses of most fetal organs in the developed hybrid pregnant female phantoms match the reference data at corresponding gestation periods. For ^{18}F-FDG, the estimated absorbed dose and effective dose to the 8-week fetus are 0.032 mGy/MBq and 0.033 mSv/MBq, respectively. Conclusion: The generated computational pregnant female phantoms can be exploited to estimate the radiation dose delivered to pregnant patients and fetus from various radiation sources used in clinical and research settings. The generated dosimetric data can be used to assess the radiation risks to pregnant woman and fetus undergoing PET studies involving the administration of ^{18}F-FDG or other tracers.

Index Terms - Pregnant female model, radiation dosimetry

I. INTRODUCTION

Pregnant females represent a critical subpopulation for which absorbed doses from radiologic imaging procedures must be evaluated to make critical decisions regarding fetal health. Over the period 1997-2006, the number of radiologic examinations performed in the US in general and those involving pregnant patients in particular, have increased by 121% and 89%, respectively [1]. The impact on health of fetal radiation exposure depends on the gestation period at the time of exposure and the absorbed dose level. At fetal doses below 50 mGy, the primary risk for the fetus is childhood cancer, an organ-specific disease with no demonstrated dose threshold. Accurate assessment of fetal absorbed dose following exposure to ionizing irradiation requires the use of reliable computational phantoms representing the physiological and anatomical characteristics of the developing fetus and maternal body. In this work, we constructed a series of pregnant female models based on existing available pregnant female, fetus and newborn models. Monte Carlo simulations were then used for the calculation of S-values in different organs/tissues of pregnant female at different gestation periods for F-18 as well as fetal/maternal absorbed doses and effective doses from six F-18 labelled radiotracers.

II. METHODS

A. Pregnant female phantoms

The Rensselaer Polytechnic Institute (RPI) pregnant female phantom series [2], the Fetal and Mother Numerical Models (FEMONUM) of Telecom ParisTech [3], the Katja phantom (24 weeks-gestation) of Helmholtz Zentrum [4] and the UF-NCI newborn model [5] were used to construct representative fetus and reference pregnant woman models. The maternal body and most maternal organs of the developed phantoms were obtained from the RPI phantoms [6]. The uterine wall, placenta, umbilical cord, amniotic fluid, vesicule vitelline and fetal body contour of 8 and 10 weeks gestation were obtained from 8 and 10 weeks FEMONUM phantoms. The fetal skeleton and fetal bone marrow of all phantoms were scaled from RPI 9-months phantoms to match the reference values of ICRP 89 [7]. The fetal esophagus, fetal thyroid, fetal salivary gland, fetal LI, fetal SI, fetal UB and fetal testis were scaled from the UF-NCI newborn phantom with the same ratios as the fetal skeleton. The fetal spinal cord was constructed as a pipe model along the spine. The fetal brain, eyes, lungs, heart, stomach, gall bladder of 8-20 weeks gestation, 25-35 weeks gestation and 38-week gestation were scaled from corresponding fetal tissues of Katja model, FEMONUM models of 26, 30 and 35 weeks and UF-NCI newborn model, respectively. The fetal kidneys and fetal liver of 8-30 weeks gestation models and 35-38 weeks gestation models were scaled from Katja model and UF-NCI newborn model, respectively. The ICRP reference organ masses were set as the target mass during the organ scaling procedure. The breast, maternal abdomen, maternal LI and SI and maternal bladder were manually adjusted at each gestation period using the Rhinoceros™ package.

B. Dosimetry calculations

The MCNPX code was used for Monte Carlo simulations of F-18 sources in 54 identified maternal and fetal organs. The MIRD formalism was adopted to calculate S-values of F-18 and to estimate radiation absorbed dose delivered to fetal and maternal organs from six F-18 labelled radiotracers. An equal average activity concentration was assumed in maternal and fetal tissues for all considered radiotracers.

III. RESULTS

A. Computational phantoms

Figure 1 shows the constructed computational pregnant female phantoms at 8-, 10-, 15-, 20-, 25-, 30-, 35- and 38-weeks gestation. Figure 2 shows the embedded computational fetus phantoms at corresponding gestation periods. The body contours and organ volumes of pregnant female and fetus were adjusted to match the reference mass of the ICRP publication 89 at different gestation periods.

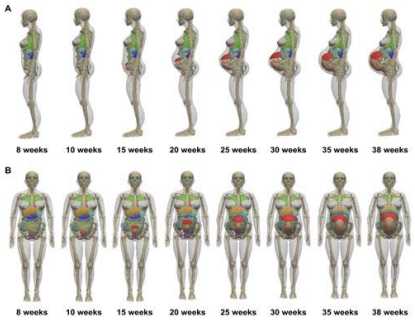

Figure 1. (A) Side view and (B) front view of the developed pregnant female phantoms at different gestation periods.

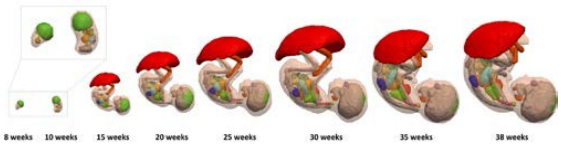

Figure 2. 3D visualization of the embedded fetus phantoms

B. S-values for F-18

Figure 3 shows the self-absorbed S-values for representative fetal organs from F-18. For all fetal organs, the self-absorbed S-values decrease with gestation age as the fetal weight increases.

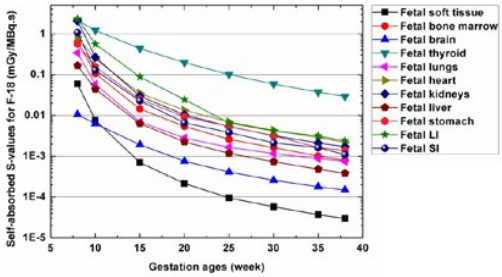

Figure 3. Self-absorbed S-values of F-18 for fetal organs

C. Absorbed dose and effective dose from radiotracers

The fetal and maternal absorbed dosed and effective dosed from ^{18}F-Amino acids, ^{18}F-Brain receptor substances, ^{18}F-FDG, ^{18}F-L-dopa, ^{18}F-FBPA and ^{18}F-FDOPA were calculated. For ^{18}F-FDG, the estimated absorbed doses to the fetal total body are 0.032 mGy/MBq, 0.026 mGy/MBq, 0.021 mGy/MBq, 0.017 mGy/MBq, 0.016 mGy/MBq, 0.015 mGy/MBq, 0.014 mGy/MBq and 0.013 mGy/MBq at 8, 10, 15, 20, 25, 30, 35 and 38 weeks gestation, respectively. The effective doses per unit administered activity to the fetus and pregnant female from ^{18}F-FDG were compared in Figure 4.

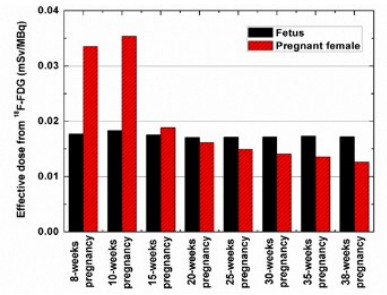

Figure 4. Effective dose per unit administered activity (mSv/MBq) to the fetus and pregnant female from ^{18}F-FDG.

IV. CONCLUSION

The generated hybrid computational pregnant female phantoms can be exploited to estimate the radiation dose delivered to pregnant patients and fetus from various radiologic examinations used in clinical and research settings. The generated dosimetric data of F-18 can be used to assess fetal radiation risks from various ^{18}F-labelled radiotracers.

ACKNOWLEDGMENT

This work was supported by the Swiss National Science Foundation under Grant SNSF 31003A-149957 and Geneva Cancer League.

REFERENCES

[1] E. Lazarus, C. DeBenedectis, D. North, P. K. Spencer and W. W. Mayo-Smith, "Utilization of imaging in pregnant patients: 10-year Review of 5270 Examinations in 3285 Patients—1997–2006 1," *Radiology*, vol.251, pp. 517-524, 2009.

[2] G. Xu, V. Taranenko, J. Zhang and C. Shi, "A boundary-representation method for designing whole-body radiation dosimetry models: pregnant females at the ends of three gestational periods- RPI-P3,-P6 and-P9," *Phys. Med. Biol.*, vol.52, pp. 7023-7044, 2007.

[3] L. Bibin, J. Anquez, J. P. de la Plata Alcalde, T. Boubekeur, E. D. Angelini *et al.*, "Whole-body pregnant woman modeling by digital geometry processing with detailed uterofetal unit based on medical images," *IEEE Trans. Biomed. Eng.,* vol. 57, pp. 2346-2358, 2010.

[4] J. Becker, M. Zankl, U. Fill and C. Hoeschen, "Katja—the 24th week of virtual pregnancy for dosimetric calculations," *Polish. J. Med. Phys. Eng.*, vol. 14, pp. 13-20, 2008.

[5] C. Lee, D. Lodwick, D. Hasenauer, J. L. Williams, C. Lee *et al.*, "Hybrid computational phantoms of the male and female newborn patient: NURBS-based whole-body models," *Phys. Med. Biol.*, vol 52, pp. 3309-3322, 2007.

[6] T. Xie and H. Zaidi, "Fetal and maternal absorbed dose estimates for positron-emitting molecular imaging probes, " *J. Nucl. Med.*, vol 55, pp. 1459-1166, 2014.

[7] ICRP, "ICRP Publication 89: Basic anatomical and physiological data for use in radiological protection: reference values," *Ann. ICRP*, vol 32, pp. 5-265, 2002.

The ACADEMY Project - A Computational Phantoms Working Group

Marc Horner[1,*], Wolfgang Kainz[2], Kerim Genc[3], and Paul Segars[4]

[1]Technical Support and Services, ANSYS, Inc. Evanston, IL, USA
[2]Center for Devices and Radiologic Health, Food and Drug Administration, Silver Spring, MD, USA
[3]Simpleware Inc., Herndon, VA, USA
[4]Carl E. Ravin Advanced Imaging Laboratories, Duke University Medical Center, Durham, NC, USA

*Corresponding author: marc.horner@ansys.com

Abstract **-** Computational modeling provides a setting to quantitatively evaluate the safety and efficacy of a device or procedure with no harm to the patient or user. This is driving the need for anatomically accurate human body computer phantoms that are accessible to a wide community and suitable for multiple modeling tasks (FEA, CFD, EM, etc.). Voxel-based phantoms are compatible with time-domain solvers, but there is a lack of surface-based phantoms suitable for solvers based on tetrahedral meshes. The goal of ACADEMY is to develop a repository of human-body phantoms in standardized surface-based format. Using the 4D extended cardiac-torso (XCAT) phantoms created by Segars *et al.* [1], we use ScanIP (Simpleware Ltd., Exeter, UK) to convert these datasets into multi-object simulation ready geometry files that can be used in any software able to import Computer Aided Design (CAD) files.

Index Terms - surface-based human computer phantoms, CAD, tissue heating, safety

I. INTRODUCTION

Advances in computational modeling are continually improving our ability to perform quantitatively accurate virtual safety assessments of implanted devices, wireless devices, and surgical procedures. Examples include the temperature rise of an implant during Magnetic Resonance Imaging (MRI), exposure assessment of a patient undergoing a Computer Tomography (CT) scan, and energy absorbed by the head when using a mobile phone. These, and other applications, are driving the need for repositories of standardized surface-based anatomically accurate human body computer phantoms.

There are two classes of phantoms suitable for computational modeling: voxel-based and surface-based. Voxel-based phantoms are developed by identifying the biological structure associated with each voxel in a medical image dataset. Surface-based phantoms are generated through a conversion of a voxel dataset to a boundary-represented format, wherein the surface of each biological structure is represented using a standard CAD format. Most research efforts to date have focused on the development voxel-based phantoms. Surface-based datasets exist, e.g. the XCAT [1] and MASH/FASH phantoms [2], but not to the same extent or level of completeness. The current lack of surface-based phantoms limits computational analysis to primarily FDTD (Finite Difference Time Domain), or other voxel-based codes. The goal of the ACADEMY project is to develop a repository of human body phantoms in a standard CAD format. The current focus is on electromagnetic (EM) simulation. Future versions of the models will be of sufficient resolution to be used in Com7putational Fluid Dynamics (CFD) and other Finite Element Analysis (FEA) applications.

II. METHODS

ACADEMY, which stands for **A**natomically Correct **CAD** Mod**E**ls of the Human Anatomy for Co**M**putational Safet**Y** Studies, is an open group currently hosted by Marc Horner of ANSYS, Inc. There have been five meetings to date, with a sixth meeting scheduled to take place before or during the 2015 Computational Phantoms workshop. The meetings are attended by medical device manufacturers, academics, industry service providers, and the US FDA.

Initial ACADEMY group meetings came to the following preliminary consensus regarding the requirements of a human phantoms repository:

A. Structures

- Internal/external structures of the human body should be represented as water-tight surface-defined volumes
- Tissue interfaces should be conformal, i.e. no gaps and no overlaps
- Resolutions of 10, 5, 2, and 1 mm are needed
  - Sub-mm resolution phantoms were also desirable, although it is important to note that these may be out of our current computational capability.

B. Population variability

- The repository should cover the entire patient or user population. Potential variations include height, age, BMI, and pregnancy stage, to name only a few.

C. Format

- Standardized CAD format
  - There should be a pathway for participants to verify compatibility with their software.

D. Distribution

- The source image data and CAD files should be freely available to academics and industry.
  - Distributing the source medical image datasets would facilitate future enhancements and/or modification of the created phantoms

E. Regulatory

- Regulatory agencies should participate in the development of the phantoms
  - Establishing partnerships with regulatory agencies, peer-reviewed publications, and review articles will bring credibility to the final product

III. SIMULATIONS

The current focus has been to establish a modeling workflow based on the 4D XCAT dataset from Prof. Paul Segars' group at Duke University [1]. This dataset was developed for multimodality imaging research and contains 173 (58 adult and 115 pediatric) 4D phantoms of varying ages from newborn to adult. The tissues in each phantom are mathematically defined and can be voxelized into 3D computational phantoms at any resolution.

Three adult male and three adult female XCAT phantoms (BMI's ranging from the 10th to 90th percentile) and a 1 year old male (50^{th} percentile BMI) were voxelized at an isotropic resolution of 2 mm. The voxelized phantoms were imported into ScanIP (Simpleware Ltd., Exeter, UK) as a stack of 2D 32-bit greyscale images. Due to the pre-segmented nature of the XCAT data, anatomical structures could be automatically segmented and categorized using the ScanIP "pre-segmented data mask generator" tool. For the sake of simplicity and phantom size, three tissue zones were included in the initial dataset: muscle, bone, and "soft tissues". Muscle and bone regions were already identified in the pre-segmented dataset. The soft tissue region was comprised of all other tissues not already identified as muscle or bone.

Spurious elements and gaps were removed using the ScanIP "Morphological Close" filter and tissue surfaces were smoothed using a recursive Gaussian filter. A multi-part surface mesh was automatically generated where each tissue was conformal to all neighboring tissues with water-tight, face-to-face contact defined by coincident nodes. The faceted solid phantom was then exported in the ACIS '.sat' format (Figure 1).

For test purposes EM simulations were conducted using ANSYS HFSS (ANSYS Inc., Canonsburg, PA). This simulation included frequency-dependent permittivities and conductivities [3] applied to each tissue. A 300 MHz incident plane wave source, which requires mesh discretization at the level needed for a 7T MRI EM simulation, was applied as an excitation. The surface mesh resolution and water-tight surfaces were found to be compatible with the automated meshing algorithm in HFSS (Figure 2).

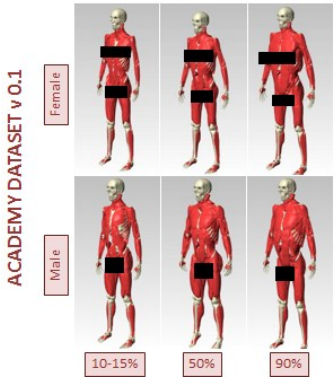

Figure 1. Muscle layers of six adult phantoms from the ACADEMY dataset, comprised of 3 adult males and 3 adult females across a range of BMI values.

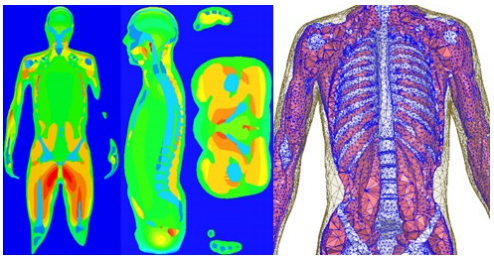

Figure 2. Local SAR distribution from a 300 MHz incident plane wave (left) and ANSYS HFSS mesh of muscle/bone behind a clip plane (right)

IV. CONCLUSION

The ACADEMY project is an on-going collaboration between industry, industry service providers, academia, and the US FDA to develop a repository of human body computer phantoms in standardized CAD format at an appropriate resolution for all computational modeling purposes. A proposed workflow from medical scan data through virtual human simulation was demonstrated with seven individuals from a newly available virtual population dataset. A semi-automated segmentation routine and automatic conformal CAD surface extraction algorithm provided the geometric phantoms for the tested EM simulation. The next stage of this project is to solicit funding to enhance the resolution of the extracted phantoms. The group welcomes your participation in this project.

REFERENCES

[1] W. P. Segars *et al.*, "Population of anatomically variable 4D XCAT adult phantoms for imaging research and optimization," *Med. Phys.*, vol. 40, 2013.
[2] R. Kramer *et al.*, "FASH and MASH: female and male adult human phantoms based on polygon mesh surfaces: I. Development of the anatomy," *Phys. Med. Biol.*, vol. 55, pp. 163-189, 2010.
[3] http://niremf.ifac.cnr.it/tissprop

Small Intestine Modeling Method for Use in Surface-based Computational Human Phantoms

Yeon Soo Yeom[1], Han Sung Kim[1], Thang Tat Nguyen[1], Zhao Jun Wang[1], Min Cheol Han[1], Chan Hyeong Kim[1,*], Jai Ki Lee[1], Maria Zankl[2], Nina Petoussi-Henss[2], Wesley E. Bolch[3], Choonsik Lee[4], and Beom Sun Chung[5]

[1]Department of Nuclear Engineering, Hanyang University, Seoul, Republic of Korea
[2]Research Unit Medical Radiation Physics and Diagnostics, Helmholtz Zentrum München Deutsches Forschungszentrum für Gesundheit und Umwelt (GmbH), Neuherberg, Germany
[3]J. Crayton Pruitt Family Department of Biomedical Engineering, University of Florida, Gainesville, Florida, USA
[4]Division of Cancer Epidemiology & Genetics, National Cancer Institute, Bethesda, Maryland, USA
[5]Department of Anatomy, Ajou University School of Medicine, Suwon, Republic of Korea

*Corresponding author: chkim@hanyang.ac.kr

Abstract **-** When converting voxel phantoms into surface format, the small intestines (SI), which are not accurately represented in voxel phantoms due to the finite voxel resolutions, cannot be directly converted to a high-quality surface model. Although stylistically designed pipe models have been developed and used to represent SI, they are not free of subjective opinions of the developers. The present study proposes a new method to construct SI models, which is a systematic procedure based on Monte Carlo approach. The proposed method was tested by constructing a new SI model for the polygon-mesh version of the ICRP reference male phantom. We believe that the constructed SI model is more anatomically realistic than the previously constructed stylistic SI model. The new model provides more similar dose values to those of the original ICRP-110 voxel male phantom for both external and internal dose calculations.

Index Terms - small intestine, voxel phantom, surface phantom, Monte Carlo

I. INTRODUCTION

Surface-based computational human phantoms have been developed mostly by converting conventional voxel phantoms into a surface format with 3D surface rendering methods. In the development, the small intestines (SI), which are not accurately modeled in voxel phantoms due to the finite voxel resolutions (normally ~ mm), cannot be directly converted to a high-quality surface format; thus, stylistically designed pipe models have been alternatively used as SI models [1-3]. However, those stylistic SI models are not free of subjective opinions of the developers.

In the present study, we propose a new modeling method to construct SI models through a systematic procedure based on Monte Carlo approach. The key idea of the new modeling method is that a large number of pipe-type SI models are randomly generated using Monte Carlo method and then, the most appropriate model is selected by comparing with the original SI voxel model for geometric and dosimetric similarities.

In order to see feasibility of the proposed method, in the present study, we constructed a new SI model for the polygon-mesh (PM) version of the ICRP reference male phantom, which is being constructed from the current voxel-type ICRP-110 male phantom [4]. Then, the constructed SI model was compared with the SI model stylistically constructed in a previous study [3].

II. METHODS

The SI model was constructed as follows. First, the frame surface enclosing the entire original SI voxel model was produced by using the alpha-shape algorithm [5] as shown in Figure 1 (a). Then, a C++ program was written to automatically generate a random SI passage line within the frame surface using the Monte Carlo method (Figure 1 (b)). Finally, a SI model was created along with the passage line by using the 'pipe' and 'mesh' functions in the *Rhinoceros* software (Robert McNeel & Associates, Seattle, Wash) (Figure 1 (c)). This procedure was repeated 1000 times, generating 1000 different SI models.

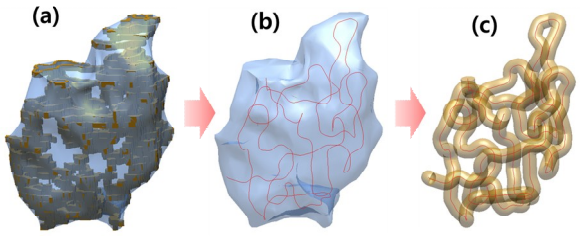

Figure 1. Small intestine (SI) model generation procedure: (a) construction of the frame surface enclosing original SI voxel model, (b) random generation of SI passage line within frame surface, and (c) generation of SI model along with passage line.

The generated SI models were compared with the original SI voxel model to evaluate geometrical similarity by using three indices: volume overlap fraction (VOF), centroid distance (CD), and mean minimum distance (MMD). Using the similarity indices, a total of 10 SI models were selected. Then the selected models were placed in the PM version of the ICRP reference male phantom, and Monte Carlo dose calculations with Geant4 code were performed to find the one which provides the most similar dose values with the original SI voxel model. In the calculations, first, the absorbed doses to the SI models were calculated for external photon beams (0.03-10 MeV) at AP, PA, RLAT, and LLAT directions. Second, specific absorbed fractions to the six representative organs (colon, stomach, liver, kidneys, pancreas, and urinary bladder) were calculated for internal exposure of photons from the SI models. For the simulations, the *G4EmLivermorePhysics* was used with 0.1 mm cut value. The relative errors of all the calculated values were less than 10%.

Table 1. Similarity indices for best 10 SI models constructed in present study and previous SI model

Similarity Index	Top 10 SI models selected in the present study										Previous SI model
	1	2	3	4	5	6	7	8	9	10	
VOF	0.40	0.39	0.39	0.37	0.40	0.40	0.40	0.39	0.39	0.40	0.31
CD [cm]	2.02	1.99	1.86	2.04	2.00	2.11	2.95	1.89	2.01	1.81	3.50
MMD [cm]	0.62	0.66	0.64	0.63	0.65	0.64	0.63	0.63	0.61	0.65	0.78

III. RESULTS AND DISCUSSION

Figure 2 shows the best 10 SI models selected from the 1000 SI models (left) and the previously constructed stylistic SI model (right). It can be seen that the new models are more anatomically realistic than the previous model. This was confirmed by an anatomist. In addition, all the three similarity indices indicated that the new models are geometrically more similar with the original SI voxel model than the previous model as shown in Table 1.

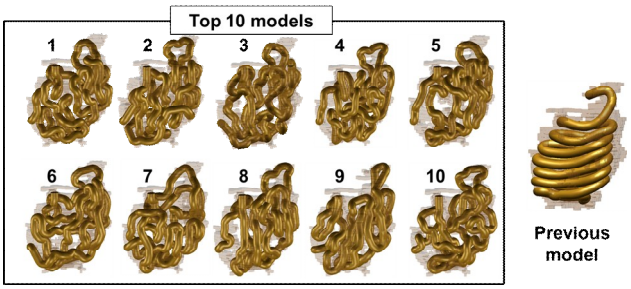

Figure 2. Top 10 small intestine (SI) models from 1000 SI models (left) and the previously constructed stylistic SI model (right)

The sixth SI model in Table 1 provided the most similar dose values with the original SI voxel model; the average dose difference was 4.19% considering all of the calculation cases. Figure 3 shows dose deviations from the original voxel model for the sixth model and the previous model. It can be seen that the sixth model provides much more similar dose values than the previous model; the dose discrepancies for the most calculation cases are within 10%.

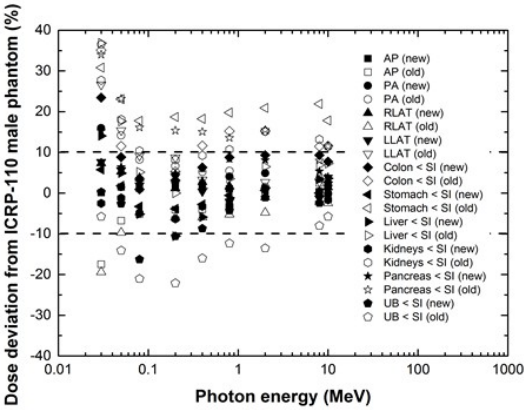

Figure 3. Dose deviations from original SI voxel model for the sixth SI model (filled) and the previously constructed SI model (hole)

IV. CONCLUSION

The present study proposed a new SI modeling method for use in surface phantoms and then, applied the proposed method to construct a new SI model for the PM version of the ICRP male phantom under development. The constructed SI model is more anatomically realistic than the previously constructed stylistic SI model, providing more similar dose values for external and internal photon exposure cases. It is expected that the proposed SI modeling method will be widely used in development of surface phantoms converted from voxel phantoms in the future.

ACKNOWLEDGMENT

This project was supported by NSSC through KORSAFe and also by Ministry of Science, ICT and Future Planning through the NRF of Korea (Project No.: 2011-0025496, 2012-K001146, 1403012). Two of the authors were supported by the Global PhD Fellowship program (Project No.: 2011-0007318, 2011-0030970).

REFERENCES

[1] C. Lee *et al.*, "Hybrid computational phantoms of the male and female newborn patient: NURBS-based whole-body models," *Phys. Med. Biol.,* vol. 52, pp. 3309-3333, 2007.
[2] C. Lee *et al.*, "The UF family of reference hybrid phantoms for computational radiation dosimetry," *Phy. Med. Biol.,* vol. 55, pp. 339-363, 2010.
[3] Y. S. Yeom, M. C. Han, C. H. Kim, and J. H. Jeong, "Conversion of ICRP male reference phantom to polygon-surface phantom," *Phy. Med. Biol.*, vol 58, pp. 6685-7007, 2013.
[4] ICRP, "Adult Reference Computational Phantoms," *ICRP Publication 110.* Ann. ICRP 39 (2), 2009.
[5] H. Edelsbrunner, D. Kirkpatrick, and R. Seidel, "On the shape of a set of points in the plane," *Information Theory, IEEE Transactions on*, vol. 29, no. 4, pp. 551 –559, 1983.

Application of Computational Human Phantom to Evaluate Annual Effective Dose by Usage of TENORM Added Consumer Products

Do Hyeon Yoo[1], Wook Geun Shin[1], Jae Gook Lee[2], Yeon Soo Yeom[3], Chan Hyeong Kim[3], Chul Hee Min[1,*]

[1]Department of Radiation Convergence Engineering and Research Institute of Health Science, Yonsei University, Wonju, Republic of Korea
[2]Korea Institute of Nuclear Safety, Daejeon, Republic of Korea
[3]Department of Nuclear Engineering, Hanyang University, Seoul, Republic of Korea

*Corresponding author: chmin@yonsei.ac.kr

Abstract - Consumer products containing Technically Enhanced Naturally Occurring Radioactive Material (TENORM) has been distributed in our life. After the accident of Fukushima nuclear power plant, the law as called 'Act on Safety Control of Radioactive Rays around Living Environment' has been implemented to prevent the unnecessary radiation exposure to the public in Korea. However, the appropriate method to effectively evaluate the annual effective dose with TENORM added consumer product was not developed despite the laws were in effect from July 2012. The aim of this study is to evaluate the exposed dose with the usage of TENORM added consumer product. To assess the annual effective dose, the Monte Carlo methods and computational human phantom were employed and the point source on the skin was suggested to effectively determine the various products shape and location. Our simulation results show that the multi-point source defined on the skin indicate the conservative dose assessment compare to the source modeled as like the real products because of the close source definition to organs. The annual effective doses with multi-point sources show less than 1 mSv over six consumer products.

Index Terms - Geant4, PSRK-Man, Monte Carlo simulation, NORM, effective dose

I. INTRODUCTION

Radioactive nuclide such as ^{40}K, ^{238}U, ^{232}Th and their decay products are naturally present in the environment and are responsible for the natural background radiation. The rapid industrialization leads to the activated exploitation of underground mineral resources including naturally occurring radioactive material (NORM) that may increase the radiation exposure to general public. Especially the general public could be significantly exposed by using the consumer products containing a technically enhanced naturally occurring radioactive material (TENORM). In this reason, the law called as 'Act on Safety Control of Radioactive Rays around Living Environment' [1] has been implemented to prevent the unnecessary radiation exposure to the public in Korea. However, the appropriate method to effectively evaluate the expose dose with TERNORM added consumer products was not developed despite the law was into effect from July 2012. For the assessment of exposure dose with NORM added consumer products, the Monte Carlo method was employed with computational human phantom. However, source modeling of each consumer products is significant burden due to the large amount of consumer products distributed in Korea. So, the current study suggests new source modeling method based on multi-point source defined on the skin surface of the computational human phantom to effectively determine the various product shape and location.

II. METHODS

A. Polygon-Surface Reference Korean-Man

The effective dose could not be directly measured from the human body. For the assessment of exposure dose with the radionuclide in a consumer products, Polygon-Surface Reference Korean-Man (PSRK-Man) phantom composed of high resolution polygons to represent the organs was developed as shown in Figure 1. PSRK-Man is developed with the reference Korean male in which the height and weight are 171 cm and 68 kg, respectively [2]. The PSRK-Man includes 27 organs and tissues. The organ equivalent doses and effective doses can be calculated from the internal and external radiation exposure.

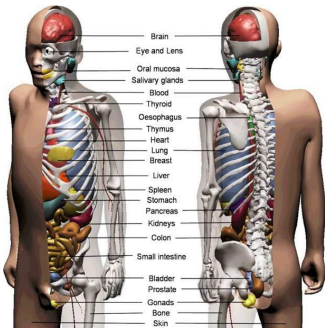

Figure 1. 3D images of PSRK-Man with the main organs

B. Source term modeling

PSRK-Man is composed of 120,850 polygons and each polygon is composed of three coordinate in x, y, z axis. Coordinates of the polygon surface, organ name and organ number are arranged as shown in Figure 2. To represent the source location of the radioactive material in the consumer product, polygons on skin under the product were selected and in the weight center in each polygon the radiation were emitted and the following organ dose and effective dose was calculated. To validate the skin point method, the organ dose was computed with the original sources defined in the products realistically modeled.

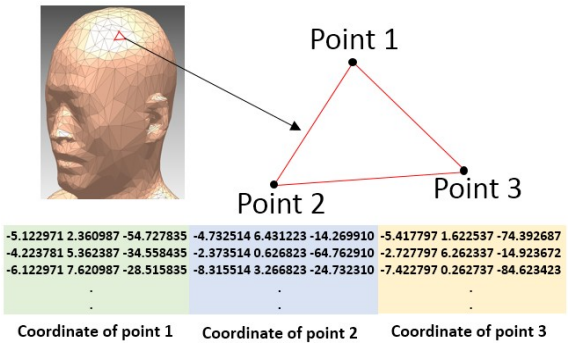

Figure 2. Three coordinates determining the polygons on skin surface of PSRK-Man phantom

III. RESULTS

A. Organ equivalent dose evaluation

Multi-point sources of the pillow products were determined near the head and neck area consist of 233 weight center point on the PSRK-Man as shown in Figure 3. For the comparison purpose, the realistic pillow also modeled with a rectangular parallelepiped shape of width, length, and height of 30 cm, 50 cm, and 13 cm, respectively.

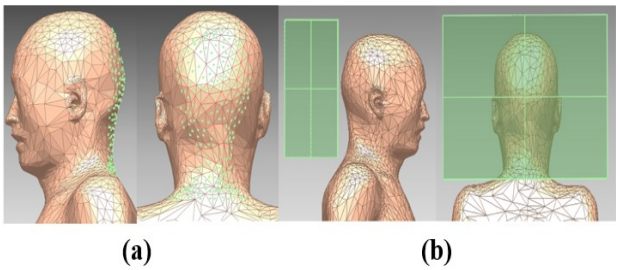

Figure 3. (a) Multi-point source methods and (b) modeling method in phantom

Figure 4 shows the organ equivalent dose with the initial gammas of 10^7 with 1 MeV isotropically emitted from the both sources. The organ equivalent dose of the modeling source of the bone and skin distributed to the whole body were evaluated as higher than that of the multi-point sources; that is, increasing the distance between the source and computational phantom increase the potential effective angle to the organs distributed in a whole body.

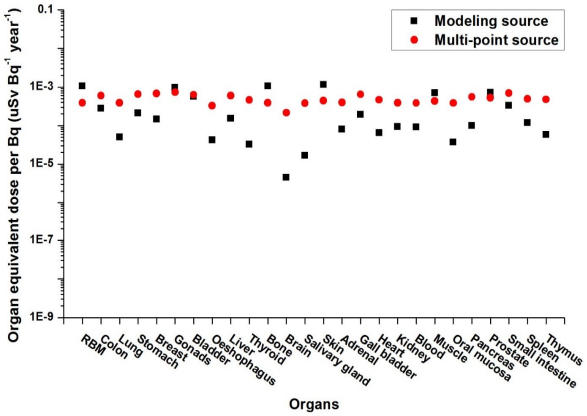

Figure 4. Organ equivalent dose with 1 MeV gamma energy

The organ dose was also assessed with other type of consumer products including belt, accessory, mat, eye patch, and cosmetic. For the evaluation of annual effective dose, the usage scenario of each product was assessed based on the data from statistics Korea.

B. Annual effective dose of the six consumer products

Finally, the annual effective dose due to the usage of the TENORM added consumer products was evaluate based on the usage time and organ equivalent doses as shown in Figure 5. The annual effective dose with the multi-point source was higher than that of modeling source. Especially, 2.5 times higher annual effective dose was assessed in mat product using multi-point source. The annual effective dose over six products was evaluated less than 1 mSv, even though the employment of conservative point source method.

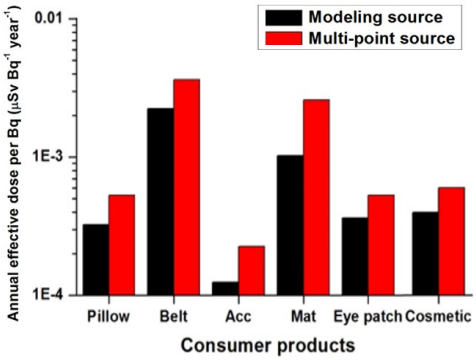

Figure 5. Annual effective dose with 1 MeV of gammas for the six consumer products with modeling and multi-point sources

IV. CONCLUSION

The current study showed the effectiveness of the multi-point source on the computational human phantom to evaluate annual effective dose by usage of TENORM added consumer products. The point source method could also be used for the other field for radiation protection to calculate the effective dose.

ACKNOWLEDGMENT

This research was supported by Korea Institute of Nuclear Safety and Global Ph.D. fellowship program through the National Research foundation of Korea (NRF) funded by the Ministry of Education (2015000666).

REFERENCES

[1] Nuclear Safety and Security Commission, "Act on safety control of radioactive rays around living environment," 2012.

[2] Kim et al., "A polygon-surface reference Korean male phantom (PSRK-Man) and its direct implementation in Geant4 Monte Carlo simulation," *Phys. Med. Biol.*, vol. 56, pp 3137, 2011.

Application of Family Phantoms to Monte Carlo Calculations of Secondary Neutron Doses from Carbon Ion Therapy

Mang Feng[1,*], Hongdong Liu[1], Zhi Chen[1], X. George Xu[1,2]

[1]School of Nuclear Science and Technology, University of Science and Technology of China, Hefei, China
[2]Nuclear Engineering Program, Rensselaer Polytechnic Institute, Troy, New York, USA

*Corresponding author: fengmang@mail.ustc.edu.cn

Abstract - Carbon ion radiotherapy has been a research focus because of its Bragg peak, which is beneficial for cancer therapy. Some researchers have pointed out that secondary neutrons and fragments will be produced when carbon ions interact with materials, but they did not evaluate organ dose absorbed by patients. In this paper, we estimate the organ equivalent dose by secondary neutrons using Monte Carlo method and voxel phantoms that are transformed from mesh-based family phantoms. As a result, the energy spectra of secondary neutron and different organs equivalent doses are acquired. The results have reference value for experiment and clinical radiotherapy.

Index Terms - phantom, carbon ion radiotherapy, Monte Carlo

I. INTRODUCTION

In recent decades carbon ion radiotherapy has been a research focus. When carbon ions enter matters, they deposit little doses at shallow depth but much doses in deep depth and form a peak named Bragg peak at the end of its range. This property is more suitable for irradiating tumors due to less harm to normal organs than X-ray and gamma-ray whose doses decrease with injection depth [1]. In addition, carbon ions exhibit a higher biological effectiveness and a lower oxygen enhancement ratio in the Bragg peak region caused by the dense ionization of individual particle tracks resulting in reduced cellular repair [1].

However, some papers reported that compared with photon and proton radiotherapy, carbon ions can produce more secondary neutrons and fragments when they interact with materials, which may do harm to patients and medical staff, especially for the young [2]. Those secondary neutrons are difficult to be measured in patients' bodies.

In this paper, MCNPX is used for Monte Carlo calculation, and mesh-based family phantoms are used as simulated patients. Considering that mesh-based geometry models cannot be imported into MCNPX software directly, those phantoms are voxelized at first.

II. METHODS

A. MCNPX software

MCNP, short for Monte Carlo N-Particle Transport Code, developed by Los Alamos National Laboratory since 1957, is a powerful Monte Carlo software for neutron, photon and electron transport calculation [3-4]. MCNPX is an enhanced version of MCNP, which can also handle heavy ion problems [5-6].

B. Mesh-based family phantoms

Mesh-based family phantoms, derived from RPI Adult Male and Female, are developed by University of Science and Technology of China [7]. They consist of different ages including children, teenagers and adults, as shown in Figure 1. Those phantoms are defined by boundary representation or BREP, and compatible with anatomical parameters for Chinese populations. Each of the phantoms has more than 100 deformable organs.

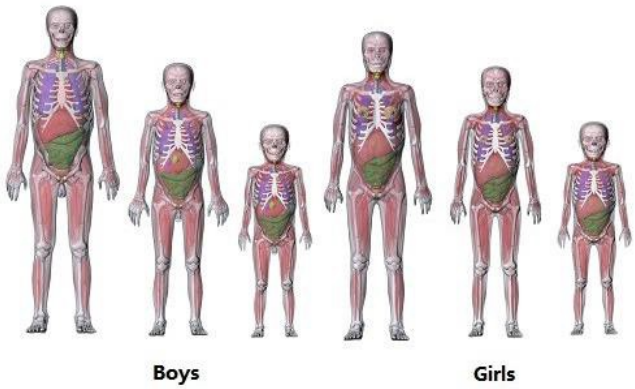

Figure 1. A series of mash-based family phantoms for Chinese people

C. Monte Carlo simulations

Considering the fact that mesh-based geometry cannot be used in MCNPX directly, we voxelize the phantoms first. The adult male phantom is chosen to be voxelized. In this voxelized phantom, each voxel is 2.5 mm × 2.5 mm × 2.5 mm, and the total number is about 24 million. It is 172 cm tall and 63 kg weight, consist of 70 organs, 45 bones, and 4 muscle structures.

The layout of simulation is shown in Figure 2. Carbon ions come through ridge filter and multi-leaf collimator (MLC) and go into phantom's brain, where there is a simulated tumor. Two different directions of carbon ions are simulated respectively. The energy of carbon ions is set to be 230 MeV/u, which makes Bragg peak located at targeted tumor. The total number of ions is 2×10^8 in order to get a reasonable accuracy of calculated dose.

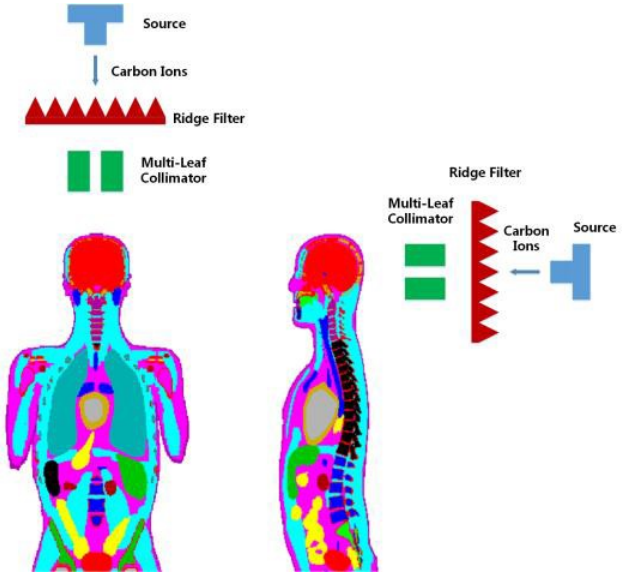

Figure 2. Scheme of Monte Carlo models with two different directions of carbon ions respectively

III. RESULTS

All of situations including different incident directions with or without nozzle are simulated in MCNPX. The doses caused by secondary neutrons in some organs are acquired, which makes it clearly to figure out the damages and risks to patients. According to our statistic results, vertical incident ions cause more doses in trunk part, but they are much less than those in head part. Besides, ridge filter and MLC result in more secondary neutrons.

In addition, we also get pictures of energy distributions of secondary neutrons in some organs and tissues, which are not attached here due to article length. In most of organs, neutron flux decreases slowly when neutron energy increases from 0 to 100 MeV, and then falls down sharply.

IV. CONCLUSION

The incident direction and nozzle can cause different dose distribution inside the body. The doses caused by secondary neutrons around targeted area have no significant difference despite of incident direction, but organs distal from target get more doses from vertical incidence than those from lateral incidence. Ridge filter and MLC can also induce more secondary neutrons. These results have reference value for experiment and clinical radiotherapy.

ACKNOWLEDGMENT

We thank Prof. Anwar Chaudhri from the University of Erlangen-Nuernberg in Germany for providing some help about the mechanism of the secondary neutrons production and the selection of some important parameters.

REFERENCES

[1] Dieter Schardt, Elsässer Thilo, and Schulz-Ertner Daniela, "Heavy-ion tumor therapy: Physical and radiobiological benefits," *Reviews of modern physics*, vol.82, p.383, 2010.

[2] Uwe Schneider, Antony Lomax, and Beate Timmermann, "Second cancers in children treated with modern radiotherapy techniques," *Radiotherapy and Oncology*, vol.89, pp.135-140, 2008.

[3] Judith F Briesmeister, "MCNP-A general Monte Carlo code for neutron and photon transport," *LA-7396-M*, 1986.

[4] Forrest B. Brown, et al., "MCNP version 5," *Trans. Am. Nucl. Soc*, vol. 87, pp. 02-3935, 2002.

[5] Michael R. James, G. W. McKinney, John S. Hendricks, Michael Moyers, "Recent enhancements in MCNPX: Heavy-ion transport and the LAQGSM physics model," *Nuclear Instruments and Methods in Physics Research Section A: Accelerators, Spectrometers, Detectors and Associated Equipment*, vol. 562, pp. 819-822, 2006.

[6] Denise B. Pelowitz, "MCNPX user's manual version 2.5.0," *Los Alamos National Laboratory*, vol. 76, 2005.

[7] Juying Zhang, Yong Hum Na, Peter F. Caracappa, X. George Xu, "RPI-AM and RPI-AF, a pair of mesh-based, size-adjustable adult male and female computational phantoms using ICRP-89 parameters and their calculations for organ doses from monoenergetic photon beams," *Physics in medicine and biology*, vol. 54, p. 588, 2009.

Application of Mesh-based Family Phantom for Radiation Dose Calculations Involving Interventional Radiology and Computed Tomography

Wanli Huo[1,*], Yao Wang[1], Zhuang Xiong[2], Yifei Pi[1], Yiming Gao[3], Zhi Chen[1], X. George Xu[1,3]

[1]School of Nuclear Science and Technology, University of Science and Technology of China, Hefei, China
[2]Department of Radiology, the First Hospital Affiliated to Anhui Medical University, Hefei, China
[3]Nuclear Engineering Program, Rensselaer Polytechnic Institute: NES Building, Troy, New York, USA

*Corresponding author: huowl@mail.ustc.edu.cn

Abstract - Radiologists need to make efforts to protect the patients by reducing their irradiation doses, especially in interventional radiology (IR) where patients are exposed to long time ionizing radiation. Excessive radiation dose may cause deterministic effects such as skin injuries. In this study, a well-established Monte Carlo package MCNPX (Monte Carlo N-Particle eXtended) and a group of mesh-based whole body family of phantoms are employed to calculate major organ doses and peak skin doses (PSDs) of patients who receive IR procedure and computed tomography (CT) scan. This paper demonstrates that the application of mesh-based family phantom under the irradiation conditions of several IR procedures and CT scans allows for calculation of doses to major organ and PSDs of patients with different ages.

Index Terms - Monte Carlo, phantom, organ dose, interventional radiology, computed tomography

I. INTRODUCTION

The interventional radiology (IR) technologies have been used for treatment and diagnose purposes since last 1960s and the use of IR has grown rapidly recently [1]. Although many patients get great benefit from IR, they are exposed to high radiation dose during guided X-ray IR procedures which have potential to cause certain harmful radiation skin injury. There is particular concern about the patient doses during an IR procedure especially the peak skin dose (PSD) [2].

X-ray CT (computed tomography) scan is one of the most popular diagnostic imaging modalities in 21st century. Although CT imaging play an important role in modern medicine, its sharp increase has resulted in a dramatic growth in the average medical radiation exposure to the worldwide [3]. In order to comply to the ALARA (As Low As Reasonably Achievable) principle in CT imaging, it is necessary to reduce the risk from the CT radiation exposure and optimizing the medical benefit of CT scans to patients.

In this study, we employed a group of mesh-based whole body family of phantoms to represent patients and a Monte Carlo method package to calculate the doses to organ and tissues of patient under different IR and CT conditions.

II. METHODS

A. Mesh-based family of phantoms

The group of whole body mesh-based computational family of phantoms were developed at University of Science and Technology of China and consisted of the triangular meshes [4]. This group of age-dependent phantoms include male and female with age of new born, 5-year, 10-year, 15-year and adult. Every phantom contains more than 100 organs and tissues and all the anatomical parameters were adjusted to agree within 0.5% with the reference people data of China. For example, the adult male with a height of 170 cm and weight of 63 kg and the adult female with a height of 158 cm and weight of 54 kg.

To adopt Monte Carlo simulation method, we converted the mesh-based phantoms to voxelized phantoms, which consist of cubic voxels with side length of 2.5 mm and the adult phantoms consist of more than 2×10^7 voxels. In order to calculate precise PSD, we added a layer of air skin with thickness of 2.5 mm above the phantoms and divided it into 2.5 mm side length cubes for the calculation of $H_p(0.07)$. On account of arms would disturb the simulation in lateral beam projections, we removed phantom arms in lateral beam projection simulations.

B. The Monte Carlo method

The Monte Carlo method is a well-established technique as well as the most accurate way to calculate radiation dose for medical physics applications. In this research, the software MCNPX (Monte Carlo N-Particle eXtended) version 2.7.0 [5] was used for Monte Carlo simulations. This production code which has been designed at the Los Alamos National Laboratory (LANL) can handle the transportation and interaction of photons, electrons, neutrons, protons and heavy ions for complex three-dimensional geometries in a wide range of energies.

C. Measurements

Measurements of the X-ray dose rate of IR procedure were carried out in the First Hospital Affiliated to Anhui Medical University. We used PTW 31013, 0.6 cc Semiflex Chamber to measure the dose rate in the center of X-ray field of different beam projections and different beam qualities. The detector was put in the center of X-ray field and above the X-ray tube with distance of 4 cm in each measurement. CT dose index (CTDI) values for several different tube voltages as well as different beam collimations were measured at Massachusetts General Hospital [6].

III. SIMULATIONS

A. Interventional radiology

In this project, several different IR exposure situations were studied, the following aspects were considered.

- Beam projections:

  PA (posterior anterior), LAO45 (left anterior oblique, 45°), RAO30 (right anterior oblique, 30°), LLAT (left lateral), RLAT (right lateral), CRAN45 (cranial, 45°) [7, 8]

- Field of view (FOV):

  40 cm × 40 cm, 30 cm × 30 cm, 20 cm × 20 cm, 10 cm × 10 cm

- Tube potential:

  60 kVp, 70 kVp, 80 kVp, 90 kVp

- Filtrations:

  3.5 mm Al + 0.1 mm Cu, 3.5 mm Al + 0.2 mm Cu, 3.5 mm Al + 0.3 mm Cu

The patients were represented by voxelized phantoms who lie on an Al bed with thickness of 2.15 mm in this study. The distance of X-ray source to skin is 72 cm in PA and 60 cm in LLAT and RLAT. A 0.6 cm^3 air ball was placed above the source as the detector to calculate the air kerma in center of filed, the constant distance of detector to source is 44 cm. The X-ray source spectrums adopted in this research were generated by using the software Xcomp5r [9]. The MCNPX F6 tally and conversion coefficients $H_p(0.07)/K_a$ [10] were used to calculate PSDs. We used the maximum dose of air skin voxel to represent the PSD in each single simulation. 5 × 10^6 histories were simulated in each simulation to keep the statistical error of most organ doses are below 5%.

B. Computed tomography

A multi-detector CT (MDCT) scanner model was developed in this paper. This model supports the tube potentials of 80, 100, 120 and 140 kVp and beam collimations of 1.25 mm, 5 mm, 10 mm, and 20 mm. Patients were placed at the isocenter of the CT scanner in these simulations. Phantoms without arms were employed in the dose calculations to simulate arm-raised position in real CT scan conditions. The F6 tally in MCNPX was used to record the organ doses of the patients. The specific histories in each run were simulated to keep the statistical error < 1% for most organ doses and < 5% for doses to organs with small volume as well as located at large distance from the primary beam.

IV. CONCLUSION

In this study, Monte Carlo software MCNPX and mesh-based whole body family phantoms were used to calculate the doses to major organs and PSDs of patients undergoing IR procedures and CT scans. This research demonstrated that the application of mesh-based family phantom under the irradiation conditions of several IR procedure and CT scans allows for calculation of doses to major organs and PSDs of patients with different ages. The PSD rates calculated in this paper show that a long time IR procedure can deliver high radiation doses to skin, which may potentially cause certain skin injury.

ACKNOWLEDGMENT

This research was funding by the National Natural Science Foundation of China (Grant No. 1137518) and the National Natural Science Foundation of China (Grant No. 11375182).

REFERENCES

[1] J. Valentin, "Avoidance of radiation injuries from medical interventional procedures," *Annals of the ICRP*, vol. 30, pp. 7-67, 2000.

[2] S. Neil, C. Pdagham and C. J. Martin, "A study of the relationship between peak skin dose and cumulative air kerma in interventional neuroradiology and cardiology," *Journal of Radiological Protection*, vol. 30, pp. 659-672, 2010.

[3] Aiping Ding, Matthew M. Mille, Tianyu Liu, Peter F. Caracappa and X. George Xu, "Extension of RPI-adult male and female computational phantoms to obese patients and a Monte Carlo study of the effect on CT imaging dose," *Physics in Medicine and Biology*, vol. 57, pp. 2441-2459, 2012

[4] X. G. Xu, T. C. Chao and A. Bozkurt, "VIP-man: An image-based whole-body adult male model constructed from color photographs of the visible human project for multi-particle Monte Carlo calculations," *Health Physics*, vol.78, pp.476-486, 2000.

[5] Denise B. Pelowitz, 2011. "MCNPX User's Manual Version 2.7.0". LLNL, Los Alamos.

[6] Aiping Ding, 2012. "Development of a Radiation Dose Reporting Software for X-ray Computed Tomography (CT)". Rensselaer Polytechnic Institute.

[7] A. Bozkurt and D. Bor, "Simultaneous determination of equivalent dose to organs and tissues of the patient and of the physician in interventiona radiology using the Monte Carlo method," *Physics in Medicine and Biology*, vol. 52, pp. 317-333, 2007.

[8] C. Koukorava, J. Farah, L. Struelens, I Clariand, L. Donadille and et al, "Efficiency of radiation protection equipment in interventional radiology: a systematic Monte Carlo study of eye lens and whole body doses," *Journal of Radiological Protection*, vol. 34, pp. 509-528, 2014.

[9] R. Nowothy and A. Hofer, "A computer code for the calculation of diagnostic-X-ray spectra," *Fortschr Geb Rontgenstr Nuklearmed*, vol. 142, pp.685-689, 1985.

[10] "Dose conversion coefficients for use in radiological protection against photon external radiation," in *The People's Republic of China National Standard of Occupation Health*, Beijing, Ministry of Health, The People's Republic of China, 2002.

Application of Korean Voxel Model to the Efficiency Calibration of Whole Body Counter

Jeong-In Kim*, Seo-Kon Kang, Byoung-Il Lee

Radiation Health Institute, KHNP, Seoul, Republic of Korea

*Corresponding author: kim.jeongin@khnp.co.kr

Abstract - The typical Korean male voxel model (KTMAN) was applied to the efficiency calculation of a bed type scanning whole body counter (WBC) by the Monte Carlo radiation transport computer code (MCNPX). The calculated efficiencies for thyroids and lungs of KTMAN are higher than those of RMC-II which is normally used for the calibration of a WBC. Considering other factors, the effect of phantom size difference between Korean model and RMC-II for whole body counting is relatively small for internal dosimetry.

Index Terms - whole body counting, KTMAN, calibration, internal dose

I. INTRODUCTION

To evaluate worker's internal doses, it is important to estimate the intake of radioactive materials properly. Generally, whole body counters (WBC) are used for the detection of high energy (>200 keV) gamma ray emitters inside a human body. This equipment cannot measure the intake directly. So, the users should know the relations between measured values and intake. To know these relations, the calibration should be done using standard sources and proper phantoms represent the human body. A Bottle Manikin Absorption phantom (BOMAB) is recommended for the calibration of WBC, but it is difficult to handle and takes long time [1]. For these reasons, commercially developed phantoms are used for convenience. One of these phantoms, an RMC-II (Canberra) is widely used. This phantom can be used for the calibration to thyroids, lungs and gastro-intestinal tract as well as whole body with suitable location of a vial of standard mixed radioactive sources.

Although these calibration phantoms can represent human body for the calibration of measurement devices, there remain potential deviations from accurate human anatomy and the body size characteristics of Korean. So, in this study, Monte Carlo simulations were carried out to calculate the efficiency of a widely used bed type whole body scanning detector for typical Korean male voxel model (KTMAN).

II. METHODS

A. Modeling of Whole Body Counter

The bed type whole body scanning detector (ACCUSCAN, Canberra) at Radiation Health Institute was used. There is one HPGe (GC4019) detector equipped in the middle of the WBC to measure the gamma ray with its energy from the body. In the measurements, the bed moves by 2 m from the end line of one side to the other side. The iron shields of each side and structures which cannot influence on detector response were ignored.

B. Phantom

For the Monte Carlo calculations, an RMC-II phantom was modeled by MCNPX [2] which is a general purpose Monte Carlo radiation transport code designed to track many particle types over broad ranges of energies. The efficiency response with this phantom was designed to replicate the ANSI N 13.30 phantoms [3] (Livermore Lung, BOMAB total body and thyroid). The RMC-II phantom has 4 holes correspond to each of calibration geometries for a single 20 ml vial with mixed radioactive sources.

The CT-based KTMAN [4] voxel model consists of 300 × 150 × 344 voxels with a voxel resolution of 2 × 2 × 5 mm^3 was also modeled. Figure 1 shows MCNPX modeling of whole body counting with KTMAN.

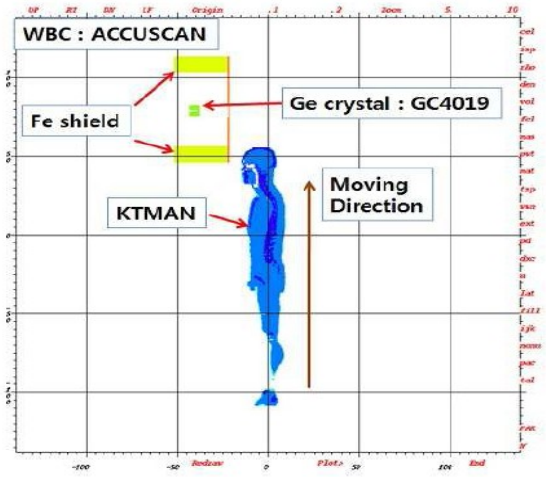

Figure 1. MCNP modeling of WBC with KTMAN

C. Monte Carlo Calculations

For the calculation of calibration efficiencies, a standard mixed source whose energies are 122 keV, 166 keV, 279 keV, 392 keV, 662 keV, 898 keV, 1173 keV and 1332 keV (correspond to ^{57}Co, ^{139}Ce, ^{203}Hg, ^{113}Sn, ^{137}Cs, ^{88}Y, ^{60}Co respectively) was inputted to be located in the middle of each holes of the RMC-II phantom. In the same way, radioactive sources in the voxels representing thyroids and lungs of KTMAN were also modeled. The F8, pulse height tally in MCNPX, which provides the energy distribution of pulse created in a detector by radiation was used for response of the germanium detector. In the real measurement, the WBC scans a human body continuously. However, there is a limitation on simulating continuous movement with MCNPX. For the alternative method, the detector was put in different places and averaged over 21 points by 10 cm intervals.

III. RESULTS AND DISCUSSIONS

Figure 2 shows the results of counting efficiencies for various photon energies at the thyroids and lungs of RMC II and KTMAN respectively. The counting efficiencies for thyroids and lungs of KTMAN are higher than those of RMC-II by about 10%. It is considered that the results come from the difference of body shape between two phantoms representing different human models.

The body size of the KTMAN is relatively small so that the distance between the phantom and the detector becomes longer and it underestimates the intake and internal dose. However, considering the other factors, the effect by the body size difference is relatively small.

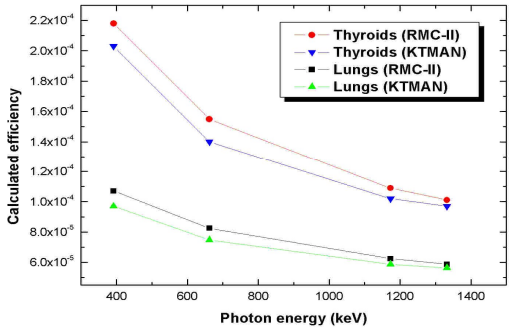

Figure 2. Calculated WBC efficiencies for RMC-II and KTMAN

IV. CONCLUSION

The typical Korean male voxel model was applied to the efficiency calculation of a bed type scanning whole body counter by the Monte Carlo calculations. The calculated efficiencies for thyroids and lungs of KTMAN are higher than those of RMC-II which is normally used for the calibration of WBC. The effect of phantom size difference between Korean model and RMC-II for whole body counting is relatively small but other models such as female and child should be considered also.

REFERENCES

[1] American National Standard, *Specifications for the Bottle Manikin Absorption Phantom*, ANSI/HPS N 13.35, 1999.
[2] Denise B. Pelowitz, *MCNPX User's manual Version 2.6.0*, LA-CP-07-1473, 2008.
[3] American National Standard, *Performance Criteria for Radiobioassay*, ANSI/HPS N 13.30, 1996.
[4] C. Lee, C. Lee, S. Park and J. Lee, "Development of the two Korean adult tomographic computational phantoms for organ dosimetry" *Med. phys.*, vol. 33(2), pp. 380-390, 2006.

Construction of a Hybrid Computational Pediatric Phantom Library: Application to the Evaluation of the Effects of Body Habitus on Internal Radiation Dosimetry

Tianwu Xie[1], Habib Zaidi[1,2,*]

[1]Division of Nuclear Medicine and Molecular Imaging, Geneva University Hospital, Geneva, Switzerland
[2]Department of Nuclear Medicine and Molecular Imaging, University Medical Center Groningen, Groningen, Netherlands

*Corresponding author: habib.zaidi@hcuge.ch

Abstract **-** In this work, a methodology is developed to modify the UF-NCI hybrid phantoms to generate a hybrid computational phantom library covering statistical distributions of body morphometry of the pediatric population. The targeted anthropometric parameters include the body weight, body length, body mass index (BMI) and sitting height/stature ratio (SSR) determined from reference databases of the National Centre for Health Statistics and the National Health and Nutrition Examination Survey. The UF-NIH phantoms were selected as representative anchor phantoms for the newborn, 1-, 2-, 5-, 10- and 15-yr-old children, respectively. A total of 1100 different male and female hybrid phantoms with 10th, 25th, 50th, 75th and 90th body morphometries were constructed. The constructed 125 5-yr-old habitus-dependent male phantoms with different body morphometries were used with MCNPX Monte Carlo transport code to investigate the effect of body habitus on the calculations of absorbed fractions (AF) and S-values of F-18 and the absorbed dose and effective dose of five ^{18}F-labelled radiotracers.

Index Terms - hybrid phantoms, radiation dosimetry

I. INTRODUCTION

Computational phantoms are commonly integrated with Monte Carlo codes simulating radiation transport inside the human body for the purpose of determining the patterns of radiation-tissue interactions enabling the calculation of the absorbed radiation dose in the human body from a variety of different medical radiation sources. However, the reliability of this methodology depends on the adopted computational model reflecting the physical characteristics (e.g. elemental composition, mass density, etc.) and anatomical features (e.g. shape, volume and size of total body and internal organs) of the human body. In this work, we developed a methodology and a C++ code to generate a large library of pediatric phantoms covering statistical distributions of body morphometry of the pediatric population to represent the human body of different habitus. The 10th, 25th, 50th, 75th and 90th body anthropometric parameters, including body weight, body length, BMI and SSR are used to remodel the anchor phantoms of the UF-NIH pediatric phantoms. A total of 1100 anthropometric computational phantoms are generated for the newborn, 1-yr-old, 2-yr-old, 5-yr-old, 10-yr-old and 15-yr-old male and female children. Monte-Carlo simulations coupled with phantom libraries can provide organ and tissue radiation dose estimations for a grid of habitus and weights, and by linear interpolation of the estimated dose for the actual anthropometric parameters of a person between the next data points of the grid, patient-specific organ dose, effective dose and cancer risks can be evaluated with high accuracy. We used the 125 developed habitus-dependent computational 5-years-old male phantoms to calculate the AFs and S-values of F-18 in 46 identified regions and evaluated the absorbed dose and effective dose of five ^{18}F-labelled radiotracers using Monte Carlo simulations. Dose comparisons were performed between habitus-dependent phantoms of different anthropometric parameters for estimation of the effect of body habitus on internal radiation dose.

II. METHODS

A. Computational phantom library

The National Health and Nutrition Examination Surveys (NHANES) data [1], including body weight, recumbent length, standing height, BMI and SSR, were used for parametrizing the pediatric population to generate habitus-dependent phantom libraries. The UF-NCI phantom series [2, 3] including the reference newborn, 1-, 5-, 10-, and 15-yr-old male and female models, were used as anchor phantoms for generation of phantom libraries of the newborn, 1-, 2-, 5-, 10-, and 15-yr-old male and female children. The schematic flowchart shown in Figure 1 illustrates the overall deformation process. The remodeling includes three basic components: the target anthropometric parameters obtained from the NHANES database; the anchor phantoms with well-defined anatomical structures that match reference data of the pediatric population; and the software tools that reconstruct the polygon mesh model from the

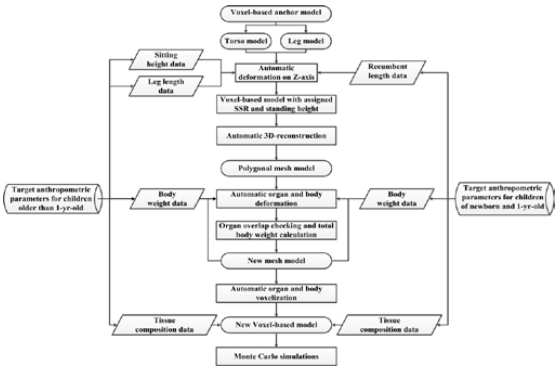

Figure 1. Flowchart of phantom remodeling for Monte Carlo simulations

corresponding voxel-based model, remodel the mesh phantom into a new one according to desired anatomical parameters and voxelize the generated mesh model into a new voxel-based model that is used as input for Monte Carlo calculations.

B. Dosimetry calculations

The 125 generated computational phantoms of the 5-yr-old male were used a input to the MCNPX Monte Carlo code to simulate the transport and interaction of emitted radiation from F-18. AFs and S-values of F-18 are calculated for 2116 source-target pairs of the 125 5-yr-old male models. The calculated S-values are then used to estimate the absorbed organ dose and effective dose from five ^{18}F-labelled radiotracers for the 5-yr-old male phantoms of different habitus.

III. RESULTS

A. S-values

Figure 2 shows the 5-yr-old male phantoms of the UF-NIH phantom series and constructed models with 10th and 90th weight, 10th and 90th BMI, 10th and 90th SSR, as well as with 50th weight, 50th BMI, 50th SSR, respectively. For most organs, the self-absorbed S-value has strong negative correlations with body weight, body height and sitting height and weak correlations with BMI and SSR (Table 1).

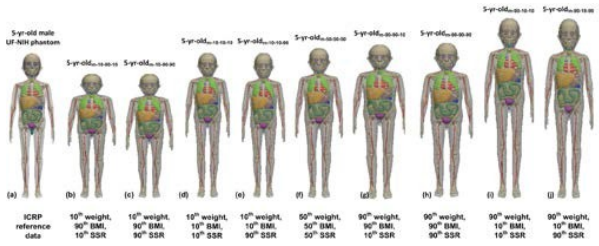

Figure 2. 3D visualization of computational phantoms of the 5-years- old male showing the original UF-NCI phantom and constructed phantoms of different habitus

Table 1. Pearson correlation coefficients between body habitus and self-absorbed S-Values of the 5-yr-old phantoms

Self-absorbed S-values of F-18	Weight	Height	BMI	SSR	Sitting Height
Adrenal	-0.92**	-0.73**	-0.01	0.16	-0.55**
Brain	-0.95**	-0.78**	0.02	0.22	-0.55**
Kidney	-0.92**	-0.74**	0.00	0.22	-0.52**
Liver	-0.85**	-0.82**	0.24*	0.26*	-0.57**
Lung	-0.90**	-0.75**	0.04	0.27*	-0.49**
Pancreas	-0.94**	-0.79**	0.04	0.19	-0.59**
Salivary Glands	-0.92**	-0.75**	0.01	0.21	-0.53**
Spleen	-0.89**	-0.74**	0.03	0.21	-0.52**
Thymus	-0.91**	-0.83**	0.15	0.16	-0.63**
Thyroid	-0.75**	-0.58**	-0.04	0.27*	-0.35**
Cortical bone	-0.99**	-0.84**	0.06	0.15	-0.65**
Spongiosa	-0.98**	-0.86**	0.09	0.14	-0.67**
Colon	-0.94**	-0.76**	-0.02	0.05	-0.65**
Gall Bladder	-0.93**	-0.71**	-0.08	0.13	-0.56**
Heart	-0.98**	-0.79**	-0.02	0.10	-0.63**
Small Intestine	-0.99**	-0.80**	-0.01	0.10	-0.65**
Stomach	-0.97**	-0.78**	-0.04	0.09	-0.63**
Urinary bladder	-0.95**	-0.76**	-0.04	0.10	-0.61**
Total body	-0.99**	-0.85**	0.06	0.15	-0.66**

*p < 0.01, **p < 0.001; SI refers to small intestine.

B. Absorbed dose and effective dose from radiotracers

The absorbed dose to 46 target organs from five ^{18}F-labelled radiotracers is calculated for the considered 125 computational phantoms. Table 2 lists the Pearson correlation coefficients of the relationship between body habitus and effective dose of five ^{18}F-labelled radiotracers.

Table 2. Pearson correlation coefficients for relation between body habitus and effective dose of ^{18}F-labelled radiotracers in the 5-years-old male phantoms

Radiotracers	Weight	Height	BMI	SSR	Sitting Height
^{18}F-Amino acids	-0.94**	-0.79**	0.05	0.22	-0.57**
^{18}F-Brain receptor substances	-0.95**	-0.80**	0.05	0.22	-0.57**
^{18}F-FDG	-0.98**	-0.86**	0.10	0.19	-0.64**
^{18}F-L-DOPA	-0.98**	-0.86**	0.12	0.17	-0.66**
^{18}F-FBPA	-0.97**	-0.86**	0.11	0.19	-0.64**

*p < 0.01, **p < 0.001; SI refers to small intestine.

IV. CONCLUSION

Based on hybrid computational phantoms, a habitus-specific phantom can be created to reflect person-specific body morphometries, thus offering an opportunity to perform person-specific dosimetry for various radiation exposure situations. A systematic study was performed to evaluate the internal dose characteristics of positron-emitting radionuclides and radiotracers in computational phantoms with different habitus. Most dosimetric parameters present high statistical correlations with total body weight and height and weak correlations with the BMI and SSR. The results support the general findings that the phantoms representing slimmer and shorter individuals receive higher absorbed organ doses. We expect that radiation dose estimates to subjects based on the most closely matched habitus-dependent phantoms has many potential applications. The detailed analysis of habitus- dependent dosimetric results for 5-yr-old children may also help frame the argument for individual patient dose assessment.

ACKNOWLEDGMENT

This work was supported by the Swiss National Science Foundation under Grant SNSF 31003A-149957 and Geneva Cancer League.

REFERENCES

[1] CDC, http://www.cdc.gov/nchs/data/nhsr/nhsr010.pdf, Accessed in 2014.

[2] C. Lee, D. Lodwick, J. Hurtado, D. Pafundi, J. L. Williams JL et al., "The UF family of reference hybrid phantoms for computational radiation dosimetry," *Phy. Med. Biol.*, vol. 55, pp. 339, 2010.

[3] C. Lee, C. Lee, J. L. Williams, W. E. Bolch, "Whole-body voxel phantoms of paediatric patients—UF Series B," *Phy. Med. Biol.*, vol. 51, pp. 4649, 2006.

Continuously Deforming 4D Tetrahedral-mesh Phantom Based on Patient 4D CT Data

Min Cheol Han[1], Yeon Soo Yeom[1], Chan Hyeong Kim[1,*], Seonghoon Kim[2], and Jason W. Sohn[3]

[1]Department of Nuclear Engineering, Hanyang University, Seoul, Republic of Korea
[2]Department of Radiation Oncology, College of Medicine, Hanyang University, Seoul, Republic of Korea
[3]Department of Radiation Oncology, Case Western Reserve University, Cleveland, Ohio, USA

*Corresponding author: chkim@hanyang.ac.kr

Abstract **-** We propose to use continuously deforming 4D tetrahedral-mesh phantoms to achieve more accurate 4D Monte Carlo dose calculation for patients. To verify our idea, a 4D tetrahedral-mesh phantom was constructed from real patient 4D CT data, which was then used in 4D Monte Carlo dose calculation. The calculated dose distribution was then compared with that of the conventional 3D simulations. The results of our study showed that the new approach can accurately reflect the patient's respiratory motion, resulting in more accurate dose distribution.

Index Terms - 4D tetrahedral-mesh phantom, 4D Monte Carlo, dose calculation, deformation vector fields

I. INTRODUCTION

Computational human phantoms are used in several areas such as radiation protection, radiation therapy, and medical imaging. Due to the development of medical imaging modalities such as CT and MR, the quality of computational phantom has been significantly improved, i.e., from stylized phantoms to 4D non-uniform rational B-spline (NURBS) phantoms [1].

However, the 4D NURBS phantoms have critical limitations for use in radiation therapy. First of all, the voxelization process has to be performed for each phase of the 4D NURBS phantom to be used in Monte Carlo codes such as Geant4 and MCNP. In addition, the 4D NURBS phantoms are composed of only organ surfaces, without detailed density distributions in each organ, which is a critical limitation to be used for patient dose calculation. For these and other reasons, several researchers performed the 4D Monte Carlo dose calculation using multiple 3D voxel phantoms [2, 3].

To solve these problems, in the present study, we propose to use continuously deforming 4D tetrahedral-mesh phantoms. The 4D tetrahedral-mesh phantom has significant advantages. First, the tetrahedral-mesh geometry can be easily deformed and the in-organ density distribution can be easily modeled [4]. In addition, the tetrahedral-mesh geometry can be directly implemented in major Monte Carlo codes such as Geant4 and MCNP6. In the present study, a 4D tetrahedral-mesh phantom was constructed using real patient 4D CT data and used for dose calculation, and then the calculation dose distributions were compared with those of the conventional multiple 3D voxel phantom simulation.

II. METHODS

Figure 1 shows the flow chart of the construction process of the 4D tetrahedral-mesh phantom. The process consists of (1) the construction of the 4D tetrahedral-mesh phantom, and (2) the implementation of the phantom in Geant4-based 4D Monte Carlo code.

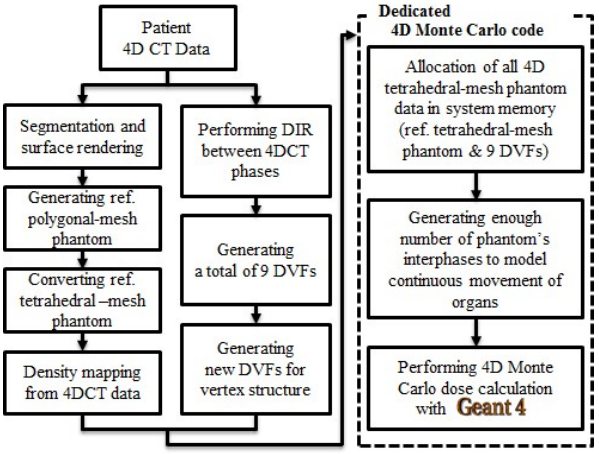

Figure 1. Flow chart of the construction process of the 4D-TETRA phantom and its dedicated 4D Monte Carlo code program

A. Construction of phantom

The 4D tetrahedral-mesh phantom consists of two parts: (1) construction of a 3D tetrahedral-mesh phantom for the reference phase of the phantom and (2) generation of deformation vector fields (DVFs) to represent continuous respiratory motion. First, for the reference 3D tetrahedral-mesh phantom, a 3D polygonal-surface phantom was constructed from the reference phase of 4D CT data (e.g. T50) via segmentation and surface rendering. Then, the constructed polygonal-mesh phantom was converted to the tetrahedral-mesh format using the TetGen library [5]. The density of tetrahedral-mesh phantom was mapped from the reference phase of the 4D CT data.

Second, the DVFs were generated by deformable image registration (DIR). In the present study, DIR was performed for 9 times, i.e., between each neighboring phases (e.g. T50→T60, …, T30→T40), and thus a total of 9 DVFs were obtained. The initial DVFs correspond to the voxel structure, not the vertex structure of the tetrahedral phantom. The DVFs, therefore, were interpolated using the tri-linear interpolation method to create new DVFs in the vertex structure.

B. Implementation of phantom in Geant4 code

A dedicated 4D Monte Carlo code was developed using Geant4 for accurate 4D dose calculation using the constructed 4D tetrahedral-mesh phantom (= reference 3D phantom + 9 DVFs). Before a 4D Monte Carlo simulation, as a pre-process, all data of 4D tetrahedral-mesh phantom was allocated in the system memory. In the present study, we assumed that the entire respiratory period can be modeled by 100 phases with sufficient accuracy. During a continuous 4D simulation, the phase of 4D tetrahedral-mesh phantom is replaced by the *UserParameterisation* class, according to the time parameter which is calculated by the event ID in Geant4 simulation.

III. RESULTS

The constructed 4D tetrahedral-mesh phantom was directly implemented in the 4D simulation code for 4D dose calculation. Figure 2 shows the image shot of 4D Monte Carlo simulation with the constructed phantom. The full animation of the developed phantom and its 4D simulation is available at below web site.

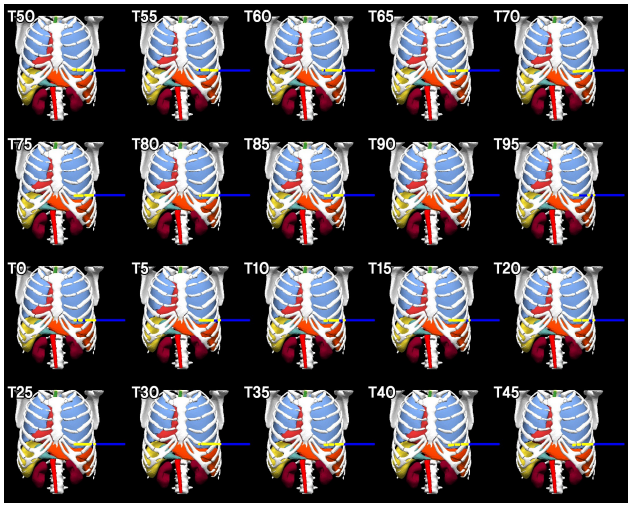

(Web site URL: http://hurel.hanyang.ac.kr/Phantom/4D.gif)

Figure 2. Image shot of 4D Monte Carlo simulation with constructed 4D-TETRA phantom in Geant4

For verification of the developed phantom and its simulation code, the dose distribution was calculated using the phantom and compared with the distribution calculated by the conventional multiple 3D simulations. For this, a proton spot beam (σ= 5 mm) was incident in the middle part of the liver, and the simulation was repeated to obtain a relative error less than 10%.

As a results, it was confirmed that the dose distributions for 4D Monte Carlo simulation approach using the constructed phantom and those of conventional 3D simulation were very close to each other. For a quantitative analysis, the dose distributions were compared using gamma index evaluation [6]. The pass rates of gamma index were very high (99.41% of 3%/3 mm criteria, and 95.78% of 2%/2 mm criteria), which means that it is possible to provide dose distributions with high accuracy by using the 4D tetrahedral-mesh phantom.

IV. CONCLUSION

We have constructed a continuously deforming 4D tetrahedral-mesh phantom using the 4D CT data of a patient. The simulation result shows that our new approach provides accurate dose distributions under patient's respiratory motion. We expect that the use of 4D tetrahedral-mesh phantoms will lead to a significant improvement of accuracy in dose calculation especially when the respiratory motion is important such as in proton spot scanning therapy.

ACKNOWLEDGMENT

This project was supported by Nuclear Safety and Security Commission (NSSC) through Korea Radiation Safety Foundation (KORSAFe) and also by Ministry of Science, ICT and Future Planning through the National Research Foundation of Korea (Project No.: 2011-0025496, 2012-K001146, 1403012). Two of the authors were supported by the Global PhD Fellowship program (Project No.: 2011-0007318, 2011-0030970).

REFERENCES

[1] W. P. Segars, G. Sturgeon, S. Mendonca, J. Grimes, and B.M.W. Tsui, "4D XCAT phantom for multimodality imaging research," *Med. Phys.*, 37, 4902-4915, 2010.

[2] S. Dowdell, C. Grassberger, G. C. Sharp, and H. Paganetti, "Interplay effects in proton scanning for lung: a 4D Monte Carlo study assessing the impact of tumor and beam delivery parameters," *Phys. Med. Biol.*, 58, 4137-56, 2013.

[3] T. C. Huang, J. A. Liang, T. Dilling, T. H. Wu, and G. Zhang, "Four-dimensional dosimetry validation and study in lung radiotherapy using deformable image registration and Monte Carlo techniques," *Radiat. Oncol.*, 5, 45, 2010.

[4] Y. S. Yeom, J. H. Jeong, M. C. Han, and C. H. Kim, "Tetrahedral-mesh-based computational human phantom for fast Monte Carlo dose calculations," *Phys. Med. Biol.*, 59, 3173-85, 2014.

[5] H. Si, "A Quality Tetrahedral Mesh Generator and 3D Delaunay Triangulator," 2006.

[6] D. A. Low, W. B. Harms, S. Mutic, and J. A. Purdy, "A technique for the quantitative evaluation of dose distributions," *Med. Phys.*, 25, 656-661, 1998.

Population of Whole-body Statistical Adult Phantoms and Assessing the Uncertainty of Organ Doses in Hyperthyroid Treatment with ^{131}I

Elie Hoseinian Azghadi, Hashem Miri Hakimabad*, and Laleh Rafat Motavalli

Physics Department, Faculty of Sciences, Ferdowsi University of Mashhad, Mashhad, Iran

*Corresponding author: mirihakim@ferdowsi.um.ac.ir

Abstract - In this paper, a series of computational phantoms (males and females) were developed based on computed tomography (CT) images of a healthy Iranian population. The Monte Carlo calculation method was then used to estimate organ doses and their uncertainties to the hyperthyroid patient from administration of iodine-l31.

Index Terms - statistical phantoms, dose uncertainty, hyperthyroidism

I. INTRODUCTION

Computational phantoms can provide an essential tool to evaluate radiation dose in extensive areas such as radiation protection, radiation imaging, and radiation treatment. Many reference phantoms are currently being developed and widely used to estimate the radiation dose in either external or internal radiation exposures. However, different organs' shape, location and mass of individuals could affect significantly the resulting radiation dose.

A population of computational phantoms would taking into account the differences between the dosimetric data of different individuals. Recently, Segars *et al.* provided the first library of 4D computational phantoms for imaging research [1]. The uncertainties of dosimetry parameters quantified by Ebrahimi-Khankook *et al.* for external photon and neutron irradiation such as an in vivo neutron activation analysis (IVNAA) facility for individuals with only different lung sizes [2-4].

The whole-body statistical phantom series developed in this study was constructed based on anatomy of Iranian subjects. The series consists of 100 (50 males and 50 females) adult phantoms. Since an accurate manual segmentation was accomplished, these datasets could be applied as an atlas for developing auto segmentation codes, which in turn would be advantageous in image-guided surgeries.

In addition to various applications, the current database could be applied in internal dosimetry area, in which patient-specific phantoms were less utilized. ^{131}I has been widely used in nuclear medicine to treat diseases of the thyroid (e.g. hyperthyroidism). The authors previously investigated the difference of organ dose estimates for ICRP voxel phantoms and stylized phantoms from administration of ^{131}I [5-7]. The goal of ^{131}I is to control hyperthyroidism by rendering the patient hypothyroid; this treatment is very effective, provided sufficient radiation is deposited in the thyroid [8].

The important questions that this study intends to answer are: what is the level of uncertainty in the organ doses when a reference model used for a group of people? And is there a systematic deviation between the results for Iranian statistical phantoms and ICRP voxel phantoms?

II. METHODS

A. Phantom construction

The body trunks of phantom series in this study were constructed from chest abdomen pelvis (CAP) CT images of a healthy population of Iranian patients collected from three Educational, Research, and Treatment Centers in Mashhad, and Tehran, Iran. CAP datasets were selected that exhibit normal anatomy of internal organs.

Selected organs were manually segmented from each dataset. The mesh models of the whole body according to trunks height, diameters and circumferences of the CAP models were created using MakeHuman software. The head and neck model was segmented from separated Image datasets and randomly added to the whole body models. The polygon models were imported into the *Rhinoceros*™ to adjust the location and orientation of models from different datasets.

B. Validation of statistical data

The authors investigated the accuracy of whole-body phantoms from statistical viewpoint by gathering the information on segmental body composition analysis of 100 individuals from clinical impedance devices. The correlation between the trunk weight and total height for constructed phantoms was in good agreement with the distribution obtained for normal subjects.

C. Evaluation of uncertainty parameters

The coefficient of variation (CV) was used to compare the amount of dose deviation from the mean value for the various situations.

III. RESULTS

Estimations of organ doses exposed to the internally deposited radionuclide, were obtained for 7 level of thyroid uptake from 5% to 95%, using similar method described in our previous paper [9]. The calculations were performed for a unit of administered activity. However, hyperthyroidism control can be accomplished equally well by either administering a fixed activity or by calculating the activity based on the size of the thyroid and its ability to trap iodine. The first method is simple, and there is evidence that 10 mCi (370 MBq) results in hypothyroidism in 69% at 1 year. The second method requires three unknowns to be determined: the thyroid uptake, the size of the thyroid, and the quantity of radiation (μCi) to be deposited per gram of thyroid (e.g., activity (μCi) = gland weight (g) × 150 μCi/g × [1/24 hour uptake on %]) [8].

IV. CONCLUSION

The series of anatomically variable phantoms developed in this work provide a valuable tool for evaluating radiation dose in various applications. In the present paper, authors try to evaluate organ dose uncertainty due to the anatomical changes of different patients undergoing hyperthyroidism treatment.

The thyroid dose and other important organ doses were calculated and the mean doses and their CV were obtained for each thyroid uptake. The results showed that the thyroid dose is strongly dependent on thyroid gland mass and uptake. In the case of constant administration activity of 10 mCi, the CV value of thyroid dose is significantly large (e.g. 37% for females) in comparison with the later method (2%). This issue was indicated in Figure 1. Therefore, obtained results imply that for effective treatment by deposit sufficient radiation in the thyroid, the later method should be recommended.

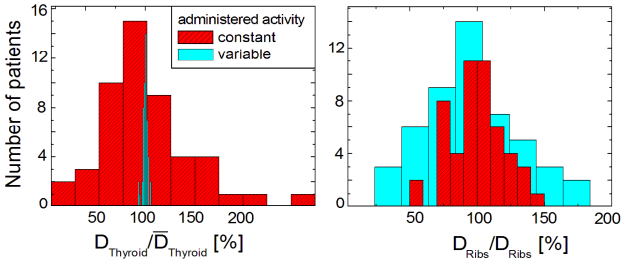

Figure 1. Histogram of thyroid, and active marrow dose in spongiosa bones of ribs per mean value for female phantoms. The mean doses are different for each thyroid uptake.

In the case of the second method of administrating activity the uncertainties in other important organ doses such as proportion of active marrow close to the thyroid, lung, and trachea were increased. Table 1 listed the CV values of dose to organs which have following properties: (1) dose dispersion larger than 20%, and (2) received considerable large dose. The later includes adjacent organs to thyroid gland, as well as major source organs in biokinetic model of radiopharmaceutical (e.g. stomach, bladder contents, and liver).

Table 1. Estimated uncertainty of thyroid dose using two method of administered activity

Administered activity	CV [%]	
	Constant	Variable
Thyroid	37	2
Trachea	49	51
Esophagus	74	67
Lung	24	44
Active marrow (T-spine)	50	86
Active marrow (Ribs)	20	44
Stomach wall	44	70
Liver	15	41

The principal contributor to the dose to nearby organs is the photons emitted by thyroid gland as thyroid uptake increases [7], which occurs in hyperthyroid patients. Therefore, larger CV values were obtained as a consequence of statistical variation of inter-organ distances between thyroid and foregoing organs in different phantoms. The highest marrow absorbed doses are delivered to the marrow in the thoracic spine, and ribs because of the short inter-organ distances between thyroid and these skeletal bones, and also their considerable fraction of total active marrow [6]. Since the administered activity is generally limited by the absorbed dose to the bone marrow, particularly in the treatment of thyroid carcinoma, assessing the level of uncertainty in this fatal tissue seems crucial.

The major contribution of the dose to the main source regions arose from self-irradiation of electrons [7]. By considering the fact that the mass of these organs are not essentially depend on thyroid gland mass, it could be concluded that various administered activities leads to a large statistical deviation from mean value.

It could be concluded that the evaluation of the uncertainty level using statistical phantoms is substantial, especially in the case of high-dose radiation fields. Also, special features of each race may have remarkable effects on resulting dose. For example, shorter necks of Iranian individuals yield to larger amount of dose delivered to lungs and other internal organs in comparison with ICRP reference adult phantoms.

REFERENCES

[1] W. P. Segars *et al.*, "Population of anatomically variable 4D XCAT adult phantoms for imaging research and optimization," *Med. phys.*, 40, 2013.
[2] A. Ebrahimi Khankook, H. Miri Hakimabad, and L. Rafat Motavalli, "The feasibility study of using lung statistical phantoms to determine the uncertainty of the lung absorbed dose in broad beams incident of photons and neutrons," under publication, 2015.
[3] A. Ebrahimi Khankook, H. Miri Hakimabad, and L. Rafat Motavalli, "A study of the effect of the lung shape on the lung absorbed dose in six standard photon and neutron exposure geometries," *Radioprotection*, 50(1), 65-72, 2015.
[4] A. Ebrahimi Khankook, H. Miri Hakimabad, and L. Rafat Motavalli, "A study of the effect of the lung shape on the lung absorbed dose in six standard photon and neutron exposure geometries," *J. Radioanal. Nucl. Chem.*, 303, 2263-2270, 2015.
[5] E. Hoseinian Azghadi, L. Rafat Motavalli, and H. Miri Hakimabad, "Internal dosimetry estimates using voxelized reference phantoms for thyroid agents," *J. Radiat. Res.*, 55 (3), 407–422, 2013.
[6] E. Hoseinian Azghadi, L. Rafat Motavalli, and H. Miri Hakimabad, "Internal dose to active marrow and endosteum from radioactive iodine," *Radiat. Prot. Dosim.*, 164 (3), 291-297, 2015.
[7] E. Hoseinian Azghadi, L. Rafat Motavalli, and H. Miri Hakimabad, "The contributions of source regions to organ doses from incorporated radioactive iodine," *Radioprotection*, 49(4), 249-256, 2014.
[8] R. S. Bahn *et al.* "Hyperthyroidism and other causes of thyrotoxicosis: management guidelines," *Thyroid* 21, 593-646, 2011.
[9] E. Hoseinian Azghadi, L. Rafat Motavalli, and H. Miri Hakimabad, "Development of a 9-months pregnant hybrid phantom and its internal dosimetry for thyroid agents," *J. Radiat. Res.*, 55 (4), 730-747, 2014.

Development of Mesh-based Age-dependent Family Phantoms

Yifei Pi[1], Mang Feng[1], Wanli Huo[1], Lian Zhang[1], Tianyu Liu[2], Hui Lin[2], Lu Yang[1], Fang Zheng[1], Huayan Tan[1], Feng Pan[1], Zhi Chen[1] and X. George Xu[1,2,*]

[1]School of Nuclear Science and Technology, University of Science and Technology of China, Hefei, China
[2]Nuclear Engineering Program, Rensselaer Polytechnic Institute, Troy, New York, USA

*Corresponding author: xgxu@ustc.edu.cn

Abstract **-** This paper describes the development of mesh-based age-dependent family phantoms that are compatible with anatomical parameters for Chinese populations. We present in detail a project to adjust the original mesh-based model, RPI-AM/AF, to phantoms with different ages: 5, 10, 15 and 20-50 years old. The organ masses were adjusted to match with the values of the reference Chinese parameters. All of these phantoms were converted to voxel formats for the purpose of organ dose calculations.

Index Terms - mesh phantoms, anatomical model, Chinese reference parameters, Monte Carlo calculations

I. INTRODUCTION

The estimate of organ doses is an essential task in radiation protection. Whole-body computational phantoms have become one of the most common research tools for computing organ doses. Based on average reference anatomical values, "Reference Man" was put forward. Most of the existing computational phantoms can be divided into three categories: stylized phantoms, voxel phantoms and boundary representation (BREP) phantoms [1-2]. Compared with the other two types of phantoms, BREP phantoms possess attractive flexibility and anatomical realism [3-4]. BREP phantoms were mostly constructed for adult anatomical parameters and phantoms for teenagers are rare. This paper reports our preliminary efforts in developing a series of mesh-based age-dependent Chinese family phantoms from a set of BREP phantoms, RPI adult male (RPI-AM) and RPI adult female (RPI-AF).

II. METHODS

This section describes the steps of construction of the series of Chinese phantoms. Figure 1 illustrates the general workflow. It starts with the gathering of initial input data including human dimensions of Chinese adults and minors [5], reference organ volume information and the RPI-AM and RPI-AF mesh phantoms. Procedures for deforming are divided into two parts: human dimensions scaling and organ volume deformation. Because most of the Monte Carlo codes are insufficiently to handle the BREP type of geometry [6], we convert the mesh-based phantoms into voxels for the purpose of particle transport simulation.

A. Original models and reference parameters

RPI-AM and RPI-AF are a pair of adult male and adult female computational phantoms that are compatible with anatomical parameters for the 50th percentile population as specified by the International Commission on Radiological Protection (ICRP) [7].

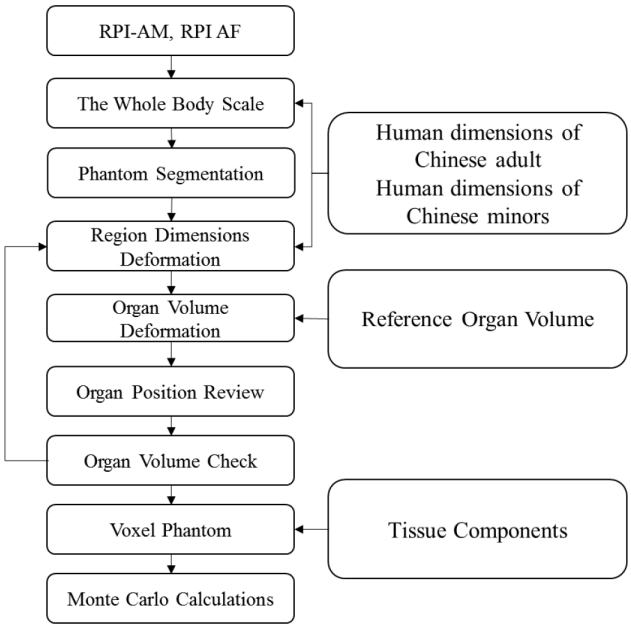

Figure 1. Flowchart of construction of mesh-based age-dependent family phantoms

They were designed entirely using polygonal mesh surface that affords the ability to sufficiently deform the dimensions of phantoms and the shape of organs. For all these reasons, we select RPI-AM and RPI-AF as our initial phantoms.

Corresponding to ICRP reports, Chinese government issued reference individuals for use in radiation protection, a national standard, to standardize Chinese 'Reference Man' [8]. Reference phantom's organ size and mass information for Chinese population are contained.

B. Adjustment

To obtain a phantom of a specific height, we developed a uniform scaling factor adjustment method for adult phantoms and different factors for different parts in teenagers' deformation. It is reasonable to deform phantoms among adults using uniform scaling [9-10]. All of these steps for scaling were done automatically through the use of MATLAB R2014B [11]. We finished human dimensions adjustment automatically and obtained rough phantoms. In order to match internal organ volume with the Chinese reference parameters, a 3D model software Rhinoceros 5 was used. As a result, the organs were eventually deformed to agree within 0.5% with the reference parameters. Finally, all of these regions were assembled together. Figure 2 displays 3D rendering pictures of these adult phantoms. Figure 3 represents the teenager phantoms.

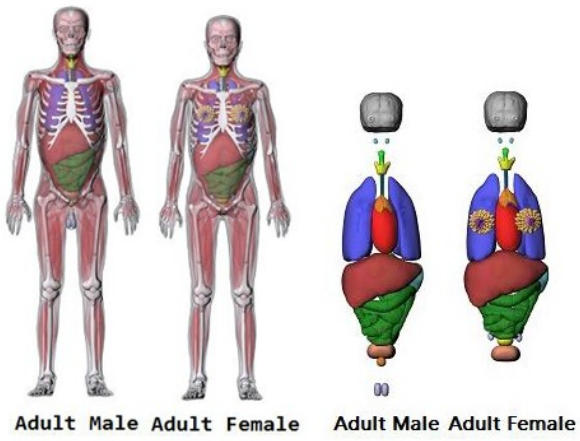

Figure 2. Adult male and female mesh phantoms

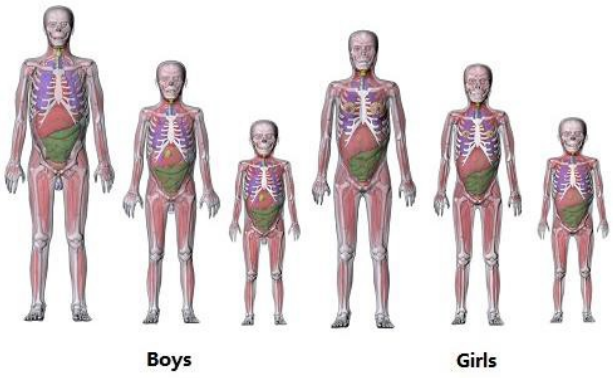

Figure 3. Boys and girls mesh phantoms

C. Tissue composition and Voxelization

The tissue element compositions were defined for the purposes of radiation transport simulations involving Monte Carlo methods. Organ-specific element compositions were based on reference value of the Chinese standard [12]. A C++ based voxelization tool was used to convert the meshed-based age-dependent phantoms into voxel formatted phantoms. The organ volumes after voxelization have been found to agree within 1% with the reference parameters.

III. CONCLUSION

In this paper, we described the preliminary efforts to develop a series of mesh-based age-dependent adult and adolescent phantoms from RPI AM and RPI AF phantoms. Automated and manual methods were implemented to deform phantoms to match with Chinese reference parameters. All phantoms were voxelized for the purposes of Monte Carlo dose calculations.

ACKNOWLEDGMENT

This work was supported in part by grants from the National Natural Science Foundation of China (Grant No. 1137518).

REFERENCES

[1] X. George Xu, "An exponential growth of computational phantom research in radiation protection, imaging, and radiotherapy: a review of the fifty-year history," *Physics in medicine and biology*, vol. 59, pp. R233-R302, 2014.

[2] X. George Xu, "Computational phantoms for radiation dosimetry: a 40-year history of evolution" in Handbook of Anatomical Models for Radiation Dosimetry. George Xu, Eds, 1st ed. London, Taylor and Francis, 2009, ch. 1, pp. 3-42.

[3] Aiping Ding, M. M. Mille, Tianyu Liu., Peter F Caracappa, and X. George Xu. "Extension of RPI-adult male and female computational phantoms to obese patients and a Monte Carlo study of the effect on CT imaging dose," *Physics in medicine and biology*, vol. 57, pp. 2441-2459, 2012.

[4] Juying Zhang, Yong Hum Na, Peter F. Caracappa, and X. George Xu, "RPI-AM and RPI-AF, a pair of mesh-based, size-adjustable adult male and female computational phantoms using ICRP-89 parameters and their calculations for organ doses from monoenergetic photon beams," *Physics in medicine and biology*, vol. 54, pp. 5885-5908, 2009.

[5] GB, "Human dimensions of Chinese minors," GB/T 26158-2010, Beijing, *Chinese Standard Press*, 2010.

[6] B. Denise, Pelowitz, "MCNPX User's Manual Version 2.7.0". LLNL, Los Alamos. 2011.

[7] J. Valentin, "Basic anatomical and physiological data for use in radiological protection: reference values: ICRP Publication 89," *Annals of the ICRP*, vol. 32, pp. 1-277, 2002.

[8] GBZ, "Reference Individuals for Use in Radiation Protection. Part 1. Physique parameters," GBZ/T200.1-2007, Beijing, *People's Medical Publishing House*, 2007.

[9] Yong Hum Na, Binquan Zhang, Juying Zhang, Peter F. Caracappa, and X George Xu, "Deformable adult human phantoms for radiation protection dosimetry: anthropometric data representing size distributions of adult worker populations and software algorithms," *Physics in medicine and biology*, vol. 55, pp.3789-3811, 2010.

[10] V. F. Cassola, V. J. de Melo Lima, R. Kramer, and H. J. Khoury, "FASH and MASH: female and male adult human phantoms based on polygon mesh surfaces: I. Development of the anatomy," *Physics in medicine and biology*, vol. 55, pp.133-162, 2010.

[11] B. R. Hunt, R. L. Lipsman, J. M. Rosenberg, 2014. "A guide to MATLAB: for beginners and experienced users". United Kingdom, CA: Cambridge University Press.

[12] GBZ. "Reference Individuals for Use in Radiation Protection. Part 5. human body elemental composition and contents of element in main tissues and organs," GBZ/T200.5-2009, Beijing, *People's Medical Publishing House*, 2009.

Development of a Male Adult Human Head Phantom Based on Polygon Mesh Surfaces

Bintuan Zhang[1], Xiaobin Xia[1,*], Yinxiangzi Sheng[2], and Yuhai Xu[1]

[1]Department of Radiation Safety, Shanghai Institute of Applied Physics, Chinese Academy of Sciences Shanghai, China
[2]Shanghai Proton and Heavy Ion Center, Fudan University Shanghai Cancer Center, Shanghai, China

*Corresponding author: xiaxiaobin@sinap.ac.cn

I. INTRODUCTION

The hippocampus is a paired brain structure where neurogenesis continues in adult humans [1]. It plays a crucial role in brain function of consolidation of information from memory and formation of new memories [2]. Since neural stem cells in the hippocampus are radiosensitive and radiation- induced injury has been linked to cognitive dysfunction in the radiotherapy [3, 4]. It is essential to develop the accurate radiation dosimetry for the hippocampus. The computational human phantoms in conjunction with the Monte Carlo dose calculations have recognized an important tool for radiation dosimetry. Current computational phantoms only consider the entire brain and do not fully consider sub-parts of the brain, such as the hippocampus. In this study, an advanced adult male head phantom was developed based on polygon mesh surfaces.

II. METHODS

The male adult head phantom was developed based on the polygonal mesh model from Anatomium™ P1 V6.0, including more than 200 parts in the brain. The software Meshlab which is an open source mesh analysis and processing tool designed for rendering, and cleaning unstructured triangular meshes was used for mesh pre-processing to improve the quality of the original mesh files. The commercial software Rhinoceros™ were mainly used for the deformation process to adjust the mass of organs or tissues in the head phantom to reference values of the International Commission on Radiological Protection (ICRP) Publication 89. In addition, algorithms were implemented in MATLAB® 2013a to avoid mesh overlapping and align the faces of adjacent mesh objects.

III. RESULTS AND DISCUSSION

For the whole brain with different parts and other organs or tissues in the head phantom, most organ or tissue masses of the mesh model agree with corresponding data of the ICRP Publication 89 within a margin of 0.5%.

IV. CONCLUSION

The male adult human head phantom was developed based on the polygon mesh surfaces. The head phantom developed in this study can be used for dose calculation of the hippocampus and dosimetric study of other brain parts.

ACKNOWLEDGMENT

The present study is funded by the Postdoctoral Fund of Chinese Academy of Sciences.

REFERENCES

[1] H. J. Song, C. F. Stevens, F. H. Gage. "Neural stem cells from adult hippocampus develop essential properties of functional CNS neurons". *Nat. Neurosci.*, vol. 5, pp. 438-445, 2002.

[2] N. J. Broadbent, L. R. Squire, R. E. Clark. "Spatial memory, recognition memory, and the hippocampus". *Proc. Natl. Acad. Sci.*, vol. 101, pp. 14515-14520, 2004.

[3] V. K. Parihar, C. L. Limoli. "Cranial irradiation compromises neuronal architecture in the hippocampus". *Proc. Natl. Acad. Sci.*, vol. 110, pp.12822-12877, 2013.

[4] F. A. Cucinotta FA, M. Alp, F. M. Sulzman, *et al.* Space radiation risks to the central nervous system. *Life Sci. Space Res.*, vol. 2, pp. 54-69, 2014.

Development of CT-based Mini-pig Physical and Computational Phantoms for Animal Dosimetry

Sooyeun Park[1,2], Byeong Ryong Park[1], Sehwan Shim[3], Wi-Ho Ha[1,*], Sunhoo Park[3], Chan Hyeong Kim[2]

[1]Health Physics Team, National Radiation Emergency Medical Center, Korea Institute of Radiological & Medical Sciences, Seoul, Republic of Korea
[2]Department of Nuclear Engineering, Hanyang University, Seoul, Republic of Korea
[3]Laboratory of Radiation Exposure & Therapeutics, National Radiation Emergency Medical Center, Korea Institute of Radiological & Medical Sciences, Seoul, Republic of Korea

*Corresponding author: lovin@kirams.re.kr

Abstract - During the past years, extensive animal irradiation researches have been carried out for the purpose of radiobiological investigation. Although mice and rats are widely used for animal experiment, their different anatomical and physiological features may lead the result considerably different in biological effect and correlated dose assessment. With the recognition of many similarities between porcine and human both anatomically and physiologically, pigs are increasingly being considered in medical research. The mini-pig is a suitable model for the study of radiation effects, and the acute radiation syndrome closely mimics that in humans. The purpose of this study was to develop mini-pig physical and computational phantoms on the basis of whole-body multi-slice CT data to provide the dose information for animal irradiation experiment. The physical and computational phantoms will be used and the calculated values will be compared.

Index Terms - mini-pig physical phantom, animal dosimetry

I. INTRODUCTION

Clinical treatment studies on radiation injury are usually preceded by experimental studies on animal model to investigate radiation-related detriment. While the small animals are commonly used with their cost effectiveness and ease in handling, they could not provide reliable results in therapeutic efficacy related to human studies due to the considerable dissimilarity in anatomy and physiology. In this light, mini-pig was selected as a dominant model for the purpose of therapeutic studies destined to apply in human.

With respect to dose delivery, however, there exists significant difference of organ dose in large animal with its location due to the attenuation and scattering of radiation [1]. Therefore, the dose assessment of large animals should be conducted with such model reflecting its anatomical structure.

The aim of this study is to develop mini-pig physical and computational phantoms which can provide corresponding dose information.

II. METHODS

A. Animal selection

A 20-kg and 7-month-old male Gottingen mini-pig was selected on the basis of his size and breed. Before irradiation experiment, the pig was certified to be disease free and had enough time to be acclimatized to the laboratory.

B. Acquisition of the mini-pig tomographic image

2D medical images were acquired by use of helical CT scanner (Asteion 4®, TOSHIBA). The X-ray tube was set at 150 kVp and 12 mAs and image reconstruction was performed with a grid of 512 × 512 pixels. The slice thickness was set at 3 mm.

C. Segmentation by each organ

For animal irradiation experiment, four interested organs were selected; skin, bone, lung and intestine. Segmentation was processed by use of Photoshop (CS5, Adobe) with Wacom tablet PC (DTH-2200).

D. Converting DICOM to STL

The CT images were saved as standardized Digital Imaging and Communications in Medicine (DICOM) format and those were used as the raw data in this project.

For 3D image processing, OnDemand3D® (Cybermed) was used for converting DICOM data to STL files [2]. Converted 3D STL image data are shown in Figure 1.

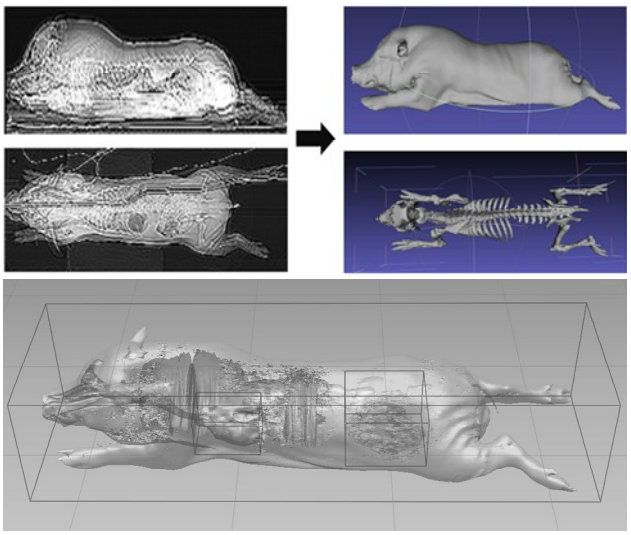

Figure 1. Conversion CT images to 3D STL polygonal image data and converted 3D polygonal mini-pig model

III. RESULTS AND DISCUSSION

The mini-pig physical phantom was constructed on a slice-by-slice basis with a resolution of 2 cm, and holes for dosimeters (alanine dosimeter and glass dosimeter) were also modeled into slices prior to assembly. Thus the slices will be

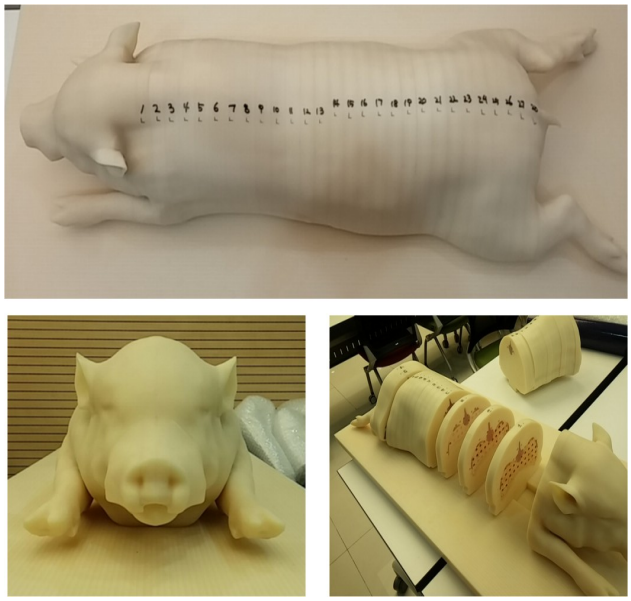

Figure 2. Outer exterior of the mini-pig physical phantom corresponding modified tomographic image. Total 1630 holes were designed to put alanine dosimeters and glass dosimeters in for the irradiation experiment.

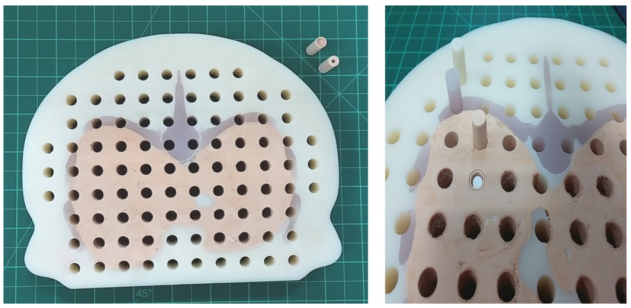

Figure 3. One slice of chest region. Lung, bone and skn were designed as interested organs for the purpose of organ dosimetry

fixed together to form the complete phantom [3]. Figure 2 shows completed mini-pig physical phantom based on segmented CT image data set.

Figure 3 shows one slice of chest including lung and bone as interested organs. In addition, intestine is developed as an interested organ in abdomen. And the other organs are assumed to be composed of same material with skin.

In consideration of two different types of dosimeters and placement of various positions, the phantom was designed to hole-holder structure. The phantom will be used in conjunction with a complementary dosimetry system which is using alanine and glass dosimeters to measure individual organ doses.

IV. CONCLUSION

Physical and computational phantoms using mini-pig model was created to provide the dose information. In particular, our group plans to carry out the animal irradiation experiment for the wide dose range to investigate radiation injury with corresponding radiation dose. Thus, to provide accurate organ dose information, comparison of simulation and measurement result is planned as future works. The measurement and simulation results will be presented in the workshop.

ACKNOWLEDGMENT

This project was supported by R&D program of the Ministry of Science, ICT and Future Planning (MSIP), Korean Government. (Project No. 50586-2015).

REFERENCES

[1] V. Nagy, "Dosimetry for Animal Irradiation Models," *International Biodosimetry Research Symposium*, Bethesda, MD, 2011.

[2] P. Mah, *et al.*, "Deriving Hounsfield units using grey levels in cone beam computed tomography," *Dentomaxillofac rad.*, vol.39, pp. 323-335, 2014.

[3] J. F. Winslow, *et al.*, "Construction of Anthropomorphic Phantoms for Use in Dosimetry Studies," *J. Appl. Clin. Med. Phys.*, vol. 10:3, pp. 557-578, 2009.

Updates of the 4D XCAT Phantom Series for Biomedical Imaging and Radiation Dosimetry

Benjamin M. W. Tsui[1,*], and W. Paul Segars[2]

[1]Department of Radiology, Johns Hopkins University, Baltimore, MD, USA
[2]Department of Radiology, Duke University, Durham, NC, USA

*Corresponding author: btsui1@jhmi.edu

Abstract **-** The four-dimensional (4D) extended cardiac-torso (XCAT) phantom series is the result of a continuous development of realistic digital phantoms for biomedical imaging and radiation dosimetry applications. The phantoms were evolved from the three-dimensional (3D) NURBS-based cardiac-torso (NCAT) phantom that was based on the Visible Human data. The organs in the torso region were modeled using non-uniform rational b-spline (NURBS) surfaces that allowed a close resemblance to the size and shapes of tissue organs. The 3D NCAT phantom was extended to the entire body from head to toe and to 4D to include models for realistic cardiac and respiratory motions derived from cardiac-gated tagged MRI images and respiratory-gated CT images from normal subjects respectively. The result was the first 4D XCAT phantoms modeling the anatomy and motions for a standard adult male and female. The XCAT has since been extended to a series of models, based on patient CT imaging data, to represent the human anatomy at different ages, and of various male and female body build types and sizes. When combined with accurate imaging simulation methods (Monte Carlo or analytical), the XCAT phantoms offer unique and useful tools for the design and development of biomedical imaging equipment, data acquisition techniques and image reconstruction and processing methods, and accurate radiation dosimetry calculations. Recent updates of the 4D XCAT phantoms include further improvement in the anatomical details (including the brain, lungs, heart, breasts, liver, vasculature, lymph nodes, etc.), the modeling of textures to simulate the heterogeneity within the tissues, and the incorporation of a model to simulate contrast perfusion. Such improvements greatly enhance the phantom's ability to simulate patient-quality data at the level necessary to assess image-quality as well as dosimetry. New applications include 3D and 4D biomedical imaging applications in PET, SPECT, CT and multi-modality PET/CT, SPECT/CT and PET/MR, and radiation dosimetry estimation for low dose imaging and radioimmunotherapy. With future medical progress focused on the personalization of medical procedures, it is highly anticipated that the 4D XCAT phantom series will continue to improve and play an increasingly important role in biomedical imaging and radiation dosimetry.

Coronary Dose Calculations with Computational Phantoms after Radiotherapy

David Broggio[1,*], Alexandra Moignier[1] and Sylvie Derreumaux[2]

[1]IRSN/PRP-HOM/SDI/LEDI, Institut de Radioprotection et de Sûreté Nucléaire, Fontenay-aux-Roses, France
[2]IRSN/PRP-HOM/SER/UEM, Institut de Radioprotection et de Sûreté Nucléaire, Fontenay-aux-Roses, France

*Corresponding author: david.broggio@irsn.fr

Abstract **-** Cardiovascular diseases following radiotherapy have been evidenced for long. However, the dose effect relationship remains difficult to establish due to confounding factors and difficulties in carrying out acute dose reconstruction. Computational models of the heart, including the coronary arteries, have been merged with thoracic models to enable dose calculation with a Treatment Planning Software. The method has been applied to study the influence of coronary topology in the case of breast radiotherapy and in a case-control study of patients treated for Hodgkin lymphoma. In the case of breast radiotherapy the presence of an arch on the Left Anterior Descending (LAD) coronary artery seems to induce higher doses than when the arch is absent. When the internal mammary chain is treated coronary doses are higher than when it is not irradiated. The result of the case control study shows that the multiplicative risk of coronary stenosis on a coronary artery segment was 1.05 at each additional gray on the median dose to the coronary artery segment.

Index Terms - radiotherapy, coronary, computational phantom, stenosis, risk

I. INTRODUCTION

Improvements in thoracic Radiation Therapy (RT) have increased patient survival and revealed late effects, making cardiovascular disease a major concern [1]. With old medical records, retrospective cardiovascular dose studies are based on mathematical phantoms or a computed tomography (CT) scan of a representative patient [2]. With current medical records, CT allows 3-dimensional (3D) visualization of the patient anatomy but does not permit precise visualization of coronary arteries because of limited resolution and contrast. The most exposed coronaries are the LAD and the Left Main artery (LM).

Here, we recall results presented elsewhere regarding the influence of coronary topology on the dose following left breast radiotherapy [3] and present unpublished results for a case control study of patients followed-up after mediastinal Hodgkin lymphoma RT.

For both cases, coronary doses were calculated with clinical tools after inclusion of a detailed heart model in the patient thoracic model.

II. MATERIAL AND METHODS

A. Computational phantoms insertion in the Treatment Planning Software

For both studies heart models obtained by CT angiographies (CTA) are delineated and exported to the Rhinoceros 3D computer aided design software. The patient thoracic images from simulation CT scans are also delineated and exported. After small adjustments a 3D model of the patient, including the coronaries, is obtained. The 3D model is then voxelized and stored in DICOM format to be exported to a Treatment Planning Software (TPS) where dose calculations are carried out with the same algorithm than in the clinical practice. Beam sets and monitor units and all other relevant parameters corresponding to the patient's RT are taken into account by the TPS.

B. Influence of coronary topology in left breast side radiotherapy

Twenty two heart models of male and female patients have been inserted in a single female thorax. The thorax was chosen to be representative of the weight and breast size of a cohort of patients treated for left breast cancer.

Dose calculations were carried out for two typical beam sets: the first with tangential and tumoral bed beams (50 Gy+16 Gy), the second added 50 Gy for treatment of the internal mammary chain (IMC). Dose statistics at the coronaries level were thus studied for different coronary topologies.

C. Case control study of mediastinal Hodgkin Lymphoma patients

Following a study of cardiovascular events for a cohort of patients who had been treated for a mediastinal Hodgkin Lymphoma [4] a refined case-control study focusing on coronary doses has been undertaken. Case patients with stenosis and matched controls without stenosis where selected. Twelve cases and 21 controls where included, for cases and controls CTAs, simulation CTs and beam sets were available. For 2 cases a surrogate beam library was used and it was checked that the dose calculations were acute enough. For each case all possible matched controls were selected, the matching criteria were hypertension, age at treatment time, and the time interval between the RT and the CCTA. Doses were calculated for the 9 segments of the LAD, LM, circumflexes and right coronaries segments as defined in [5]. Univariate risk analysis with conditional logistic regression was carried out.

III. RESULTS AND DISCUSSION

A. Influence of coronary topology in left breast side radiotherapy

The 3D dose maps revealed that the internal mammary IMC beams induced hot spots between 20 and 30 Gy on the LM and the proximal LAD for some coronary topologies. Without IMC beams, hot spots between 5 and 26 Gy are located on the middle and distal LAD. It was noticed that when the LAD presents an arch in the proximal part hot spots seem to be of higher magnitude, as illustrated on Figure 1.

Figure 1. Dose map for the coronary tree without internal mammary chain irradiation (left) and with (right).

Moreover the inter-model standard deviation of the mean dose to the LAD was 19% without IMC irradiation and 35% with IMC irradiation.

B. Case control study of mediastinal Hodgkin Lymphoma patients

The stenotic CA segments were mainly associated to high doses: 80% of them received a median dose superior to 20 Gy. But, as thoroughly evidenced in the literature, it is not the only significant risk factor for cardiovascular disease. Indeed, similar high doses were sometimes found in damaged and normal coronary artery segments, as illustrated on Figure 2.

In eleven cases out of twelve, the highest dose of the coronary distribution was on a damaged segment. Logistic regression with CA segments yielded an odds ratio associated to the risk of coronary stenosis of 1.049 per additional gray with the CA segment median dose (95% confidence interval, 1.004 to 1.095; p-value < 0.05).

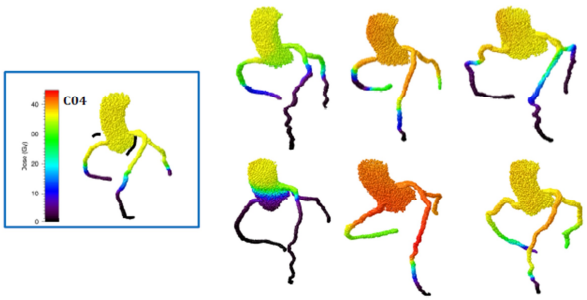

Figure 2. Dose map for a case (C04) and its matched controls. The black lines along the case's coronaries outline the stenotic parts.

IV. CONCLUSION

Detailed heart models and thoracic models have been merged into a computational phantom and then exported to a treatment planning software. The increase in anatomy detail at the coronary level enabled to carry out dose calculations that are not possible with conventional medical images used in radiotherapy.

Such a process might be undertaken for larger cohort but using dedicated clinical tools since the process exposed here is too time-consuming for larger studies.

ACKNOWLEDGMENT

The medical physicists and radiotherapists of Hôpital de la Pitié-Salpétriere (Paris) and of Institut Gustave Roussy (Villejuif) are thanked for their efficient support and enthusiasm. Dr. Jean-François Paul (Clinique Marie Lannelongue, Le Plessis-Robinson) also actively took part in this work.

REFERENCES

[1] SC. Darby, M. Ewertz, P. McGale, *et al.* "Risk of ischemic heart disease in women after radiotherapy for breast cancer," N Engl J Med, 368, pp. 987-998, 2013.

[2] CW. Taylor, A. Nisbet, P. McGale, *et al.* "Cardiac exposures in breast cancer radiotherapy: 1950s-1990s," *Int. J. Radiat. Oncol. Biol. Phys.*, 69, pp. 1484-1495, 2007.

[3] A. Moignier, D. Broggio, S. Derreumaux, *et al.* "Dependence of coronary 3-Dimensional dose maps on coronary topologies and beam set in breast radiation therapy: a study based on CT angiographies," *Int. J. Radiat. Oncol. Biol. Phys.*, 89, pp. 182-190, 2014.

[4] T. Girinsky T, R. M'Kacher, N. Lessard *et al.* "Prospective coronary heart disease screening in asymptomatic Hodgkin lymphoma patients using coronary computed tomography angiography: Results and risk factor analysis," *Int. J. Radiat. Oncol. Biol. Phys.*, 89, pp. 59-66, 2014.

[5] The principal investigators of CASS and their associates, "The National Heart, Lung, and Blood Institute Coronary Artery Surgery Study (CASS)," *Circulation*, 63 (suppl I), pp. I1–I81, 1981

Evaluation of Motion Compensation Using Component Analysis in Nuclear Medicine Imaging: Phantom Simulation Study

Kyeong Min Kim*, Se Jong Oh

Korea Institute of Radiological & Medical Sciences, Seoul, Republic of Korea

*Corresponding author: kmkim@kirams.re.kr

Abstract **-** Motion correction in PET or SPECT imaging is one of important issues for the accurate quantitation of physiological parameters. For motion correction in both abdomen and brain imaging, many approaches using external monitoring device have been suggested. In this study, we suggest an alternative approach using multi-frame image data only, without additional motion monitoring device. For the evaluation of the new approach, simulation experiments using Zubal brain and XCAT phantom were performed. In the generation of simulated images, abrupt motion was applied to dynamic images of brain and tumor in lung, respectively. Both images of glucose uptake and dopamine receptor binding were generated for brain. Periodic motion by breathing was also applied to abdomen including tumor region. To all simulated images, gaussian smoothing filter and gaussian noise were applied to mimic clinical PET data. In the extraction of interested region, factor analysis based on principal component analysis was applied. The extracted component images of interested regions were close to those without motion. The curve of factor-weight with time reflected the degree of motion. Accuracy of motionless factor of images with abrupt motion was better than that of periodic motion. The smoothing contributed to reduce the error in motion extraction. These results shows that this approaches can be feasible to compensate the abrupt or random motion in the dynamic brain study with long acquisition duration, without additional motion monitoring devices.

Index Terms – PET, motion, dynamic image, respiration, factor analysis

I. INTRODUCTION

In the quantitative study using PET or SPECT, the correction of patient's motion is one of important issues for the improved image quality and the accurate estimation of physiological parameters. Patient's motion during image acquisition degrades the image contrast, consequently, image quality and results in the error in quantitative measurement. Many researchers have suggested various approaches for motion compensation in brain and abdomen regions. Many studies among the approaches motion correction have been based on the use of multi-frame imaging techniques and additional motion-monitoring device. In the use of multi-frame imaging, image- or sonogram-based approaches have been suggested. Although sinogram-based approach can be more effective, because of its theoretical flexibility of implementing motion correction to image reconstruction, image-based approach of motion correction has been still preferable for clinical implementation.

Representative method of image-based motion correction is the use of co-registration of images acquired between motions [1]. This approach also requires the additional information of patient motion during image acquisition. To get the motion information without motion monitoring device, many number of multi-frame or dynamic frame is required to extract motion information extracted from multi-frame images. And based on the extracted motion information, the multi-frame images are summed for motionless images and co-registered to the image with motion. This approach is, however, laborious and inefficient to be applied to clinical cases with various and many motion during imaging acquisition. Therefore to increase the applicability to clinical study, additional motion monitoring is still recommended [2-5].

Kinetic analysis using dynamic imaging has been widely used in the quantitative estimation of physiological parameter, such as blood flow, binding potential, glucose metabolic rate. Usually dynamic imaging needs long acquisition duration, which may result in patient's motion during acquisition. Therefore the variation of pixel values on each time-frame image, due to the motion, induces the error in the parameter estimation and the parametric images.

In the image of abdomen region, patient breathing using PET imaging induces the motion artifact of target shape distortion and activity underestimation. For the correction of artifact due to respiration motion, gated acquisition incorporating the periodic breathing cycles information obtained from external device, has been widely used. Acquired gated sonogram are reconstructed to images for evaluation of activity and size of tumor. Gated image can provide the motion reduced images. However, increased image noise on gated image, compared to non-gated image, limit the improvement of tumor detectability [6-7].

Factor analysis based on principal component analysis is a use tool of blind extraction from data mixture including various information sources. Factor analysis has been successfully applied and validated to dynamic PET studies for extracting image-based input function and elimination of spill-over activity from neighbor organs. Factor analysis uses only multi-frames images and provides images and time-variation information of factors assumed. Therefore, in the motion correction using data with multi-frames, such as dynamic and gated study, factor analysis can be applied.

In this study, we evaluated the applicability of factor analysis in the extraction of image with motion compensation, using human phantoms and simulation.

II. MATERIAL AND METHODS

A. Generation of phantom images with motion

Zubal brain phantom [8] and XCAT phantom [9] were used in the generation of image for brain and abdomen regions, respectively. For brain images, the dynamic images of FDG and

FP-CIT were assumed and generated. The dynamic images with 24 frames were generated for both of FDG and FP-CIT. All images were reformed to matrix of 128 × 128 size, and Gaussian smoothing filter with 4 mm kernel size was applied to images of all dynamic frames. The Gaussian noise close to clinical image was added to images of all frames.

For abdomen images, dynamic and gated image of FDG were generated using XCAT phantom was used. The number of dynamic and gated frames were 24 and 8, respectively. The size of image matrix was 128 × 128. The same processing of blurring filter and adding noise were applied to image.

Abrupt motion within 10 mm range was applied to both brain and abdomen region. In the gated image generation, realistic respiration motion information was applied.

B. Motionless image extraction

For brain images, the number of 2 was used in separation and extraction of components of gray matter and white matter for FDG, and striatal and other brain regions for FP-CIT. For number of 3 was used in separation and extraction of components of lung, liver, tumor regions. Factor analysis algorithm based on the methods of Di Paola [10] and Wu [11] was used.

The dynamic images of initial 8 frames were summed to single frame image to clarify the target region in the dynamic images. In the transverse slices of the summed image, the rectangular mask was put on the target region, and applied to whole dynamic images. The masked dynamic images were used in the extracting time-activity curves of target regions. The dynamic data of 4-dimension was transformed to 2-dimensional data. Two or Three components were separated and extracted from the masked dynamic data. Time weight curves (TWCs) and images of extracted factors were used in estimated the motion-induces variation and motionless image.

III. RESULTS

The curve of factor-weight with time (time-weighted curve, TWC) reflected the degree of motion. In the noiseless data, the information abrupt motion could be estimated by TWC of the extracted factor and the factor images of separated components were very similar to the image without motion for both brain and tumor in abdomen region. Even for the data with noise, the error in the estimation of motion from TWC was small (~5% of area under the TWC).

In the case of abdomen image with periodic respiration motion, TWC and images of 3 factors could be separated and extracted. The shape of tumor region was distorted and the motion variation was underestimated. As noise increased, the amount of distortion and error increased.

IV. CONCLUSION

Factor analysis could be applied to image-based motion compensation in the dynamic PET study, without any external motion monitoring device. The use of only dynamic image data set in motion correction can provide flexibility and simplicity in kinetic analysis using images with patient's reposition during acquisition. For the image with respiration motion, factor analysis in this study was not sufficient to be used. To be applicable to abdomen images, the combinational use of new multi-frame binding and modified data separation algorithm is needed.

REFERENCES

[1] R. Woods *et al.,* "Automated image registration: Ii. Intersubject validation of linear and nonlinear models," *J. Comput. Assist. Tomogr.,* vol. 22, pp.153-165, 1998.

[2] Y. Picard and C. Thompson, "Motion correction of PET images using multiple acquisition frames," *IEEE Trans. Med. Imaging,* vol. 16, pp.137 –144, 1997.

[3] B. Lopresti *et al.,* "Implementation and performance of an optical motion tracking system for high resolution brain PET imaging," *IEEE Trans. Nucl. Sci.,* vol. 46, pp.2059-2067, 1999.

[4] R. Fulton *et al.,* "Correction for head movements in positron emission tomography using an optical motion-tracking system," *IEEE Trans. Nucl. Sci.,* vol. 49, pp.116-123. 2002.

[5] S-K Woo et al, "Sinogram-based motion correction of PET images using optical motion tracking system and list-mode data acquisition," *IEEE Trans. Nucl. Sci.,* vol. 51, pp. 782-788, 2004.

[6] E. Rietzel, et al, "Four-dimensional computed tomography: Image formation and clinical protocol," *Med. Phys.*, vol. 32, pp. 874–889, 2005.

[7] SA. Nehmeh and Y E. Erdi, "Respiratory Motion in Positron Emission Tomography/Computed Tomography: A Review," *Sem. Nucl. Med.,* vol. 38, pp.167-176, 2008.

[8] I.G. Zubal *et al.,* "Two dedicated software, voxel-based, anthropomorphic (torso and head) phantoms," *in Proceedings of the International Workshop,* National Radiological Protection Board, edited by P. J. Dimbylow (NRPB, Chilton), pp. 105-111, 1996.

[9] W.P. Segars *et al.,* "4D XCAT phantom for multimodality imaging research," *Med. Phys.,* vol. 37, pp. 4902-4915, 2010.

[10] D.R. Paola *et al.,* "Handling of dynamic sequences in nuclear medicine," *IEEE Trans. Nucl. Sci.,* vol. 29, pp. 1310-1321, 1982.

[11] H.M. Wu *et al.,* "Factor analysis for extraction of blood time-activity curves in dynamic FDG_PET studies," *J. Nucl. Med.,* vol. 36, pp.1714-1722, 1995.

Simultaneous Algebraic Reconstruction Technique (SART) in Digital Breast Tomosynthesis Using Voxelized 3D Breast Phantom

Sunghoon Choi[1], Ye-seul Kim[1], Haeng-Hwa Lee[1], Donghoon Lee[2], Shouchih Mu[2], and Hee-Joung Kim[1,2,*]

[1]Department of Radiological Science, Yonsei University, Wonju, Republic of Korea
[2]Department of Radiation Convergence Engineering, Yonsei University, Wonju, Republic of Korea

*Corresponding author: hjk1@yonsei.ac.kr

Abstract **-** We conducted a simultaneous algebraic reconstruction technique (SART) in order to reconstruct the projection data acquired from analytically simulated digital breast tomosynthesis (DBT). In this study, we simulated a computerized 3D anthropomorphic breast phantom. The results indicated that SART gave better reconstructed images compared to FBP by comparing overall root-mean-square errors (RMSEs) for both lesion and ductal tissue in-plane tomosynthesis images. As a result, our simulations and reconstruction scheme could give basic information in further tomosynthesis studies.

Index Terms - SART, DBT, Computerized 3D breast phantom

I. INTRODUCTION

Digital breast tomosynthesis (DBT) has been considered as an innovative imaging modality because it can solve the problem of poor depth resolution in conventional digital mammography by utilizing multiple slices of breast volume [1]. Similar to breast computed tomography (CT), projection data which are generated from DBT also needed to be reconstructed in order to produce axial cross sectional images of scanned breast. Several reconstruction methods have been introduced in commercialized DBT system such as filtered back-projection (FBP) and algebraic reconstruction technique (ART). Since the breast is mostly composed of low density materials, the iterative reconstruction algorithms present better image qualities compared to FBP because a high pass filter mainly used in FBP suppress low frequency components [2].

In order to overcome the difficulty in FBP, we conducted a simultaneous algebraic reconstruction technique (SART) which could produce better image qualities in DBT. The purpose of this study was to apply SART algorithm and quantitatively evaluate its performance in analytically simulated DBT system with computerized 3D breast phantom.

II. METHODS

A. Analytic simulation of DBT system

Figure 1 shows the analytically simulated DBT system by using MATLAB ver.8.0. (MathWorks Inc., USA). This tomosynthesis system has an arc motion of X-ray tube and stationary detector, pivoting around a center-of-rotation (COR). As moving total ±21° sweep angle range, we acquired 15 projection images with 3° step angle by using ray-driven forward projector. The specifications of simulated DBT are summarized in Table 1.

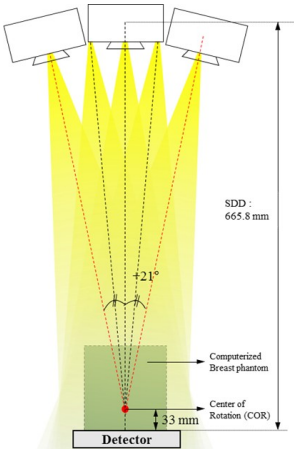

Figure 1. Schematic illustration of analytically simulated DBT system

Table 1. Specifications of simulated DBT

Source to detector distance	665.8 mm	Detector dimensions	634(W) × 722(H)[b]
COR to detector distance	33 mm	Pixel pitch	0.25 mm
Number of projections	21	Volume dimensions	122(W) × 252(H) × 230(T)[b]
Angle step	1.5°	Voxel size[a]	0.5 mm

a. Isotropic voxels were used.
b. W: Width, H: Height, T: Thickness.

B. Voxelized 3D breast phantom

We used a statistically simulated 3D breast phantom proposed by J. M. Shorey [3]. This phantom contains duct, adipose, and fibro-glandular tissue, skin, fat, muscle, and lesion followed by stochastic growth model introduced by Burgess and Chakraborty [4]. Schematic view of anthropomorphic breast phantom is shown in Figure 2.

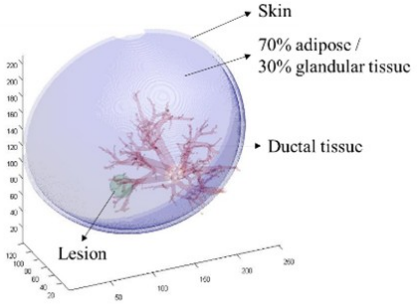

Figure 2. 3D visualization of voxelized breast phantom

C. Simultaneous algebraic reconstruction technique (SART)

SART was firstly proposed by A. H. Andersen and A. C. Kak [5] in order to reduce noise and computational time arisen from algebraic reconstruction technique (ART) for solving linear equation which could be expressed as follows:

$$A_{ij}x_j = b_i \tag{1}$$

where A_{ij} is a sparse matrix that contains weighting coefficients for j[th] voxel on i[th] ray, x_j is the solution, and b_i is the measured ray-sum. SART is simultaneously updating the solutions at k[th] iteration by averaging all correction terms for each scan direction which could be described as follow equation:

$$x_j^{(k+1)} = x_j^{(k)} + \frac{\Sigma_{i\epsilon\theta}\left[A_{ij}\frac{b_i - A_{ij}^T x_j^{(k)}}{\Sigma_{j=1}^N A_{ij}}\right]}{\Sigma_{i\epsilon\theta}A_{ij}} \tag{2}$$

III. RESULTS AND DISCUSSIONS

Resulted forward projection images of voxelized breast phantom are shown in Figure 3 and reconstructed images using FBP and SART of 10 iterations are shown in Figure 4. As shown in Figure 4, SART gave better image qualities compared to FBP in both lesion and ductal tissue in-plane tomosynthesis images.

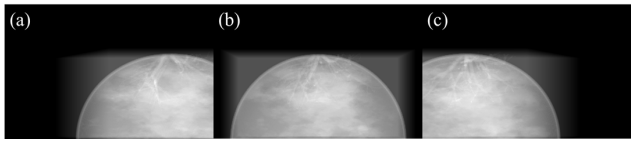

Figure 3. Resulted forward projection images from (a) -21° (b) 0° and (c) 21° using ray-driven forward projector

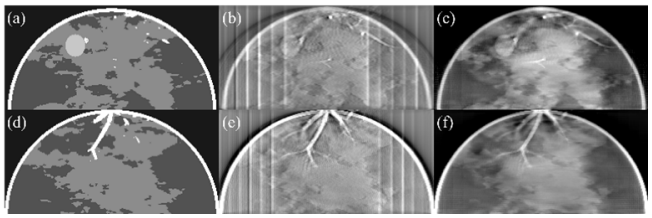

Figure 4. Reconstructed axial cross sectional images using FBP and SART of 10 iterations were shown as follows: (a) and (d) were original voxelized breast phantom of lesion and ductal tissue in-plane, respectively, (b) and (e) were reconstructed images from FBP and (c) and (f) were reconstructed images from SART, showing same in-plane as original breast phantom.

In order to quantitatively evaluate the performances of FBP and SART, we calculated overall root-mean-square errors (RMSEs) between the referenced original breast phantom and the reconstructed images. As shown in Figure 5 (a), the resulted overall RMSEs from SART showed lower value compared to those from FBP, which indicated that SART described the breast phantom more closely. We also compared overall RMSEs at lesion in-plane reconstructed images as a function of iteration numbers in SART as summarized in Figure 5 (b). The result showed that overall RMSE was reduced as increasing the iteration times.

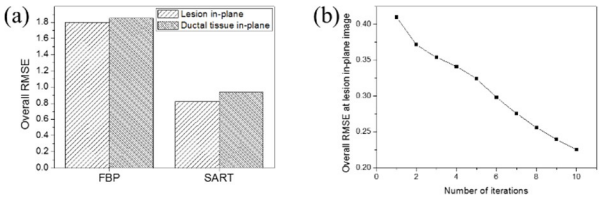

Figure 5. Calculated overall RMSE of (a) lesion and ductal tissue in-plane between the original breast phantom and reconstructed volume produced by FBP and SART and (b) lesion in-plane tomosynthesis image as a function of iteration numbers

IV. CONCLUSION

We analytically simulated DBT system and computerized anthropomorphic breast phantom which containing statistically generated duct and ellipsoidal lesion. After acquiring forward projection images in each angle using ray-driven forward projector, we reconstructed them by using SART and FBP. The results indicated that SART gave better image qualities than FBP by comparing overall RMSEs for both lesion and ductal in-plane tomosynthesis images. As a result, our simulations and reconstruction scheme could give basic information in further tomosynthesis studies.

ACKNOWLEDGMENT

This research was financially supported by the Ministry of Trade, Industry & Energy (MOTIE), Korea Institute for Advancement of Technology (KIAT) and Gangwon Institute for Regional Program Evaluation (GWIRPE) through the Economic and Regional Cooperation Industry (No. R0002898).

REFERENCES

[1] J. T. Dobbins and D. J. Godfrey, "Digital x-ray tomosynthesis: current state of the art and clinical potential," *Phys. Med. Biol.*, vol. 48, pp. R65-R106, 2003.

[2] D. V. Sompel, M. Brady, and J. Boone, "Task-based performance analysis of FBP, SART and ML for digital breast tomosynthesis using signal CNR and Channelised Hotelling Observers," *Medical Image Analysis*, vol. 15, pp. 53-70, 2011.

[3] J. M. Shorey, "Stochastic Simulations for the Detection of Objects in Three Dimensional Volumes: Applications in Medical Imaging and Ocean Acoustics," *Electrical and computer engineering*, Durham, NC: Duke University, 2007.

[4] A. E. Burgess and S. Chakraborty, "Producing lesions for hybrid mammograms: extracted tumors and simulated microcalcifications," *Proceedings of SPIE*, *SPIE Medical Imaging*, 1999, pp. 316-322.

[5] A. H. Andersen and A. C. Kak, "Simultaneous algebraic reconstruction technique (SART): A superior implementation of the ART algorithm," *Ultrasonic Imaging*, vol. 6, pp. 81-84, 1984.

ICRP Adult and Pediatric Reference Computational Phantoms

Maria Zankl[1,*], Janine Becker[1], Choonsik Lee[2], Wesley E. Bolch[3], Yeon Soo Yeom[4], and Chan Hyeong Kim[4]

[1]Research Unit Medical Radiation Physics and Diagnostics, Helmholtz Zentrum München – German Research Center for Environmental Health (GmbH), Neuherberg, Germany
[2]Radiation Epidemiology Branch, National Cancer Institute, National Institutes of Health (NIH), Rockville, MD, U.S.A.
[3]J. Crayton Pruitt Family Department of Biomedical Engineering, University of Florida, Gainesville, FL, U.S.A.
[4]Department of Nuclear Engineering, Hanyang University, Seoul, Korea

*Corresponding author: zankl@helmholtz-muenchen.de

Abstract **-** The paper summarizes the current ICRP reference computational phantoms – adult voxel phantoms, pediatric boundary representation phantoms, and the project presently converting the adult reference voxel phantoms into high- quality polygon mesh versions.

Index Terms **-** reference computational phantoms, adult, pediatric, voxel, boundary representation

I. INTRODUCTION

Phantoms simulating the human body or parts thereof play a central role in radiation dosimetry. The first computational body phantoms have been based upon mathematical expressions representing planes, cylindrical, conical, elliptical, and spherical surfaces describing the shape and position of idealized body organs [1-6]. For this first generation of computational body phantoms, the organ masses and volumes were in accordance with the ICRP data of former Reference Man [7].

With the advent of more powerful computers in the 1980s, various groups have developed voxel phantoms as an extension and improvement to these earlier models [8-21]. Being based on three-dimensional images of single individuals, they offer a more realistic replication of human anatomy. Various authors have shown that the organ shapes of the earlier mathematical phantoms present an over-simplification that has an influence on the energy distribution which may deviate for some cases systematically from that calculated for voxel phantoms [22-29].

However, despite their obvious advantages compared to the previously used stylized phantom type, most of these phantoms do not represent the average Caucasian man or woman, due to being derived from a specific individual. Hence, the International Commission on Radiological Protection (ICRP) decided to construct voxel phantoms being representative of the adult Reference Male and Reference Female [30] with respect to their external dimensions, their organ topology, and their organ masses [31], for the update of organ dose conversion coefficients following the recent ICRP Recommendations [32].

A further disadvantage of all voxel phantoms is their limited flexibility concerning changes in size, shape, and posture. Therefore, further work on phantom development has focused on the development of phantoms that seek to combine the realism of patient-based voxel phantoms with the flexibility of mathematical phantoms. So-called "hybrid" phantoms may be based on voxel geometry, but their stepped surfaces are replaced by polygon meshes (PM) and/or non-uniform rational B-splines (NURBS), thus resulting in so-called boundary representation (BREP) based phantoms. Hence this phantom type has been chosen for the family of pediatric reference phantoms being developed for the ICRP.

Finally, as the voxel resolution of the adult reference computational phantoms is of the order of a few mm, smaller tissues, like, for example, the eye lens, skin and micron-thick target tissues in respiratory and alimentary tract regions could not be properly segmented. The calculated doses for these tissues have, therefore, some limitations, particularly for weakly-penetrating radiation. In this context, ICRP Committee 2 recently initiated a research project to convert the ICRP 110 phantoms into polygon mesh format with the goal of producing replica of the ICRP 110 phantoms in polygon mesh format, including all source and target regions, even those with micron resolution.

II. METHODS

A. Adult reference computational voxel phantoms

Voxel phantoms were selected with external dimensions close to the reference data. These were then adjusted to the reference values of ICRP Publication 89 [30]. The method is described in detail in ICRP Publication 110 [31].

B. Pediatric reference computational phantoms

Major organs and tissues were segmented from CT data of patients at ages close to newborn, 1 year, 5, 10, and 15 years. NURBS and polygon mesh surfaces were then used to model individual organs and tissues and subsequently match anthropometric data and reference organ masses [30].

C. Adult reference phantom conversion project

The ICRP 110 voxel phantoms are being converted into high-quality polygon mesh format.

III. RESULTS

A. Adult reference computational voxel phantoms

The adult reference computational phantoms of ICRP Publication 110 are the official computational models representing the Reference Male and Reference Female [30, 32].

B. Pediatric reference computational phantoms

The UF hybrid phantom series is provided in two formats. The first is via NURBS and polygon mesh surface renderings; the

second are voxelized versions of these same reference phantoms. They are in very close agreement with the reference data of ICRP Publication 89 [30].

C. Adult reference phantom conversion project

It is expected that the converted phantoms would lead to the same, or very similar, dose coefficients as the ICRP 110 reference phantoms for penetrating radiation and, at the same time, provide more accurate dose coefficients for weakly penetrating radiation and small tissues. In addition, the reference phantoms in polygon mesh format would be easily deformable and could serve as a starting point to create phantoms of various postures to be used, for example, in accidental dose calculations.

REFERENCE

[1] M. Cristy, *Mathematical phantoms representing children of various ages for use in estimates of internal dose*, ORNL Report TM-367, Oak Ridge National Laboratory, 1980.

[2] M. Cristy and K. F. Eckerman, *Specific absorbed fractions of energy at various ages from internal photon sources*, Part I: Methods, ORNL Report TM-8381/V1, Oak Ridge National Laboratory, 1987.

[3] H. L. Fisher and W. S. Snyder, *Distribution of dose in the body from a source of gamma rays distributed uniformly in an organ,* ORNL-4168, Oak Ridge National Laboratory, 1967.

[4] H. L. Fisher and W. S. Snyder, "Distribution of dose in the body from a source of gamma rays distributed uniformly in an organ," Proceedings of First International Congress on Radiation Protection, 1968, pp. 1473- 1486.

[5] W. S. Snyder, M. R. Ford and G. G. Warner, *Estimates of specific absorbed fractions for monoenergetic photon sources uniformly distributed in various organs of a heterogeneous phantom*, MIRD Pamphlet 5, Revised, Society of Nuclear Medicine, 1978.

[6] W. S. Snyder, M. R. Ford, G. G. Warner and H. L. Fisher, *Estimates of absorbed fractions for monoenergetic photon sources uniformly distributed in various organs of a heterogeneous phantom. Medical Internal Radiation Dose Committee (MIRD).* Pamphlet No. 5, Society of Nuclear Medicine, 1969.

[7] ICRP, Reference man: *Anatomical, physiological and metabolic characteristics,* ICRP Publication 23, Pergamon Press, 1975.

[8] J. Becker, M. Zankl, U. Fill and C. Hoeschen, "Katja — the 24th week of virtual pregnancy for dosimetric calculations," *Pol J Med Phys Eng.*, vol. 14, pp. 13-19, 2008.

[9] M. Caon, "Voxel-based computational models of real human anatomy: a review," *Radiat. Environ. Biophys.*, vol. 42, pp. 229-235, 2004.

[10] M. Caon, G. Bibbo and J. Pattison, "An EGS4-ready tomographic computational model of a forteen year-old female torso for calculating organ doses from CT examinations," *Phys. Med. Biol.*, vol. 44, pp. 2213-2225, 1999.

[11] P. Dimbylow, "Development of the female voxel phantom, NAOMI, and its application to calculations of induced current densities and electric fields from applied low frequency magnetic and electric fields," *Phys. Med. Biol.*, vol. 50, pp. 1047-1070, 2005.

[12] P. J. Dimbylow, "The development of realistic voxel phantoms for electromagnetic field dosimetry," Proceedings of Workshop on Voxel Phantom Development, 1996, pp. 1-7.

[13] U. Fill, M. Zankl, N. Petoussi-Henss, M. Siebert and D. Regulla, "Adult female voxel models of different stature and photon conversion coefficients for radiation protection," *Health Phys.*, vol. 86, pp. 253- 272, 2004.

[14] R. Kramer, H. J. Khoury, J. W. Vieira and V. J. M. Lima, "MAX06 and FAX06: update of two adult human phantoms for radiation protection dosimetry," *Phys. Med. Biol.*, vol. 51, pp. 3331-3346, 2006.

[15] R. Kramer, *et al.*, "All about FAX: a female adult voxel phantom for Monte Carlo calculations in radiation protection dosimetry," *Phys. Med. Biol.*, vol. 49, pp. 5203-5216, 2004.

[16] R. Kramer, J. W. Vieira, H. J. Khoury, F. R. A. Lima and D. Fuelle, "All about MAX: a male adult voxel phantom for Monte Carlo calculations in radiation protection dosimetry," *Phys. Med. Biol.*, vol. 48, pp. 1239-1262, 2003.

[17] N. Petoussi-Henss, M. Zankl, U. Fill and D. Regulla, "The GSF family of voxel phantoms," *Phys. Med. Biol.*, vol. 47, pp. 89-106, 2002.

[18] X. G. Xu, T. C. Chao and A. Bozkurt, "VIP-MAN: An image-based whole-body adult male model constructed from color photographs of the Visible Human Project for multi-particle Monte Carlo calculations," *Health Phys.*, vol. 78, pp. 476-486, 2000.

[19] H. Zaidi and X. G. Xu, "Computational anthropomorphic models of the human anatomy: The path to realistic Monte Carlo modeling in radiological sciences," *Annual Review of Biomedical Egineering*, vol. 9, pp. 471-500, 2007.

[20] M. Zankl, *et al.*, "The construction of computer tomographic phantoms and their application in radiology and radiation protection," *Radiat. Environ. Biophys.*, vol. 27, pp. 153-164, 1988.

[21] M. Zankl and A. Wittmann, "The adult male voxel model "Golem" segmented from whole body CT patient data," *Radiat. Environ. Biophys.*, vol. 40, pp. 153-162, 2001.

[22] T. C. Chao, A. Bozkurt and X. G. Xu, "Conversion coefficients based on the VIP-Man anatomical model and EGS4-VLSI code for external monoenergetic photons from 10 keV to 10 MeV," *Health Phys.*, vol. 81, pp. 163-183, 2001.

[23] D. G. Jones, "A realistic anthropomorphic phantom for calculating organ doses arising from external photon irradiation," *Radiat. Prot. Dosim.*, vol. 72, pp. 21-29, 1997.

[24] S. Kinase, *et al.*, "Evaluation of specific absorbed fractions in voxel phantoms using Monte Carlo simulation," *Radiat. Prot. Dosim.*, vol. 105, pp. 557-563, 2003.

[25] R. Kramer, H. J. Khoury and J. W. Vieira, "Comparison between effective doses for voxel-based and stylized exposure models from photon and electron irradiation," *Phys. Med. Biol.*, vol. 50, pp. 5105-5126, 2005.

[26] R. Kramer, J. W. Vieira, H. J. Khoury and F. de Andrade Lima, "MAX meets ADAM: a dosimetric comparison between a voxel-based and a mathematical model for external exposure to photons," *Phys. Med. Biol.*, vol. 49, pp. 887-910, 2004.

[27] T. Smith, N. Petoussi-Henss and M. Zankl, "Comparison of internal radiation doses estimated by MIRD and voxel techniques for a 'family' of phantoms," *Eur. J. Nucl. Med.*, vol. 27, pp. 1387-1398, 2000.

[28] M. Zankl, U. Fill, N. Petoussi-Henss and D. Regulla, "Organ dose conversion coefficients for external photon irradiation of male and female voxel models," *Phys. Med. Biol.*, vol. 47, pp. 2367-2385, 2002.

[29] M. Zankl, N. Petoussi-Henss, U. Fill and D. Regulla, "The application of voxel phantoms to the internal dosimetry of radionuclides," *Radiat. Prot. Dosim.*, vol. 105, pp. 539-548, 2003.

[30] ICRP, *Basic anatomical and physiological data for use in radiological protection: reference values*, ICRP Publication 89, Pergamon Press, 2002.

[31] ICRP, *Adult reference computational phantoms*, ICRP Publication 110, International Commission on Radiological Protection, 2009.

[32] ICRP, *The 2007 Recommendations of the International Commission on Radiological Protection*, ICRP Publication 103, Elsevier, 2007.

Development of Skeleton Model for Polygon-mesh Version of ICRP Reference Phantoms

Zhao Jun Wang[1], Yeon Soo Yeom[1], Thang Tat Nguyen[1], Han Sung Kim[1], Min Cheol Han[1], Chan Hyeong Kim[1,*], Jai Ki Lee[1], Maria Zankl[2], Nina Petoussi-Henss[2], Wesley E. Bolch[3], Choonsik Lee[4], and Beom Sun Chung[5]

[1]Department of Nuclear Engineering, Hanyang University, Seoul, Korea
[2]Research Unit Medical Radiation Physics and Diagnostics, Helmholtz Zentrum München Deutsches Forschungszentrum für Gesundheit und Umwelt (GmbH), Neuherberg, Germany
[3]J. Crayton Pruitt Family Department of Biomedical Engineering, University of Florida, Gainesville, Florida, USA
[4]Division of Cancer Epidemiology & Genetics, National Cancer Institute, Bethesda, Maryland, USA
[5]Department of Anatomy, Ajou University School of Medicine, Suwon, Korea

*Corresponding author: chkim@hanyang.ac.kr

Abstract **-** The ICRP reference adult phantoms described in ICRP Publication 110 are voxel phantoms based on whole-body computed tomography scans of adult male and female patients. The voxel resolutions are on the order of a few mm; therefore, smaller tissues such as the eye lens, skin or the walls of some organs could not be defined in the phantom. In order to address the limitations of the ICRP-110 phantoms, ICRP Committee 2 recently initiated a research project to convert the current ICRP-110 voxel phantoms into a polygon-mesh (PM) format. As a part of the conversion project, the present study developed the skeleton model. In this development, most of bones were constructed by directly converting the voxel models into PM format, whereas some complex bones (spine, hands, and feet) were constructed by adjusting existing high-quality bone models to the ICRP-110 voxel models. In addition, the conversion project has also addressed several problems in the current skeleton model of the ICRP-110 phantoms. The conversion work was evaluated by comparing photon dose (coefficient) values of the red bone marrow (RBM) and endosteum with those of the ICRP-110 phantoms. The comparison results show good agreement; dose discrepancies were less than 6% for all calculation cases except for the 0.03 MeV cases, for which the difference is 18% at the maximum.

Index Terms **-** ICRP reference phantoms, polygon-mesh phantom, skeleton, conversion

I. INTRODUCTION

The voxel resolutions of the current ICRP reference adult phantoms in ICRP Publication 110 [1] are on the order of several mm and thus those phantoms have certain limitations in dose calculations. For example, ICRP Publication 116 [2] reported that the breast doses resulting from isotropic- geometry (ISO) proton beam irradiations-a highly improbable scenario-are significantly overestimated owing to the fact that the phantoms are not uniformly covered by skin. In addition, micron-thick target tissues are not defined in the respiratory and alimentary tract regions of the phantom; thus, several stylized models are separately used instead.

To avoid limitations of the ICRP reference phantoms, ICRP Committee 2 recently initiated a research project to convert the voxel-type ICRP reference phantoms into a polygon-mesh (PM) format. The ultimate goal of the conversion project is to reproduce the ICRP reference phantoms in high-quality PM format, preserving anatomical structures and at the same time including all the source and target regions for consistent ICRP dose calculations.

As a part of the conversion project, the present study developed the skeleton model, a very complex framework of the body, while addressing some limitations of the skeleton of the ICRP reference voxel phantoms. Then, photon dose values for RBM and bone surface (endosteum) were calculated and compared with those of the current ICRP reference voxel phantoms to see how the skeleton conversion work influences dose assessment.

II. METHODS

In the present study, most bones were constructed by directly converting voxel models to a high-quality PM format. For this, the primitive polygonal models were constructed by using 3D rendering methods. Then, the primitive polygonal models were refined to produce a high quality model via several refinement procedures using the *Rapidform* software (INUS Technology Inc., Korea), which provides powerful refinement tools for polygonal models. On the other hand, it was difficult to convert some complex bones (spine, hands, and feet) to high-quality PM models. In this case, therefore, other existing high-quality bone models were employed and carefully adjusted to the voxel models, minimizing the difference of the centroids and maximizing the volume overlap fraction to preserve the original bone shape as much as possible.

During the skeleton conversion, two limitations of the skeleton in the ICRP reference voxel phantoms were identified and addressed. First, it is anatomically incorrect that the non-segmented part of cartilage is included in spongiosa. Therefore, the cartilage has been extracted from the spongiosa, by recalculating the mass and elemental composition of spongiosa for the PM version of the ICRP reference phantoms. After the extraction of the cartilage, the costal cartilage and intervertebral discs were modelled following the methodology used for the UFH-NURBS pediatric phantoms [3] which were recently adopted as ICRP reference pediatric phantoms. The non-modelled part of cartilage will be included in residual soft tissue (RST) in the future.

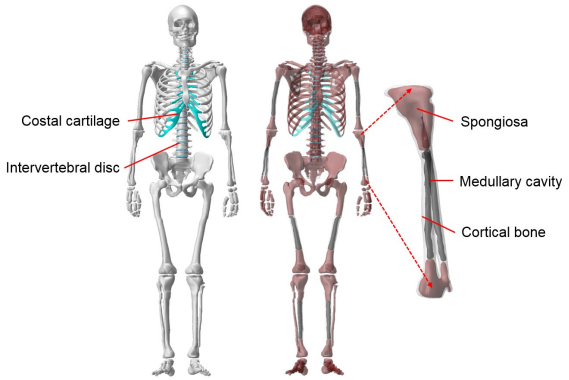

Figure 1. Skeleton model developed in the present study

Second, the sacrum bones are anatomically incorrect in ICRP reference voxel phantoms in the sense that the sacrum does not include cortical bone in the female phantom [1]. For the correction, the present study assigned the cortical bone mass for the female sacrum following the cortical bone mass fraction of the male sacrum, while reducing the cortical bone mass of the female tibiae to maintain the total cortical bone mass. For the male phantom, the dorsal sacral foramina are absent; thus, the foramina were modeled in the present study.

To evaluate the conversion work, the present study calculated the skeletal-averaged photon absorbed dose for the RBM and endosteum and compared the values with those of ICRP reference voxel phantoms. For simulation, the phantoms were irradiated with photon beams of 0.03-10 MeV in the AP, PA, LLAT, and RLAT directions.

III. RESULTS AND DISCUSSION

The present study developed skeleton models for use in the PM version of the ICRP reference phantoms. Figure 1 shows the male skeleton model as an example. The skeleton system consists of 17 bones and 2 cartilages. Each bone was segmented into cortical bone, spongiosa, and medullary cavity regions. The spongiosa and medullary cavity were fully enclosed by cortical bone in the developed models.

Figure 2 shows the dose differences between PM and voxel models for the RBM and endosteum. It can be seen that dose values for the PM models are generally in good agreement with those of the voxel models; dose differences were less than 6% for all calculation cases except for 0.03 MeV, for which the maximum difference was 18%.

IV. CONCLUSION

As a part of the ICRP-110 phantom conversion project, the present study developed skeleton models for use in the PM version of the ICRP reference phantoms. The developed skeleton models maintain the original skeletal structure of the ICRP reference voxel phantoms, providing very similar dose values for external photon exposures.

ACKNOWLEDGMENT

This project was supported by NSSC through KORSAFe and also by Ministry of Science, ICT and Future Planning through the NRF of Korea (Project No.: 2011-0025496, 2012-K001146, 1403012). Two of the authors were supported by the Global PhD Fellowship program (Project No.: 2011-0007318, 2011-0030970).

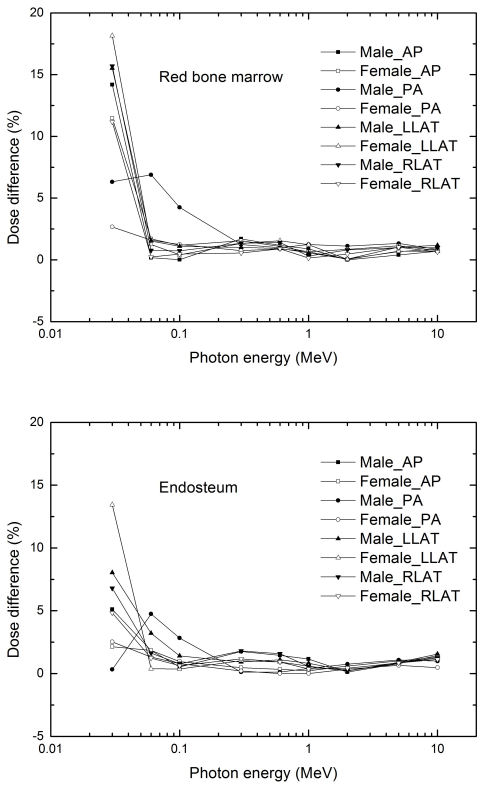

Figure 2. Dose differences (PM vs. voxel) for RBM (upper) and endosteum (lower)

REFERENCES

[1] ICRP, 2009. Adult Reference Computational Phantoms. ICRP Publication 110. Ann. ICRP 39 (2).

[2] ICRP, 2010. "Conversion Coefficients for Radiological Protection Quantities for External Radiation Exposures". ICRP Publication 116.

[3] C. Lee *et al.* "The UF family of reference hybrid phantoms for computational radiation dosimetry", *Phy. Med. Biol.*, 55, 339-363, 2010.

Modeling Target Regions of Alimentary Tract in Polygon-mesh Version of ICRP Reference Phantoms

Han Sung Kim[1], Yeon Soo Yeom[1], Thang Tat Nguyen[1], Zhao Jun Wang[1], Min Cheol Han[1], Chan Hyeong Kim[1,*], Jai Ki Lee[1], Maria Zankl[2], Nina Petoussi-Henss[2], Wesley E. Bolch[3], Choonsik Lee[4], and Beom Sun Chung[5]

[1]Department of Nuclear Engineering, Hanyang University, Seoul, Korea
[2]Research Unit Medical Radiation Physics and Diagnostics, Helmholtz Zentrum München Deutsches Forschungszentrum für Gesundheit und Umwelt (GmbH), Neuherberg, Germany
[3]J. Crayton Pruitt Family Department of Biomedical Engineering, University of Florida, Gainesville, Florida, USA
[4]Division of Cancer Epidemiology & Genetics, National Cancer Institute, Bethesda, Maryland, USA
[5]Department of Anatomy, Ajou University School of Medicine, Suwon, Korea

*Corresponding author: chkim@hanyang.ac.kr

Abstract **-** Recently, the ICRP Committee 2 initiated a research project to convert the voxel-type ICRP-110 reference phantoms into high-quality polygon-mesh (PM) format. As a part of the conversion project, the present study defined the target and source regions in the alimentary tract regions of the PM version of the ICRP reference male phantom, to be used for calculations of Specific Absorbed Fractions (SAF) of charged particles. The electron SAF values were calculated and compared with those of the ICRP-100 stylized models. The present study shows that it is possible to calculate charged particle SAF values for the alimentary tract regions using the PM version of the ICRP reference phantoms without using any additional supplementary models. The new models provided very similar dose values to those of the ICRP-100 stylized models.

Index Terms **-** ICRP reference phantoms, polygon-mesh, alimentary tract, specific absorbed fractions (SAF)

I. INTRODUCTION

The ICRP-110 reference phantoms [1], which are voxel phantoms with voxel resolution of a few mm, have limitations in dose calculations for weakly-penetrative radiations and very small tissues. For example, the ICRP-110 phantoms cannot define micron-thick target tissues of the respiratory and alimentary tract regions which are necessary for charged particle dosimetry and separate stylized models have been alternatively used.

Recently, the ICRP Committee 2 initiated a research project to develop an exact replica of the ICRP-110 phantoms in high-quality polygon-mesh (PM) format, including all source and target regions of the phantoms. As a part of this research project, the present study defined the target and source regions of the alimentary tract regions of the PM version of ICRP reference male phantom for charged particle SAF calculation. Furthermore, electron SAF values were calculated and compared with those of the ICRP-100 stylized models.

II. METHODS

Following the detailed morphometric data given in ICRP Publication 100 [2], the target and source regions of the alimentary tract regions of the PM version of ICRP male phantom were defined. For most of the alimentary tract organs (oesophagus, stomach, small intestine, and colon), target and source regions were defined using the *offset* function of the *Rapidform* software (INUS Technology Inc., Korea). The target and source regions of the oral cavity are complicated and they were defined by using several functions (*offset, divide,* and *thicken*).

The values of the source volumes are different between the ICRP Publication 89, based on which the PM version of the ICRP phantoms are being developed, and the ICRP-100 stylized models, resulting in significant deviations of the calculated SAF values for charged particles from those of the ICRP-100 stylized models. These deviations could be decreased by adjusting the PM-defined source volumes to those of the ICRP-100 stylized models; however, this unnatural adjustment of the source volumes would significantly change the overall shapes of the alimentary tract regions of the PM version of the ICRP phantoms, resulting in significant discrepancies of the external dose coefficients with the ICRP-110 phantoms, which is unacceptable. Instead, it was decided to use a simple correction factor, called volume correction factor (VCF), which is simply defined as the ratio of the source volumes in the PM version of the ICRP phantoms and the ICRP-100 stylized models. The deviation problem was addressed by multiplying the correction factor to the calculated SAF value from the PM version of ICRP phantoms. This approach makes it possible to use the PM version of the ICRP reference phantoms for both internal and external dose coefficient calculations.

For the present study, calculations of electron SAF values for the alimentary tract regions were performed using the Geant4 code and the PM version of the ICRP male phantom. To improve computation speed, the PM phantom was converted into the tetrahedral-mesh format [3] and then, the tetrahedralized phantom was implemented in the Geant4 code for Monte Carlo simulations. Primary electrons (0.15-4 MeV) were uniformly generated for the source regions in the phantom by using a sampling method based on the barycentric coordinate system [4]. The *G4EmLivermorePhysics* model was used with 1 μm cut value. The relative errors of all the calculated values were less than 10%.

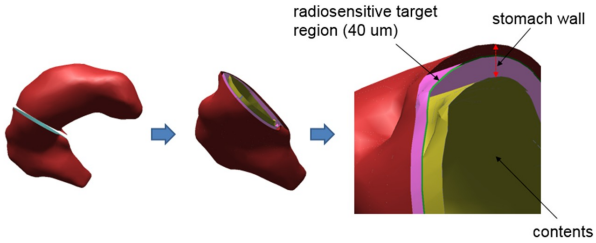

Figure 1. Stomach of the polygon-mesh version of the ICRP male phantom including radiosensitive target region.

III. RESULTS AND DISCUSSION

In the present study, all the target and source regions of the alimentary tract were defined in the PM version of the ICRP male phantom under development. As an example, Figure 1 shows the micron-thick target regions of the stomach.

The electron SAF values, calculated for the PM version of the ICRP male phantom and the ICRP-100 stylized model were compared [2]. Figure 2 shows the electron SAF values for stomach content as source and for stomach as target. It can be seen that there is a good agreement for all energies considered; the maximum difference was found to be 10% at 4 MeV. Figure 3 compares the electron SAF values to the small intestine, for content and villi sources. For the villi as a source, there is also good agreement; the maximum difference was only 8% at 4 MeV. For the content source, however, the maximum difference was observed to be 36% at 4 MeV, but the discrepancies were less than 12% for energies less than 2 MeV. The SAF values for the other tubular-shaped organs showed similar trends as for the small intestine.

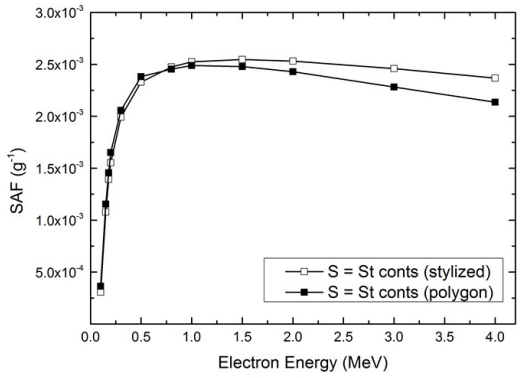

Figure 2. Electron specific absorbed fraction (SAF) to stomach for stomach content as a source.

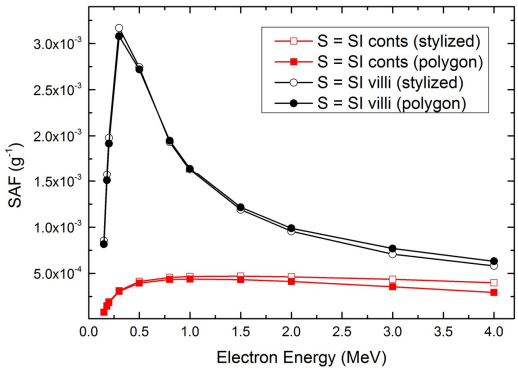

Figure 3. Electron specific absorbed fraction (SAF) to the small intestine for content (square) and villi (circle) as sources.

IV. CONCLUSION

As a part of the ICRP-110 phantom conversion project, the present study defined the target and source regions of the alimentary tract, as part of the PM version of the ICRP male phantom which is currently under development. The present study shows that it is possible to calculate charged particle SAF values for the alimentary tract regions using the PM version of the ICRP reference phantoms without using any additional supplementary models. Based on the present study, the target and source regions in alimentary tract regions will also be defined in the female phantom.

ACKNOWLEDGMENT

This project was supported by NSSC through KORSAFe and also by Ministry of Science, ICT and Future Planning through the NRF of Korea (Project No.: 2011-0025496, 2012-K001146, 1403012). Two of the authors were supported by the Global PhD Fellowship program (Project No.: 2011-0007318, 2011-0030970).

REFERENCES

[1] ICRP, 2009. Adult Reference Computational Phantoms. ICRP Publication 110. Ann. ICRP 39 (2).
[2] ICRP, 2006. "Human Alimentray Tract Model", ICRP Publication 100. Ann. ICRP 36 (1-2).
[3] Y. S. Yeom, J. H. Jeong, M. C. Han, and C. H. Kim, "Tetrahedral- mesh-based computational human phantom for fast Monte Carlo dose calculations," *Phy. Med. Biol.*, vol 59, pp. 3173-3185, 2014.
[4] C. Rocchini and P. Cignoni, "Generating Random Points in a Tetrahedron," *J. Graph. Tools*, vol. 5, pp. 9-12, 2001.

Incorporation of Detailed Eye Model into Polygon-mesh Version of ICRP Reference Phantoms for Lens Dose Assessment

Thang Tat Nguyen[1], Yeon Soo Yeom[1], Han Sung Kim[1], Zhao Jun Wang[1], Min Cheol Han[1], Chan Hyeong Kim[1,*], Jai Ki Lee[1], Maria Zankl[2], Nina Petoussi-Henss[2], Wesley E. Bolch[3], Choonsik Lee[4], and Beom Sun Chung[5]

[1]Department of Nuclear Engineering, Hanyang University, Seoul, Korea
[2]Research Unit Medical Radiation Physics and Diagnostics, Helmholtz Zentrum München Deutsches Forschungszentrum für Gesundheit und Umwelt (GmbH), Neuherberg, Germany
[3]J. Crayton Pruitt Family Department of Biomedical Engineering, University of Florida, Gainesville, Florida, USA
[4]Division of Cancer Epidemiology & Genetics, National Cancer Institute, Bethesda, Maryland, USA
[5]Department of Anatomy, Ajou University School of Medicine, Suwon, Korea

*Corresponding author: chkim@hanyang.ac.kr

Abstract **-** The recent reduction of dose limit for eye lens makes lens dose assessment more important. The ICRP adopted a detailed stylized eye model to avoid the limitation of the ICRP-110 reference phantoms in which the detailed structure of the eyes cannot be modeled due to the low voxel resolutions. The ICRP used for the calculations of external idealized exposures (ICRP Publication 116) both a stylized model and the voxel model of the eye as in the phantom, depending on types of radiations, energies, and irradiation geometries. In the present study, we incorporated the ICRP-116 detailed eye model into the polygon-mesh version of the ICRP reference phantoms, which were converted from the ICRP-110 reference phantoms. After the incorporation, the lens doses coefficients were calculated and then compared with those of the ICRP-116 data.

Index Terms **-** ICRP reference phantom, polygon-mesh model, eye lens, dose coefficients

I. INTRODUCTION

The reduction of the occupational annual equivalent dose limit for the eye lens from 150 mSv to 20 mSv recommended by ICRP Publication 118 [1] makes the assessment of lens doses more important. The ICRP-110 reference phantoms [2] due to their voxel resolution of the order of mm, cannot describe the detailed structure of the eyes; therefore, the ICRP used for defining the reference dose coefficients for external radiation (Publication 116 [3]), and for some types of exposure a detailed stylized eye model [4] for lens dose assessment.

In order to keep consistency in the lens dose assessment, in the present study, we incorporated the ICRP-116 detailed eye model into the polygon-mesh (PM) version of the ICRP reference phantoms [5], which were converted from the ICRP-110 reference phantoms [3]. After the incorporation, the lens dose coefficients were calculated by using the PM version of the ICRP reference phantoms and compared with those of the ICRP-116 reference data.

II. METHODS

Firstly the ICRP-116 detailed eye model was generated in a PM format. For this purpose, a NURBS-surface-based eye model was produced by using the *Sphere, Corn,* and *Boolean* functions in the *Rhinoceros* software (Robert McNeel & Associates, Seattle, Wash). This NURBS-surface model was then converted to the PM model by using the *Mesh* function in the same software.

The PM eye model was then placed in the PM version of the ICRP reference phantoms. During the placement, for the male phantom, the centroids of the eye models, except for the eyelids, were matched to those of the eyes of the ICRP reference phantom. On the other hand, for the female phantom, the centroids of the eye models in the PM phantom were about 3 mm lower, which was necessary to avoid interference with the cranium. The eyelid in the eye model was adjusted to be a part of the skin using the *Deform* function in the *Rapidform* software (INUS Technology Inc., Korea).

After incorporation, the PM version of the ICRP reference phantoms were implemented into the Geant4 Monte Carlo code (ver. 10.01) to calculate lens dose coefficients for external exposures for photons and electrons. For precise simulation, the *G4EmLivermorePhysics* was used with 1 μm cut value. The relative errors of all the calculated values were less than 10%. The calculated coefficients were then compared with those of ICRP-116 reference data [3].

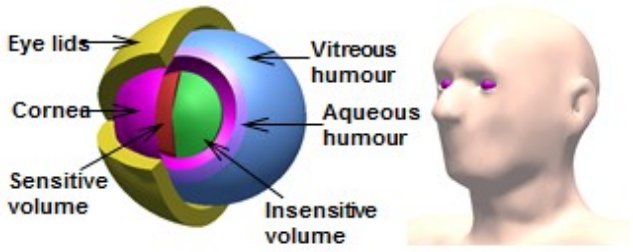

Figure 1. Polygon-mesh eye model (left) and head of polygon-mesh version of the ICRP reference male phantom including eye models (right).

III. RESULTS AND DISCUSSION

Figure 1 shows the PM detailed eye model constructed in the present study and the head of the PM version of the ICRP male phantom including the eye model. The masses of the sensitive and insensitive volumes of the lens are 38.9 and 189.3 mg, respectively which are very close to those of original stylized eye model (~1% difference).

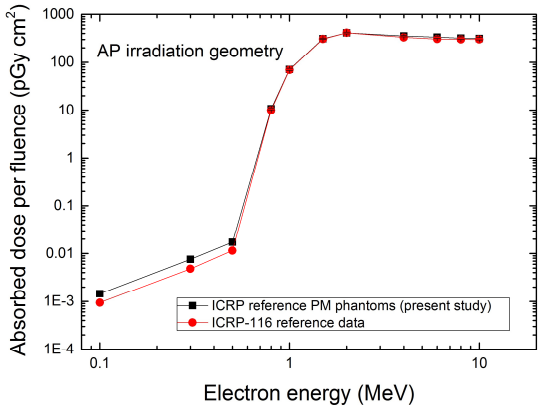

Figure 2. Comparison of dose coefficients calculated with polygon-mesh version of ICRP reference phantoms including detailed eye model and ICRP-116 data for electron beams in AP direction.

Figure 2 compares lens dose coefficients for broad parallel electrons beams in the AP direction. For electron energies (> 0.5 MeV), there was a good agreement between the values; the maximum difference was 12% at 6 MeV. For the low-energy region, however, the lens dose coefficients calculated with the PM version of the ICRP reference phantoms were significantly higher than those of the ICRP-116 data; the maximum difference was as large as 55% at 0.3 MeV. The significant differences are due mainly to the fact that the ICRP-116 data was calculated with the bare-eye model and therefore do not reflect the dose contribution of the secondary radiations from the head.

Figure 3 compares the lens dose coefficients for broad parallel photon beams in the AP, PA, and LAT directions. For the AP direction, there was a good agreement; the dose differences were less than 8% for all the calculation cases. On the other hand, for the PA direction, there were significant differences, i.e. higher than 20% for photon energies (≤ 0.1 MeV); the highest difference was a factor of 6 times at 30 keV. This significant difference is caused by the difference in size and composition of the head structure between the PM version of the ICRP phantoms and the mathematical phantom used to calculate the ICRP-116 data. The difference in the head models also makes slight dose discrepancies in the LAT direction; the maximum difference was 20% for 0.05 MeV.

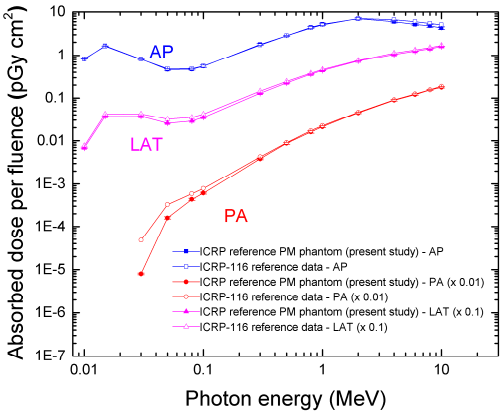

Figure 3. Comparison of dose coefficients calculated with polygon- mesh version of ICRP reference phantoms including detailed eye model and ICRP-116 data for photon beams in AP, PA, and LAT directions.

IV. CONCLUSION

In the present study the ICRP-116 detailed eye model was incorporated into the PM version of the ICRP reference phantoms. Then, the developed models were used to calculate the dose coefficients for the eye lenses and the calculated values were compared with those of the ICRP-116 data. The results of the present study show that there is significant difference of dose coefficients, and we believe that the current approach provides more consistent dose values for the eye lenses.

ACKNOWLEDGMENT

This project was supported by NSSC through KORSAFe and also by Ministry of Science, ICT and Future Planning through the NRF of Korea (Project No.: 2011-0025496, 2012-K001146, 1403012). Two of the authors were supported by the Global PhD Fellowship program (Project No.: 2011-0007318, 2011-0030970).

REFERENCES

[1] ICRP, 2012. ICRP statement on tissue reactions and early and late effects of radiation in normal tissues and organs: threshold doses for tissue reactions in a radiation protection context. ICRP Publication 118. Ann. ICRP 41 (1–3).
[2] ICRP, 2009. Adult Reference Computational Phantoms. ICRP Publication 110. Ann. ICRP 39 (2).
[3] ICRP, 2010. "Conversion coefficients for Radiological Protection Quantities for External Radiation Exposures", ICRP, Publication 116, Ann. ICRP 40 (2-5), Elsevier.
[4] Behrens, R., Dietze, G., Zankl, M., 2009. Dose conversion coefficients for electron exposure of the human eye lens. Phys. Med. Biol. 54(13), 4069-4087.
[5] Y. S. Yeom, M. C. Han, C. H. Kim and J. H. Jeong, "Conversion of ICRP male reference phantom to polygon-surface phantom," *Physics in Medicine and Biology*, vol. 58, pp. 6985-7007, 2013.

CAD-and Image-based Monte Carlo Radiation Modeling Techniques and Its Application in Rad-HUMAN

Yican Wu, Mengyun Cheng, Wen Wang, Ting Li, Jing Song, Lijuan Hao, Shengpeng Yu, Tao He, Shaoheng Zhou, Pengcheng Long, Liqin Hu, FDS Team

Key Laboratory of Neutronics and Radiation Safety, Institute of Nuclear Energy Safety Technology, Chinese Academy of Sciences, Hefei, China

*Corresponding author: yican.wu@fds.org.cn

Index Terms - Rad-HUMAN, SuperMC, radiation protection, nuclear medicine

I. INTRODUCTION

To assess the effects of the ionizing radiation and risk of the radiation exposure by using Monte Carlo (MC) simulations with the computational phantom was one of the most important research fields of the radiation shielding and medical physics [1]. Radiation dosimetry aims to determine the amount and distribution pattern of energy deposited in various organs of the human body by radiation sources. The accuracy of assessment strongly depends on the adopted modeling approach include Monte Carlo codes and computational phantom [2].

This contribution gives an overview of a systematic research of FDS Team on the CAD-based Monte Carlo modeling and transport simulation technique. Based on the above techniques, FDS Team has developed the Super Monte Carlo Simulation Program for Nuclear and Radiation Process (SuperMC) and constructed the Chinese Adult Female Phantom Rad-HUMAN.

II. METHODS

A. CAD-based Fast Monte Carlo Particle Transport Technique

CAD-based fast Monte Carlo n, γ, p and e transport simulation technique were developed; in order to improve the calculation speed, transport simulation acceleration algorithm were innovative developed, including source convergence of preliminary sample and adaptive weight window smoothing variance reduction, and the computing speed were largely improved.

B. CAD- and Image-based Monte Carlo Human Modeling Technique

CAD- and image-based Monte Carlo modeling technique were developed, and a coupled modeling method of linac treatment head, MLC and patient phantom was also developed based on the hierarchical geometry method.

C. Visualized Analytics and Real-time Organ Dose Assessment Technique

Several specialized visualization techniques were developed, such as visual analytics workflow for radiation shielding; data field cutting based on geometry model and coupled visualization of 3D time varying data map. And based on the parallel technique, developed the real-time organ dose assessment method.

III. THE SUPERMC PROGRAM

Based on the above techniques, the Super Monte Carlo Simulation Program for Nuclear and Radiation Process (SuperMC) has been developed by FDS Team. SuperMC is a general purpose, intelligent and multi-functional program for the design and safety analysis of nuclear systems. The latest version of SuperMC can accomplish the transport calculation of n, γ, p, e and can be applied for criticality and shielding design of reactors, medical physics analysis, etc. [3-4].

The automatic modeling module of SuperMC can achieve automatic conversion from CT/segmented sectioned images to computational phantoms, the automatic and accurate modeling of the whole process of radiotherapy, as well as bi-directional automatic conversion between CAD models and MC models (SuperMC, MCNP, TRIPOLI, Geant4, FLUKA models) [5].

The visualization module of SuperMC can directly process the output files of multiple codes (SuperMC, MCNP, etc.), and virtual maintenance simulation along with real-time organic dose evaluation in radiation environment, as low as reasonably achievable (ALARA) evaluation of work scenarios in radiation environment including shut-down maintenance and nuclear accident.

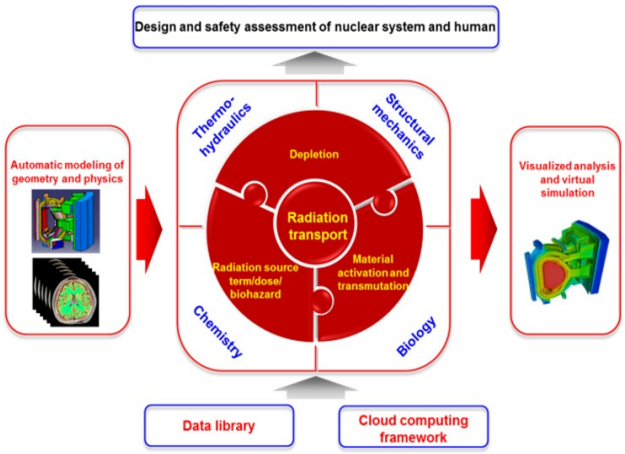

Figure 1. Framework of SuperMC

IV. MODELING AND APPLICATION

A. Construction the Chinese Adult Female Phantom Rad-HUMAN

Following manual segmentation and 3D reconstruction, the Rad-HUMAN's internal and external models with various precision, which contains 46 organs and tissues, were created by using SuperMC program from sectioned images of the Chinese Visible Human (CVH) dataset.

A set of complete conversion coefficients and the effective dose of Chinese female for external and internal monoenergetic photon and neutron beams have been simulated based on Rad-HUMAN [6-7]. Rad-HUMAN is a precise computational phantom of Chinese adult female whose detailed information can be used to improve the Chinese female radiological datasets.

Rad-HUMAN has been chosen as the dose assessment phantom of SuperMC. Based on the Rad-HUMAN voxel model, SuperMC can realize accurate evaluation of organic dose rates instead of considering the worker as a point, which is mainly employed by other nuclear and radiation virtual simulation systems.

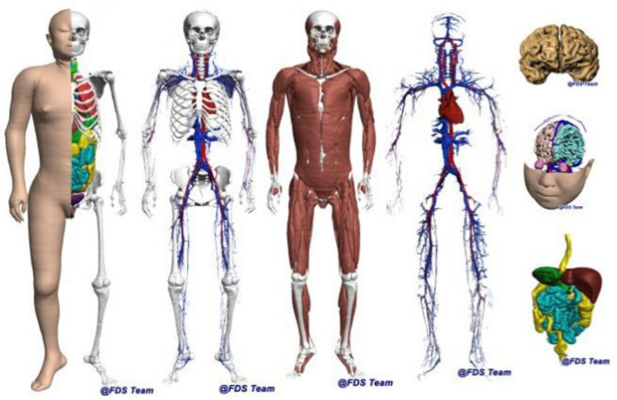

Figure 2. 3D view of Rad-HUMAN

B. Application in Radiation Protection

Based on the Rad-HUMAN voxel models and the dose conversion coefficients, the Accelerator Driven Sub-critical System (ADS) spallation target replacement simulation was performed by SuperMC. According to the ADS spallation target replacement task design, the maintenance worker's absorbed dose was assessed. The simulation and preliminary assessment of the replacement maintenance program can get the following conclusions: in the maintenance work, the maximum effective dose rate is 0.69 μSv/h, under the dose limit design 100 μ Sv/h. Repair process cumulative dose is 0.27 mSv, which doesn't exceed the 20 mSv/year limit. The result showed that the SuperMC could real-timely and accurately assess radiation dose based on Rad-HUMAN model.

C. Application in Nuclear Medicine

Rad-HUMAN can be used in nuclear medicine, such as the radionuclide imaging and radioactive seed implantation in brachytherapy for tumor. Based on the Rad-HUMAN internal dosimetry data, we can evaluate the absorbed dose of organs which using ^{99m}Tc injected into the liver. The result can be used as reference for radiation assessment of nuclear medicine, such as dose verification after surgery and potential radiation evaluation for radionuclides in preclinical research.

IV. CONCLUSION

Super Monte Carlo Simulation Program for Nuclear and Radiation Process (SuperMC) can accomplish the transport calculation of n, γ, p, e and can be applied for criticality and shielding design of reactors, medical physics analysis, etc. A set of complete conversion coefficients and the effective dose of Chinese female for external and internal monoenergetic photon and neutron beams have achieved based on Rad-HUMAN. SuperMC program and Rad-HUMAN phantom have been applied to predict and evaluate dose distributions in the radiation protection, nuclear medicine and radiation therapy.

ACKNOWLEDGMENT

This work was supported by the Strategic Priority Research Program of Chinese Academy of Sciences (No. XDA03040000), the National Special Program for ITER (No. 2014GB1120001).

REFERENCES

[1] Xu X and Eckerman KF, "Handbook of anatomical Models for radiation dosimetry," *Taylor & Francis, 1st Ed.,* September 1, 2009.

[2] Y. Wu and X. Xu, "The need for further development of CAD/MCNP interface codes", *Invited presentation at the American Nuclear Society Annual Meeting, Transactions of American Nuclear Society*, 96: TRANSAO 961-882, ISSN: 0003-018X, June 24-28, Boston, Massachusetts, 2007.

[3] Wu Yican, Song Jing, Zheng Huaqing, *et al.*, "Development of super Monte Carlo calculation program SuperMC 2.0," *Annals of Fusion Energy*, doi:10.1016/j.anucene, 2014

[4] SONG Jing, SUN Guangyao, CHEN Zhenping, *et al.* "Benchmarking of CAD-based SuperMC with ITER benchmark model[J]," *Fusion Engineering and Design*, 89(11), 2499-2503, 2014.

[5] Y. Wu, FDS Team. "CAD-based Interface Programs for Fusion Neutron Transport Simulation," *Fusion Engineering and Design*, 84, 1987-1992, 2009.

[6] Kai Zhao, Mengyun Cheng, Pengcheng Long, *et al*, "Human organ geometry construction from segmented images," *Proceedings of the 2013 International Conference on Innovative Computing and Cloud Computing, ICC2013*, Wuhan.

[7] Wang Wen, Mengyun Cheng, Pengcheng Long, Liqin Hu, "Specific Absorbed Fractions of Electrons and Photons for Rad-HUMAN Phantom Using Monte Carlo Method," *Chinese Physics C*, 010201-1~7, 2015.

Real-time Radiation Dose Assessment Method Based on Voxel Phantom Using Parallel Technology

Ting Li, Tao He, Liqin Hu, FDS Team

Key Laboratory of Neutronics and Radiation Safety, Institute of Nuclear Energy Safety Technology, Chinese Academy of Sciences, Hefei, China

*Corresponding author: liqin.hu@fds.org.cn

Index Terms - dose assessment, voxel phantom, real-time, Rad-HUMAN

I. INTRODUCTION

With regard to ADS system, spallation target is a key component to connect the accelerator and subcritical reactors, spallation reactions producing neutrons for subcritical neutron source reactor to provide high-energy protons. Due to the high energy proton bombardment and intense neutron irradiation, while a large number of nuclear heat deposition also need to be cooled, and thus general life of the spallation target window is shorten. Spallation target window is designed to replace once a year and should be carried out by manual.

In order to ensure the smooth implementation and to protect the personal safety of worker, the intervention process is needed to be simulated for dose assessment. In this paper, we have studied radiation dose assessment based on voxel phantom during the spallation target replacement by using SuperMC/RVIS [1]. SuperMCN/RVIS is a Virtual reality-based Simulation System for Nuclear and Radiation Safety, developed by FDS Team [2]. Main capabilities of RVIS include: 1) CAD-based modeling and virtual assembly simulation of complex components; 2) visualized analysis of dynamical 3D radiation field coupled with geometry model; 3) virtual roaming simulation and organic dose assessment in radiation environment.

II. METHODS

This paper studies the maintenance simulation based on Rad-HUMAN model and RVIS. We present the application of VR technology in radiation dose assessment during the ADS spallation target replacement maintenance.

A. Voxel phantom: Rad-HUMAN

Rad-HUMAN (Figure 1) is created by FDS Team using sectioned images of a Chinese visible human dataset. The model took six months and more than 20 professionals to segment the organs on the sectioned images. The model contains about 28.8 billion voxels and 46 organs. FDS Team uses self-developed Multi-Physics Coupling Analysis Modeling Program (SuperMC/MCAM) [3-8], with full-fill mode using voxel model space, filled with more than 700 million of voxels, generating 3 mm × 3 mm × 3 mm of Rad-HUMAN's SuperMC input file. This file contains the repetitive structure of the voxel model space distribution and geometry description.

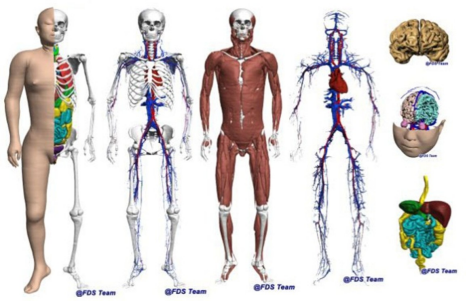

Figure 1. 3D view of Rad-HUMAN

Rad-HUMAN model has been used to calculate the radiation protection infrastructure dose data, in which the results of organ dose conversion factors fluxes with ICRP 116 publication [9] are in good agreement.

B. Real-time dose assessment based on voxel phantom

Dose calculation accuracy of voxel model lies in that absorbed doses of the human organs are calculated for each voxel, with the average absorbed dose treated as the organ dose.

$$D_T = \frac{1}{N}\sum_{j=1}^{N} D_{T,j} = \frac{1}{N}\sum_{j=1}^{N} \Phi_j * F \qquad (1)$$

D_T is the absorbed dose to tissue or organ is organ absorbed dose for the voxel *j* and Φ_j is the flux of the voxel *j*, *F* is dose conversion factor for the flux, *N* is for the amount of voxels organ. Figure 2 shows the flow of organ equivalent dose calculation.

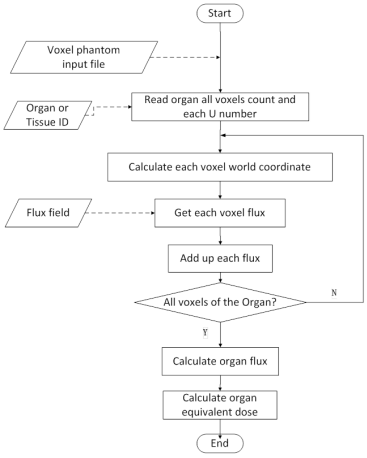

Figure 2. Flow chart of organ equivalent dose calculation

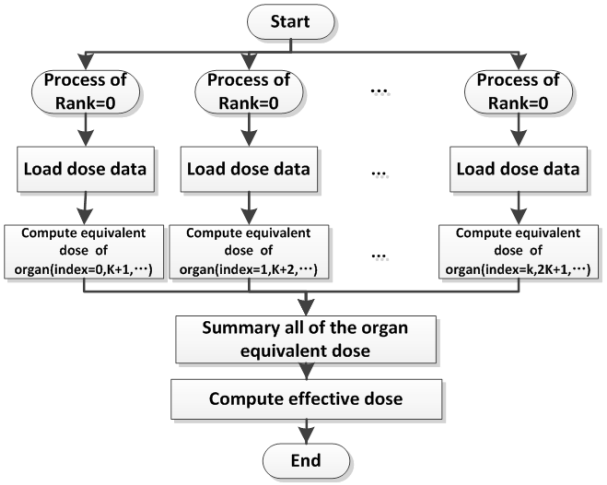

Figure 3. Flow chart of dose calculation with multi-core and GPU parallel technology

Due to the huge number of voxels, often in the millions, method based on multi-core and GPU parallel technology, is introduced to achieve real-time calculation of the dose. To achieve real-time dose calculation, all of the voxel model is divided into several groups, each group is computed by each core or thread. The method is applied to the voxel model of radiation dose calculation, in the organ of the voxel on the basis of the calculation of all the voxels consisting of organ doses to achieve the purpose of accurately calculating organ doses. Flow chart of dose calculation with multi-core and GPU parallel technology is showed in Figure 3.

III. SIMULATION AND RESULTS

According to the ADS spallation target replace task design, maintenance worker first walks into the radiation environment, then climbs the ladder to the target place to carry out the replace task (path and position shown in Figure 4), taking 310 man·h.

The simulation and preliminary assessment of the replacement maintenance program can get the following conclusions:

(1) In the maintenance work, the maximum effective dose rate is 0.69 μSv/hr, under the dose limit design 100 μSv/hr. Repair process cumulative dose is 0.27 mSv, which meets the relevant requirements (workers radiation dose does not exceed 20 mSv / year).

(2) Based on the human external dose assessment methods, the voxel model reflects the human anatomy more detail, the model more realistic, and elaborates much more precise radiation dose calculations.

(3) With the multi-core and GPU parallel technology, organ dose calculation was processed real-timely, the result showed that the proposed method could real-timely assess accurate radiation dose based on voxel model.

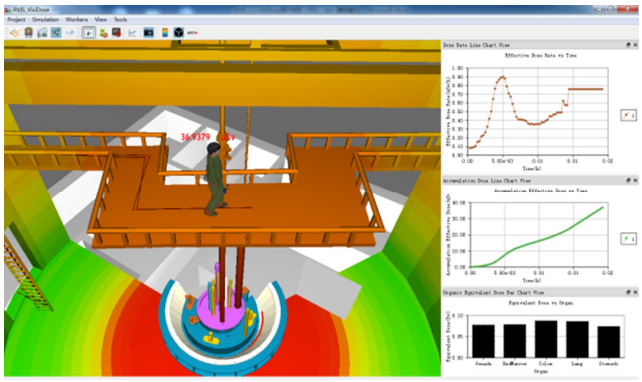

Figure 4. The spallation target replacement repair simulation with RVIS

ACKNOWLEDGMENT

This work was supported by the Strategic Priority Research Program of Chinese Academy of Sciences (Grant No. XDA03040000), the National Natural Science Foundation of China (Grant No. 91026004 and 11305205), the National Special Program for ITER (No. 2014GB1120001).

REFERENCES

[1] TANG Z, LONG P, HUANG S, *et al.*, "Real-time dose assessment and visualization of radiation field for EAST tokamak [J]," *Fusion Eng. Des.*, 85 (7–9): pp. 1591-1594, 2010.

[2] www.fds.org.cn [OL].

[3] Y. Wu, Y. Li, L. Lu, A. Ding, "Research and development of the automatic modeling system for Monte Carlo particle transport simulation," *Chinese J. Nucl. Sci. Eng.*, 26[1]. pp. 20-27, 2006.

[4] Y. Wu, FDS Team, "CAD-based interface programs for fusion neutron transport simulation," *Fusion Engineering and Design*, 84(7-11), pp.1987-1992, 2009.

[5] Y. Wu, J. Song, H. Zheng, *et al.*, "CAD-basd Monte Carlo program for integrated simulation of nuclear system SuperMC[J]," *Annals of Nuclear Energy*, In Press, doi:10.1016/j.anucene.2014.08.058, 2014.

[6] J. Song, G. Sun, H. Zheng *et al.*, "Benchmarking of CAD-based SuperMC with ITER Benchmark Model[J]," *Fusion Engineering and Design*, 89(11):2499-2503, 2014.

[7] CHENG M, HUANG S, LI J *et al.*, "Progress of HUMOP: Human Automatic Modeling Program [J]," *Transactions American Nuclear Society*, 104, 648-652, 2011.

[8] Wu Yican, Hu Liqin, Long Pengcheng *et al.*, "Development of design and analysis software for advanced nuclear sysytems [J]," *Chinese Journal of Nuclear Science and Engineering*, 30(1):55-64, 2010.

[9] Y. C. Wu, J. J. Li, Y. Li *et al.*, "An integrated multi-functional neutronics calculation and analysis code: VisualBUS [J]," *Chinese Jouranl of Nuclear Science and Engineering*, 27(4): 365-373, 2007.

Near Real-time GPU and MIC-based Monte Carlo Code ARCHER for Radiation Dose Calculations in Voxelized and Mesh Phantoms

Tianyu Liu[1], Noah Wolfe[2], Lin Su[1], Christopher D. Carothers[2], Bryan Bednarz[3], and X. George Xu[1,*]

[1]Nuclear Engineering Program, Rensselaer Polytechnic Institute Troy, New York, USA
[2]Computer Science Department, Rensselaer Polytechnic Institute Troy, New York, USA
[3]Departments of Medical Physics and Human Oncology, University of Wisconsin-School of Medicine and Public Health Madison, Wisconsin, USA

*Corresponding author: xug2@rpi.edu

Abstract - The ARCHER code being developed at RPI is a very fast Monte Carlo simulation code for radiation dose calculation. Currently it is capable of coupled photon-electron transport simulation and simplistic heavy ion simulation. It is designed and optimized for multiple computing devices, including the conventional CPU and the newly emerging GPU and MIC accelerators. In this paper we highlight some of our latest result.

Index Terms - GPU, Xeon Phi, MIC, triangular mesh phantom, parallel computing

I. INTRODUCTION

For decades the Monte Carlo (MC) simulation has been widely used as the gold standard in radiation dosimetry. The development of sophisticated, deformable human phantoms that contain accurate, detailed anatomical information enables MC simulation to provide very reliable dose estimate. The lengthy computation time can be effectively reduced by modern computing hardware. State-of-the-art Central Processing Units (CPUs) allow most of the present-day applications to scale well. Meanwhile, "accelerators" such as Nvidia's Graphics Processing Units (GPU) and Intel's Many Integrated Core (MIC) coprocessors (also known as Xeon Phi) implement very different architecture and currently do not offer binary compatibility. This has driven many interested developers, including us, to redesign their MC codes (to make it *work* on accelerators), and conduct low-level, architecture-specific optimization and tuning (to make it *work well*).

It remains unclear what specific computing architecture may become the mainstream in the future. Aware of this issue, we have been developing a suite of MC code called "ARCHER" (Accelerated Radiation-transport Computations in Heterogeneous EnviRonments) that is optimized for both the conventional CPU and the new GPU and MIC platforms. Our goal is to provide a heterogeneous computing solution to achieve maximum system usage and best single node performance for MC dose calculation.

II. METHODS

ARCHER consists of several functional units, including physics, geometry, random number generator, application- specific modules, etc. The physics unit currently contains a coupled photon-electron transport kernel and a simplistic heavy ion kernel. The photon part is developed from scratch while the electron part is a modified version of the Dose Planning Method (DPM) code. In the geometry unit, Woodcock delta tracking is currently adopted as the tracking method, and collision estimator as the tally method. The path-length based tracking and tally that is implemented in MCNP is still in development and testing. Two random number generators are supported, including the Xorshift and Linear Congruential Generator (LCG). Additionally, ARCHER has a set of high- level modules that share the above three central units but have their own unique components. These modules are designed for different applications, including CT dosimetry, tomotherapy dosimetry, radiation shielding design, etc. Each module has three versions to run on the CPU, GPU and MIC platforms respectively. To make a fair comparison, the CPU version of the code is multithreaded and optimized.

III. SIMULATIONS

A. Fast dose calculation in voxel phantoms

ARCHER supports radiation transport in voxel phantoms, either the one that is well defined up front, or the DICOM CT images that will be converted by ARCHER into an unsegmented phantom. These two cases are tested in CT and tomotherapy dose calculations, respectively. In the CT imaging dose calculation, a whole body scan over RPI-Adult Male (73kg) phantom is simulated. The beam width is 20 mm; the X-ray is 120 kVp; a total of 90 axial scans are used; statistical uncertainty of organ doses is restricted to 0.5%. The performance of ARCHER on different computing platforms is shown in Figure 1. The GPUs outperform the MIC and the state-of-the-art Haswell CPU, while the latter two outperform the

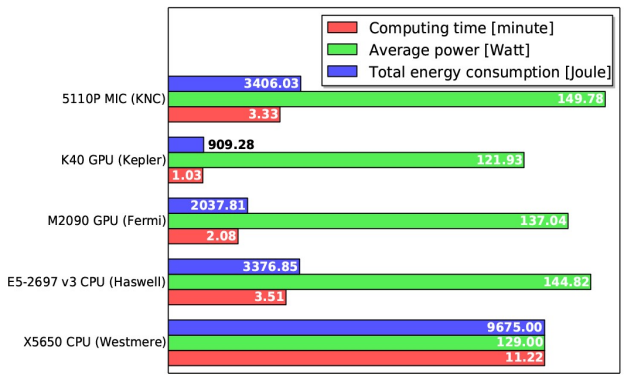

Figure 1. Performance of ARCHER for a CT imaging dose calculation (*lower is better*)

Table 1. Concurrent execution of different hardware devices

Hardware	Speedup factor
X5650 CPU (Westmere)	Baseline
X5650 CPU (Westmere) 4 × M2090 GPU (Fermi) Titan GPU (Kepler) K20 GPU (Kepler) K40 GPU (Kepler) 5110P MIC (KNC)	34.25 ×

Westmere CPU which serves as the baseline in our comparison. Beyond the computation time alone, we are also interested in programmatically determining the average power draw and the total energy consumption of each hardware device, given the fact that energy efficiency is nowadays the topmost concern in exascale system design. While all the devices require approximately the same level of instantaneous power, the GPUs appear the most energy efficient overall, exceeding the Westemere CPU by a factor of 5~10. Besides, in order to maximally exploit the computing power of our heterogeneous platform, we have established a generic execution model such that the CPU, GPU and MIC devices can all work concurrently and efficiently. As is shown in Table I, a speedup factor of 34 can be obtained by fully utilizing the entire sever.

In the tomotherapy dose calculations, the phase space files generated from a 6 MV linear accelerator are used; statistical uncertainty of dose to the planning target volume is restricted to 1%. The GPUs again exhibit excellent performance and complete the simulation on the order of 1 minute and less (Table 2).

Table 2. Performance of ARCHER for 3 tomotherapy dose calculations

Hardware	Prostate [sec]	Lung [sec]	Head & neck [sec]	Speedup
E5-2620 CPU (Sandy Bridge)	729	507	876	Baseline
M2090 GPU (Fermi)	63.4	49.8	79.1	10.18 ~ 11.50 ×
6 × M2090 GPU	10.9	8.9	13.4	56.97 ~ 66.88 ×
K20 GPU (Kepler)	44.7	35.6	59.4	14.24 ~ 16.31 ×
K40 GPU (Kepler)	36.0	29.9	44.2	16.96 ~ 20.25 ×

B. Fast ray tracing in triangular mesh phantoms

The boundary representation (BREP) phantoms are distinctive of its flexibility in geometric morphing and convenience in creating customized phantoms. Still, they cannot be handled in many widely used MC codes and need to be voxelized by in-house software. The voxelization process is usually very computationally expensive. The capability of performing radiation transport directly in the BREP phantom is often desired and is a new functionality of ARCHER currently being developed. Recently, Intel has developed a ray tracing API called "Embree" primarily for computer graphics applications. It has very efficient bounding volume hierarchies implementation and adopts highly optimized algorithms. In our preliminary work, we have evaluated the feasibility of applying this computer graphics API to MC radiation transport. The phantom we use is RPI-Adule Male

Table 3. Performance comparison of different ray tracing implementations

Hardware	Implementation	Performance [rays/second]
X5650 CPU (Westmere)	Brute force	2.68×10^2
X5650 CPU (Westmere)	Embree	4.10×10^5
5110P MIC (KNC)	Embree	5.72×10^5

Obese (142 kg) that has over 1 million triangular meshes. The Embree API is compared against a brute force ray-tracing method that implements Möller-Trumbore intersection calculation. Embree is found to be more computationally efficient by 3 orders of magnitude, and is even faster on the MIC coprocessor (Table 3).

IV. CONCLUSION

ARCHER is a young and growing code for Monte Carlo simulation of radiation transport. It can perform coupled photon-electron transport simulation and simplistic heavy ion simulation. Working as a test bed, it allows us to have a better understanding of the new computing hardware in terms of the computation speed and energy efficiency. In our early tests, ARCHER has demonstrated good performance in CT and tomotherapy dosimetry and shown promising potential in clinical use.

ACKNOWLEDGMENT

This research is funded in part by the National Institute of Biomedical Imaging and Bioengineering (NIBIB) (R01EB015478).

Cloud-based Software Methods for Managing a Large Phantom Database - Example of VirtualDose

Mang Feng[1,*], Aiping Ding[2], Yiming Gao[2], Zhi Chen [1,X]. George Xu[1,2]

[1]School of Nuclear Science and Technology, University of Science and Technology of China, Hefei, China,
[2]Nuclear Engineering Program, Rensselaer Polytechnic Institute, Troy, New York, USA

*Corresponding author: fengmang@mail.ustc.edu.cn

Abstract - This paper describes a cloud-based software – VirtualDose, a software as a service (SaaS) for reporting organ doses for adult and pediatric patients who undergo CT examinations. SaaS design pattern enables users simultaneously to access the software application via internet without pre-installation requirement. It was found that VirtualDose was more accurate owing to the use of anatomically realistic geometries.

Index Terms - VirtualDose, phantom, CT, SaaS

I. INTRODUCTION

X-ray computed tomography (CT) has been widely used as a diagnostic modality [1]. However, the potential radiation risk to the patient population, particularly to children, has increased much concern both from the public and radiology community over past few years [2]. The International Commission on Radiological Protection (ICRP) emphasized the importance of managing patient dose [3], and dose evaluation methodologies have been developed, including CT dose index (CTDI), dose-length product (DLP), effective dose (E), etc. [4-6]. VirtualDose is developed as a new cloud-based software for reporting organ doses to patients. It is based on a comprehensive organ database retrieved from the Monte Carlo simulation results with 25 anatomically realistic patient phantoms. With the adoption of new Software as a service (SaaS) design pattern, the users may access the web application via internet without pre-installation. This paper summarizes the methods and results in developing a database for this large phantom library.

II. MATERIALS AND METHODS

A. A Phantom Set of Twenty-five "Virtual Patient" Models

25 whole-body Boundary Representation (BREP) phantoms were used [7], including newborn babies, children, male and female adults and pregnant females, which were developed by Rensselaer Polytechnic Institute (RPI) and the University of Florida (UF) [8-10]. Those phantoms were converted to voxel-based phantoms by an in-house voxelization algorithm for the purpose of dose calculations in the Monte Carlo program [8].

B. Monte Carlo Organ Dose Calculations

The process of CT scan was simulated in a Monte Carlo radiation transport code-MCNPX [11]. For the purpose of reporting organ doses, the scan range was first deconstructed into the individual tube rotations or slices of the scan. A series of separate axial scans from head to toe were successively simulated by using the combination of each specific tube voltage and each transverse beam width in the MCNPX code. For each slice simulated, the direct dose within the scan volume and the scattered radiation dose outside of the scan volume were calculated. Once the axial slice-by-slice dose database had been established, organ doses from a contiguous axial scan corresponding to a specific protocol can be obtained by directly summing the corresponding single axial slices in the scan range.

C. SaaS Architecture

VirtualDose was designed as a SaaS (Software as a Service) application [12] which hosted all its associated data and up-to-date resources centrally on a remote computer server and allow multiple users to simultaneously access the software functions via the Internet. To implement this architecture, a "Service-Orientated Architecture (SOA)" design was adopted [13], as shown in Figure 1. Programming languages, including Hypertext Markup Language (HTML), Cascading Style Sheets (CSS) and JavaScript, were used to provide an interactive graphical user interface (GUI). For the server-side scripting, C# was used as the primary programming language. And JavaScript Object Notation (JSON) was used to send user's request and feedback server's data information.

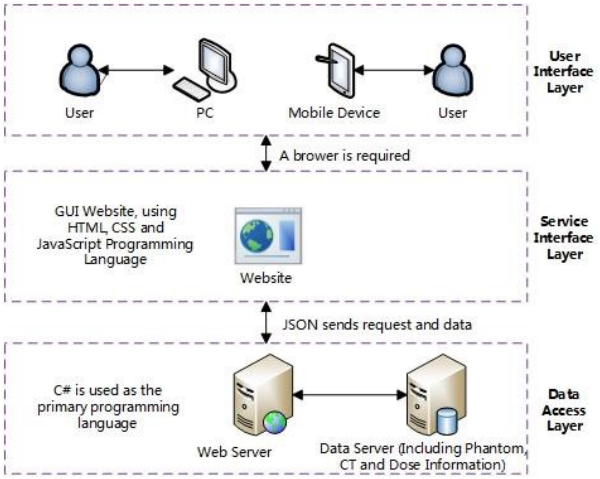

Figure 1. Schematic diagram of the SOA architecture for VirtualDose

In VirtualDose, all the detailed distributions of radiation doses to different organ/tissues were derived from a large organ dose database. To efficiently integrate this database into VirtualDose, an "Entity Framework" (EF) technology in the .NET development

environment [14] was used to create various types of entity data modes (e.g. patient phantoms, doses for each different beam thickness).

III. RESULTS

A. VirtualDose Architecture

The completed VirtualDose contains client-side and server-side. The client-side interface consists of parameter selection panel, a patient model/scan range display, and a dose result display. These allow users to specify the operating conditions of a particular CT scan for a particular patient.

The server-side stores data of 25 different phantoms and their organ doses with various CT scanning produced by Monte Carlo simulations. Based on the user-specified scan parameters, VirtualDose fetches and calculates the patient- specific organ dose data from the remote server-side database. The results are displayed as a table and a figure on user's browser.

B. Comparison of Organ Dose Data in VirtualDose with CT- Expo and ImPACT

We compared the dose data of VirtualDose with CT-Expo [15] and ImPACT [16], which are two dosimetry tools that were based on the stylized pediatric and adult patient models that were known to be anatomically simple. The results showed dose discrepancies among these three software packages. The anatomical variations contribute the most to the difference, which confirm previous report that the lack of realism offered by stylized phantoms caused significant discrepancies in reported CT dose results [17].

IV. CONCLUSION

Based on an extensive and latest library of 25 patient phantoms of both genders and various ages, VirtualDose has been shown in this study to be fully functional in reporting organ doses for a variety of patient types. When compared against the CT-Expo and ImPACT software that are based on anatomically simplified models, VirtualDose is found to be more accurate owing to anatomically realistic geometries. The development of VirtualDose as a SaaS platform allows multiple users to access the software simultaneously via Internet without having to install the software locally.

ACKNOWLEDGMENT

The development of VirtualDose as a commercial software was supported by an STTR grant to Virtual Phantoms, Inc. from the National Institute of Biomedical Imaging and Bioengineering (NIBIB) (1R42EB010404).

REFERENCES

[1] IMV's 2014 CT Market Outlook Report 2015 IMV's 2014 CT Market Outlook Report. http://www.imvinfo.com/index.aspx?sec=ct&sub=dis&itemid=200081, 2015.
[2] Amy Berrington de González, *et al.*, "Projected cancer risks from computed tomographic scans performed in the United States in 2007," *Archives of internal medicine*, vol. 169, pp. 2071-2077, 2009.
[3] J. Valentin, "Managing patient dose in multi-detector computed tomography (MDCT). ICRP Publication 102," *Annals of the ICRP*, vol.37, pp. 1-79, 2006.
[4] Denis Tack, Pierre Alain Gevenois, and Hicham T. Abada, *Radiation dose from adult and pediatric multidetector computed tomography*, Berlin, Germany: Springer, 2007.
[5] E. Seeram, "Computed tomography-physical principles, clinical applications, and quality control," *St Louis: Saunders*, 2009.
[6] Mahadevappa Mahesh, *MDCT physics: the basics: technology, image quality and radiation dose*, Lippincott Williams & Wilkins, 2012.
[7] X. George Xu, "An exponential growth of computational phantom research in radiation protection, imaging, and radiotherapy: a review of the fifty-year history," *Physics in medicine and biology,* vol. 59, p. R233, 2014
[8] Juying Zhang, Yong Hum Na, Peter F Caracappa, and X. George Xu, "RPI-AM and RPI-AF, a pair of mesh-based, size-adjustable adult male and female computational phantoms using ICRP-89 parameters and their calculations for organ doses from monoenergetic photon beams," *Physics in medicine and biology*, vol. 54 p.5885, 2009
[9] Wesley Bolch, Choonsik Lee, Michael Wayson, and Perry Johnson, "Hybrid computational phantoms for medical dose reconstruction," *Radiation and environmental biophysics*, vol.49, pp. 155-168, 2010
[10] X. George Xu, Valery Taranenko, Juying Zhang, and Chengyu Shi, "A boundary-representation method for designing whole-body radiation dosimetry models: pregnant females at the ends of three gestational periods—RPI-P3,-P6 and-P9," *Physics in medicine and biology*, vol.52, p.7023, 2007
[11] Denise B. Pelowitz, 2005. "MCNPX user's manual version 2.5. 0" *Los Alamos National Laboratory 76*.
[12] Aiping Ding, "Development of a radiation dose reporting software for X-ray computed tomography (CT)," 2012.
[13] Erl. Thomas, *Service-oriented architecture: concepts, technology, and design*, Pearson Education India, 2006.
[14] Microsoft 2012a The ADO.NET Entity Framework Overview, http://msdn.microsoft.com/en-us/library/aa697427(v=vs.80).aspx, 2012.
[15] HD. Nagel, "CT-Expo–ein neuartiges Programm zur Dosisevaluierung in der CT," 2002.
[16] ImPACT's ct dosimetry tool, http://www.impactscan.org/ctdosimetry.htm, 2012
[17] Haikuan Liu, Jianwei Gu, Peter F Caracappa, and X. George Xu, "Comparison of two types of adult phantoms in terms of organ doses from diagnostic CT procedures," *Physics in medicine and biology*, vol.55, p.1441, 2010.
[18] Choonsik Lee, *et al.*, "Organ doses for reference adult male and female undergoing computed tomography estimated by Monte Carlo simulations", *Medical physics*, vol.38, pp.1196-1206, 2011.
[19] Choonsik Lee, Kwang Pyo Kim, Daniel J. Long, and Wesley E. Bolch, "Organ doses for reference pediatric and adolescent patients undergoing computed tomography estimated by Monte Carlo simulation," *Medical physics*, vol.39, pp.2129-2146, 2012.

The Combined Chinese Reference Man/woman Voxel Phantom and the Construction of Multi-scale Dosimetry

Junli Li, Rui Qiu, Chunyan Li, Zhen Wu

Department of engineering physics, Tsinghua University, Beijing, China

*Corresponding author: lijunli@mail.tsinghua.edu.cn

Abstract - When the radiation interacts with the human body, the radiation dose is distributed inside the human body in a very heterogeneous way due to the different shape, structure and materials of different organs/tissues. The radiation protection quantities used now, i.e. the effective dose and the equivalent dose, are both based on the average dose of organs/tissues, although the maximum dose possesses special significance for health effects. To improve the radiation dosimetry system, a new dosimetric model called as the multi-scale dosimetry is proposed here. Firstly, a combine human phantom is made, which describes most organs in mm level, with some radiation sensitive sub-structure in μm level such as cancellous bone, breast, respiratory tract, etc. To establish the base for evaluating the health effects, the atom DNA model in the cell nucleus is made in nm level. Then, a series of dosimetric quantities are proposed for different spatial levels, such as equivalent dose and maximum voxel dose for macro-dosimetry, linear energy, specific energy, cell dose for micro-dosimetry, and DNA double strand breaks for nano-dosimetry. Finally, two biological effect models will be added, including the cell death model based on the cell survival curve and the cancer model based on the epidemiology investigation. A lot of test will be done to verify the dosimetry calculation results. This multi-scale dosimetry idea will help us to extend our understanding the detail dose distribution in the human body and to evaluate the radiation health effects more accurately.

Index Terms - human phantom, Monte Carlo method, radiation protection

The Development of Resolution Enhanced Chinese Reference Adult Female Voxel Phantom and Its Application on Organ Dose Calculation

Tsi-Chian Chao[1,*], Yi-Chun Tsai[1], Pei-Shuan Lu[1], Chung-Chi Lee[1], Chuan-Jong Tung[1], and Junli Li[2]

[1]Department of Medical Imaging and Radiological Sciences, College of Medicine, Chang Gung University, Taipei, Taiwan
[2]Department of Engineering Physics, Tsinghua University, Beijing, China

*Corresponding author: chaot@mail.cgu.edu.tw

Abstract **-** The purpose of this study is to enhance resolution of Chinese Reference Adult Female (CRAF) voxel phantom and to calculate its organ doses using EGS4-VLSI Monte Carlo simulation. To calculate the organ dose, Monte Carlo method and voxel phantoms are often used to simulate the energy deposition in human body and the voxel size of phantom will influence the accuracy and precision of these dose calculations. In this study, axial resolutions of 56 organs in CRAF phantom were enhanced by using an objective interpolation method. An axial-resolution enhanced voxel phantom was reconstructed and named CRAF66. Good neighbor method was implemented to solve the overlapping and defect voxels near organ boundaries on CRAF66. After CRAF66 phantom was ready, Monte Carlo code EGS4-VLSI was applied to calculate organ doses of CRAF and CRAF66 against external and internal photon /electron exposure. Fisher's least significant difference (LSD) was used to evaluate if voxel sizes significantly affect the organ dose calculation. Results show that axial resolution of CRAF phantom was successfully enhanced from 1.98 mm in head and from 3.96 mm in body to 0.66 mm in CRAF66. The LSD results show that organ dose differences between CRAF66 and CRAF in vessel, bone and muscle are small but statistically significant against external photon/electron exposure. The organ dose differences between CRAF66 and CRAF in small source organs are small but statistics significant against internal photon exposure. We found out that the voxel sizes of phantom influence organ dose mostly and the organ doses difference between CRAF66 and CRAF are statistically significant in most source organs against internal electron exposure.

Index Terms - voxel phantom, Monte Carlo, objective interpolation, good neighbor method, Fisher's least significant difference

I. INTRODUCTION

The purpose of this study is to enhance resolution of Chinese reference adult female (CRAF) voxel phantom and to calculate its organ doses from external/internal photon/electron exposure using Monte Carlo.

The study is divided by three parts:

(1) Enhancing Z-resolution of CRAF voxel phantom
(2) Calculating organ doses using MC simulation
(3) Comparing organ doses of CRAF with CRAF66 by using Fisher's least significant difference (LSD)

II. METHODS

A. Enhancing Z-resolution of CRAF voxel phantom

Axial resolutions of 56 organs in CRAF phantom were enhanced by using objective interpolation method.

(1) The input scene is first converted to a "binary" scene (a scene with only two intensities, 0 and 1) by a segmentation operation.
(2) The "shape" of the region represented by the 1-valued voxels (the object) is then utilized to create an output binary scene with similar shape via interpolation.
(3) Converting the binary scene V_b into a scene V_g, by assigning to each voxel v in V_g a number that represents the shortest distance between v and the boundary
(4) The number is positive if v has an intensity 1 in V_b, otherwise the number is negative.
(5) Now we interpolate V_g using linear, trilinear, or other interpolation rules to create another scene V_b'.
(6) Assigning a voxel in V_b' the intensity 1 if the corresponding voxel in V_g has positive value. All other voxels are assigned the intensity 0.

A voxel phantom with enhanced axial resolution was reconstructed and named CRAF66. Good neighbor method, which replaced the defected voxels with their 26 neighbors that with lowest mass ratio after to before interpolation, was implemented to solve the overlapping and defect voxels near organ boundaries on CRAF66.

B. Calculating organ doses using MC simulation

After CRAF66 phantom was ready, Monte Carlo code EGS4-VLSI was applied to calculate organ doses of CRAF and CRAF66 against external and internal photon/electron exposure. For external exposure, we selected broad parallel beams (60 × 200 cm^2) of monoenergetic photon/electron beam. The range of photon energies were from 15 keV to 10 MeV. The range of electron energies were from 100 keV to 10 MeV. The direction of photon/electron beam incidence were AP, PA, LLAT, RLAT, ROT, and ISO. For internal exposure, specific absorbed fractions (SAF, Φ) were calculated for each of these energies for the 20 source organs to 16 target organs. The range of photon energies were from 15 keV to 10 MeV and the range of electron energies were from 100 keV to 10 MeV.

C. Comparing the organ dose of CRAF with CRAF66 by using Fisher's least significant difference (LSD)

III. RESULTS

Figure 1 shows the results that axial resolutions of CRAF phantom were enhanced by using objective interpolation method. Figure 1 (c) shows a new CRAF66 phantom with overlapping and defect voxels near organ boundaries and which can be solved by the Good neighbor method.

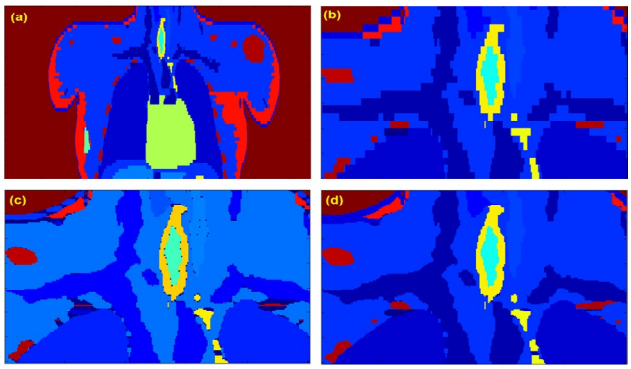

Figure 1. (a) and (b): coronal views of CRAF, (c) and (d): same view of (b) in CRAF 66 before and after good neighbor correction

After been constructed CARF and CRAF66 were implemented into MC to calculate organ doses for external/internal photon/electron exposures, and these results were compared using Fisher's LSD method.

- For external photon exposure, when photon energy is smaller than 100 keV, the difference of muscle, vessel, skin and bone dose between CRAF and CRAF66 are small but statistically significant.
- For external electron exposure, the difference of muscle, vessel, and skin dose between CRAF and CRAF66 are small but statistically significant in most energy.
- For internal photon exposure, when source organ was also target organ, SAF between CRAF and CRAF66 are small but statistically significant.
- For internal electron exposure, voxel size affects the SAF very significantly. When source organ was also target organ, SAF always decreased when energy increased. When source organ differed from target organ, SAF always increased when energy decreased (Figure 2).

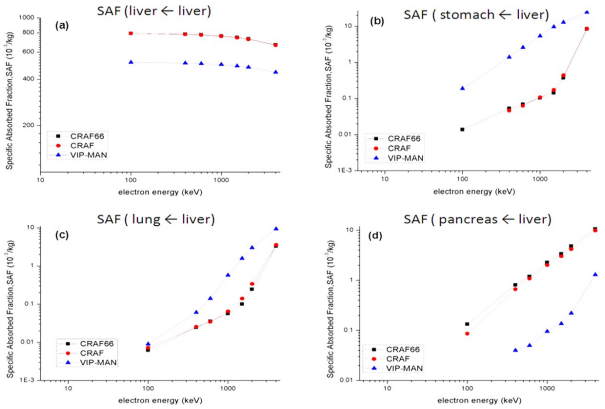

Figure 2. SAF of electron sources in liver and target organ in (a) liver (b) stomach (c) lung and (d) pancreas

Table 1. The resolution of CRAF and CRAF66

	CRAF	CRAF66
Number of voxels [billion]	0.22	1.18
Voxel size [mm^3]	Head: 0.613 × 0.613 × 1.98 Body: 0.613 × 0.613 × 3.96	0.613 × 0.613 × 0.66
Resolution	571 × 858	571 × 858
Number of slices	Head: 108	2401

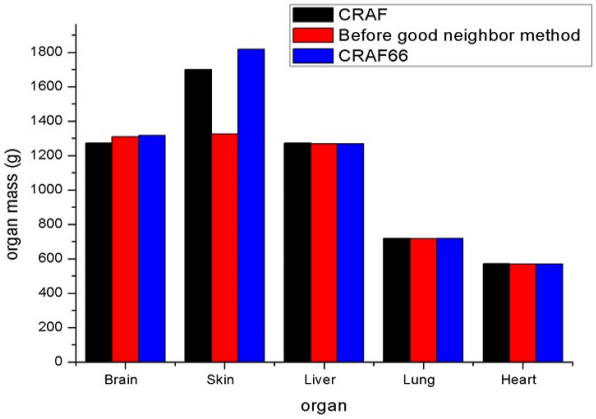

Figure 3. Organ mass comparison among CRAF, CRAF66 before and after good neighbor correction

IV. CONCLUSION

The axial resolution of CRAF phantom was successfully enhanced from 1.98 mm in head and from 3.96 mm in body to 0.66 mm in CRAF66 (Table 1). Organ mass comparison of CRAF and CRAF66 after good neighbor correction showed good agreement between each other (Figure 3). The LSD results show that organ dose differences between CRAF66 and CRAF in vessel, bone and muscle are small but statistically significant against external photon/electron exposure. The organ dose differences between CRAF66 and CRAF in small source organs are small but statistics significant against internal photon exposure. We found out that the voxel sizes of phantom influence organ dose mostly and the organ doses difference between CRAF66 and CRAF are statistically significant in most source organs against internal electron exposure.

Monte Carlo Calculated Conversion Factors Based on a 3D Detailed Breast Model for the Estimation of Mean Glandular Dose in Mammography

Wenjing Wang[1,2,3], Rui Qiu[1,2,3,*],Li Ren[1,2,3], Huan Liu[1,2,3], Chenxing Jiang[1,2,3],and Junli Li[1,2,3]

[1]Department of Engineering Physics, Tsinghua University, Beijing, China
[2]Key Laboratory of Particle & Radiation Imaging (Tsinghua University), Ministry of Education, Beijing, China
[3]Key Laboratory of High Energy Radiation Imaging Fundamental Science for National Defense, Beijing, China

*Corresponding author: qiurui@mail.tsinghua.edu.cn

Abstract - Mammography has been recognized internationally as the primary choice for breast cancer screening. In China, more than 300,000 women were exposed in mammography for breast cancer screening in 1998, and the number is increasing rapidly. However, there is a risk of breast cancer induced by the exposure in mammography. The female breast is one of the most radiosensitive organs and the recommended tissue weighting factors for breast tissue of ICRP has changed from 0.05 to 0.12 (ICRP 1991, 2007). Therefore the risk of radiation-induced breast cancer in mammography should be paid more attention.

In order to estimate the risk of radiation-induced breast cancer more precisely, a 3D detailed breast model is constructed in this paper, which contains skin, subcutaneous fat, Cooper's ligaments, fibroglandular region, and so on. The detailed breast model constructed with mathematical models was then voxelized to a voxel model with a voxel size of 0.2 mm. The voxel model was compressed in craniocaudal direction to get a deformation model, and Monte Carlo stimulation for dose estimation in mammography was performed based on it with Geant4.

Compressed breast models of four different glandularities (25%, 50%, 75%, 100%) and four different thicknesses (3 cm, 4 cm, 5 cm, 6 cm) were simulated at four different X-ray tube voltages (25 kV, 30 kV, 35 kV, 40 kV) for the Mo/Mo X-ray spectrum. The absorbed dose to glandular tissue was calculated and was expressed in the form of conversion coefficients by normalizing to the air kerma free-in-air at the entrance surface without backscattering radiation. The effects of the scattering from the female human body were studied by attaching the 3D detailed breast model to the whole-body Chinese reference adult female voxel model.

It was shown that the difference between glandular tissue dose conversion coefficients with scattering considered and that without scattering considered was smaller than 3%. A series of glandular tissue dose conversion coefficients for mammography based on the 3D detailed breast model were calculated. The comparison between the data calculated and the old data base on the simplified breast model was carried out. A discrepancy up to 30% was observed, which might come from both the breast model and the Monte Carlo code used.

Development of "4D Voxel Phantom" Reflecting Continuous Respiratory Motion of Patient

Jeong Min Seo[1,2], Min Cheol Han[1], Se Hyung Lee[1,3], Seong hoon Kim[4], Chan Hyeong Kim[1,*], Yeon Soo Yeom[1]

[1]Department of Nuclear Engineering, Hanyang University, Seoul, Republic of Korea
[2]Department of Radiologic Science, Daewon University College, Jecheon, Republic of Korea
[3]Department of Radiation Oncology, Bundang Jesaeng General Hospital, Seongnam, Republic of Korea
[4]Department of Radiation Oncology, College of Medicine, Hanyang University, Seoul, Republic of Korea

*Corresponding author: chkim@hanyang.ac.kr

Abstract **-** In the present study, we propose a new type of voxel phantom, called "4D voxel phantom," which is directly generated from the patient 4D CT data and continuously deformed to accurately model the continuous patient's respiratory motion. The results show that the patient's continuous respiratory motion was reflected in the developed 4D voxel phantom without any constrained-movement.

Index Terms **-** 4D voxel phantom, patient 4D CT, respiration motion, deformation vector field (DVF)

I. INTRODUCTION

In radiation oncology, the Monte Carlo (MC) simulation with a patient voxel phantom based on CT data has been performed to verify the planned dose distribution. As it is important for accurate dose distribution due to the respiratory motion, recently, several investigators performed the multiple 3D voxel simulations based on different 10 available phase images of the patient 4D CT [1-2] to assess the effects of respiratory motion. However, 10 phases with a temporal resolution of ~0.4 sec may not be suitable for more complex studies, such as interplay effect between the movement of the scanning proton beam and the deforming target organ [3].

We propose a new type of 4D phantom reflecting continuous respiratory motion of patient, called "4D voxel phantom," which is directly generated from the patient 4D CT data. To test the reliability of our new approach, a 4D voxel phantom was constructed and evaluated by performing point tracking [4] and voxel's dose tracking [5] corresponding to arbitrary points and voxels in liver parts of the reference phase, respectively.

II. MATERIALS AND METHODS

This construction process is divided into two parts: (1) construction of DVFs for interphase images and dose registrations, and (2) implementation of the 4D voxel phantom in the dedicated 4D Monte Carlo simulation code.

A. Construction of DVFs

Generally, the deformation vector field (DVF) was constructed by deformable image registration (DIR). In the present study, we constructed the two kinds of DVFs according to the following methods: (1) all DVFs were defined by DIRs, and (2) all DVFs were defined by DIRs and Inverse DVF (iDVF). Figure 1 shows the construction methods of DVF.

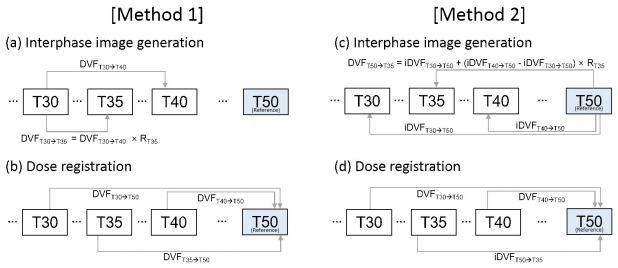

Figure 1. Two construction methods of DVF proposed in the present study

In *Method 1*, DVFs for interphase images are generated by DIR between the neighboring phase images of 4D CT set [6] and interpolation. Then, DVFs for dose registration are produced by DIR between the all phase images and the reference image (e.g. T50).

In *Method 2,* DVFs for the interphase images are generated by equation 1:

$$DVF_{T50\to N} = iDVF_{N1\to T50} + (iDVF_{N2\to T50} - iDVF_{N1\to T50}) \times R_N \quad (1)$$

where N is interphase, $N1$ and $N2$ are neighboring phases of N, and R_N is interpolation ratio of N. Then, DVFs for dose registration can be generated simply by using the inverse of the DVFs for the interphase images.

B. Implementation of voxel phantom in 4D Monte Carlo simulation code

A dedicated 4D Monte Carlo simulation code for 4D voxel phantom was written using the Geant4 toolkit. The roles of the developed code include: (1) to upload the 4D voxel phantom and DVFs in memory, (2) to perform continuous 4D simulation according to the time-relevant parameter, and (3) to perform the dose registration between the interaction phase and the reference phase using tri-linear interpolation method in real-time.

III. SIMULATION

A. Implemented 4D Voxel Phantom

Finally, the 4D voxel phantom was successfully developed and implemented in the dedicated 4D simulation code. Figure 2 shows 100 snapshot images of 4D simulation constructed by *Method 2.* The full 4D Monte Carlo simulation animation is available (see the URL in Figure 2).

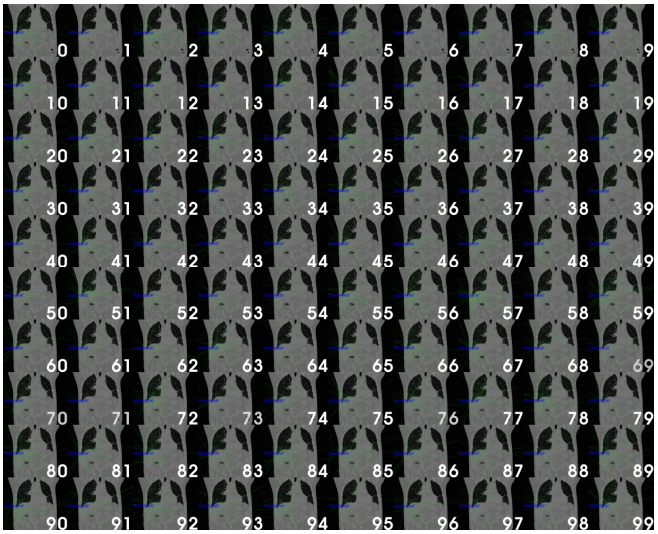

(Web site URL: http://hurel.hanyang.ac.kr/Phantom/4DVoxel.gif)

Figure 2. Snapshot images of 4D simulation with 4D voxel phantom constructed by Method 2

B. Point and voxel's dose tracking results

To test our new approach, we constructed 4D voxel phantoms by applying two DVF construction methods and performed continuous 4D Monte Carlo simulations. The phantoms were irradiated by a 100 MeV spot-scanning proton beam (spot size σ = 5 mm). The fixed spot beam was directed to the middle part of the liver, considering organ's deformation (~12 mm mostly in the superior-inferior (SI) direction). The simulations were repeated to obtain a relative error less than 10%.

Figure 3 shows the results of point tracking and voxel's dose tracking for 4D voxel phantoms constructed by *Method 1* and *Method 2.* As shown in point tracking results, the point's movement by *Method 2* (Figure 3-c) was presented more continuously than that of *Method 1* (Figure 3-a). This difference seems due mainly to the registration error by DIR. In case of *Method 1*, because the DIR was used twice for generation of interphase image and dose registration, the registration error for interphase images was twice as compared with that of the existing phase images of 4D CT data set. Besides, in case of *Method 2*, the registration error of interphase images was equal to that of existing phase images caused by using the inverse DVF. For such a reason, the voxel's dose tracking result also shows that the dose distribution by *Method 2* (Figure 3-d) is more continuous than that of *Method 1* (Figure 3-b).

IV. CONCLUSION

In the present study, we have developed a new type of voxel phantom, called "4D voxel phantom," which is directly generated from the 4D CT data of a patient and continuously deformed during patient respiratory motion. The results show that the developed phantom could provide accurate movement reflecting continuous respiratory motion. We expect that the use of 4D

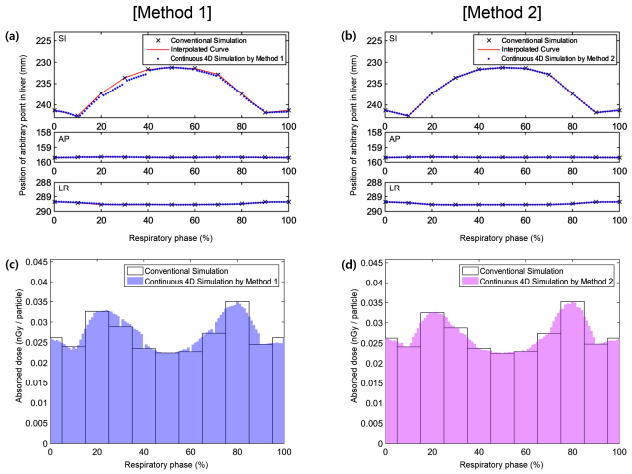

Figure 3. The results of point tracking (top) and voxel's dose tracking (bottom) for 4D voxel phantoms constructed by *Method 1* (left) and *Method 2* (right)

voxel phantoms could significantly improve the dose calculation accuracy where the organ movement is important such as in interplay effect study in proton therapy and IMRT.

ACKNOWLEDGMENT

This project was supported by Nuclear Safety and Security Commission (NSSC) through Korea Radiation Safety Foundation (KORSAFe) and also by Ministry of Science, ICT and Future Planning through the National Research Foundation of Korea (Project No.: 2011-0025496, 2012-K001146, 1403012). Two of the authors were supported by the Global PhD Fellowship program (Project No.: 2011-0007318, 2011-0030970).

REFERENCES

[1] S. Dowdell, C. Grassberger, G. C. Sharp, and H. Paganetti, "Interplay effects in proton scanning for lung: a 4D Monte Carlo study assessing the impact of tumor and beam delivery parameters," *Phys. Med. Biol.*, 58, 4137-56, 2013

[2] T. C. Huang, J. A. Liang, T. Dilling, T. H. Wu, and G. Zhang, "Four-dimensional dosimetry validation and study in lung radiotherapy using deformable image registration and Monte Carlo techniques," *Radiat. Oncol.*, 5, 45, 2010

[3] H. Paganetti, H. Jiang, J. A. Adams, G. T. Chen and E. Rietzel, "Monte Carlo simulations with time-dependent geometries to investigate effects of organ motion with high temporal resolution," *Int. J. Radiat. Oncol. Biol. Phys.*, 60, 942-50, 2004

[4] J. R. McClelland, J. M. Blackall, S. Tarte, A. C. Chandler, S. Hughes, S. Ahmad, D. B. Landau, and D .J. Hawkes, "A continuous 4D motion model from multiple respiratory cycles for use in lung radiotherapy," *Med. Phys.*, 33, 3348-3358, 2006

[5] E. Heath, and J. Seuntjens, "A direct voxel tracking method for four-dimensional Monte Carlo dose calculations in deforming anatomy," *Med. Phys.*, 33, 434-445, 2006

[6] E. Schreibmann, G. T. Y. Chen and L. Xing, "Image interpolation in 4D CT using a BSpline deformable registration model," *Int. J. Radiat. Oncol.*, 64, 1537-50, 2006

Development of the Functionalized Virtual Population based on Different Anatomies and Its Application to Implant Effectiveness and Safety Evaluations

Niels Kuster[1,2,*]

[1]IT'IS Foundation, Zurich, Switzerland
[2]ETH Zurich, Zurich, Switzerland

*Corresponding author: nk@itis.ethz.ch

Abstract **-** Detailed, high-resolution, functionalized computational phantoms are essential for performing reliable and realistic simulations of biological and physical processes for life sciences applications. Here we present the functionalized computable models of the Virtual Population and illustrate several examples of their features and applicability in medical implant effectiveness and safety evaluations.

Index Terms **-** computational phantomsm, Virtual Population, functionalization, computational life sciences, implant safety evaluation

I. COMPUTABLE VIRTUAL POPULATION FOR MEDICAL APPLICATIONS

Numerical modeling is rapidly becoming the preferred approach for conducting research in life sciences and especially for evaluating medical implant effectiveness and safety. Until recently, medical devices and diagnostic and therapeutic tools were modeled only in simplified environments, compromising the transferability of results to complex living systems consisting of tissues and organs. As a result, the formal application of simulation and modeling approaches to support safety and efficacy evaluations has received limited recognition in the regulatory approval process. The development of more advanced numerical tools and computational phantoms representing a simulation environment has become crucial to facilitating the acceptance of simulations in the regulatory approval process. As these computational phantoms have evolved from stylized models to extremely detailed models represented by polygon meshes or non-uniform rational B-spline (NURBS) surfaces (as reviewed in [1]), their advanced capabilities have broadened the scope of their applicability beyond historical dosimetric assessments of ionizing and non-ionizing radiation.

The development and release of the Virtual Family computational phantoms in 2008 [2] and the Virtual Population (ViP) in 2011 by the IT'IS Foundation and the United States Food and Drug Administration (FDA) has transformed the field of computational life sciences. The wide usage of these phantoms by more than 400 research teams worldwide and their expansion to new fields has created an urgent demand for the development of enhanced capabilities to accommodate increasingly more specific and complex applications. Significant effort has been invested on improving the models, resulting in the total resegmentation of the first generation models to achieve higher resolution, detailedness, and consistency and the development of novel surface generation methods to improve surface quality [3] (Figure 1).

Figure 1. Vertebrae, intervertebral discs, and spinal cord of Ella in Versions 1.0 and 3.1 (left). Generic thoracolumbar stabilization implant inserted in the L2, L3, and L4 vertebrae of Ella Versions 1.0 and 3.1 (right)

Concomitantly, the models have been significantly enhanced to include the functional information necessary for conducting realistic simulations of biological and physical processes, such as neuron and fiber orientation, and tissue-specific biological and physical properties, such as thermal, dielectric, or acoustic properties [4]. When used with powerful physical solvers, the latest version of ViP3.1 (Table 1, Figure 2) represents the most reliable and preferred computational phantoms for applications ranging from implant safety and effectiveness assessments to

Table 1. Estimated uncertainty of thyroid dose using two method of administered activity

Model Name	DOI
Duke	10.1099/VIP11001-03.1
Ella	10.1099/VIP11002-03.1
Billie	10.1099/VIP11003-03.1
Thelonious	10.1099/VIP11004-03.1
Dizzy	10.1099/VIP11005-03.1
Louis	10.1099/VIP11006-03.1
Eartha	10.1099/VIP11007-03.1
Roberta	10.1099/VIP11008-03.1

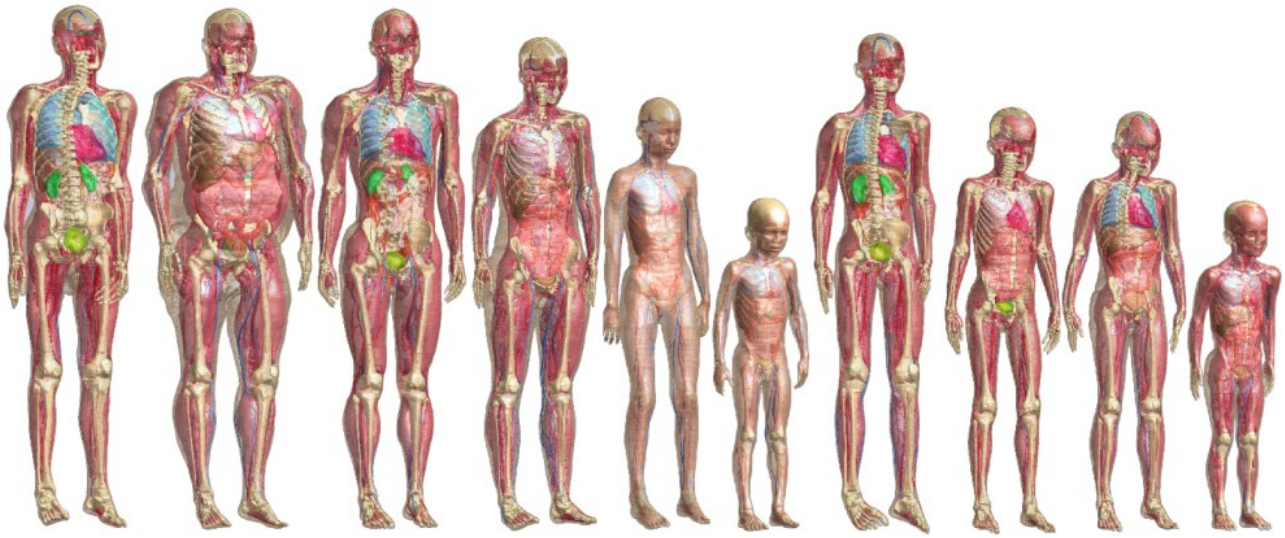

Figure 2. From left to right: the elderly and obese models, the 4 models of the Virtual Family, and the 4 models of the Virtual Classroom V3.1

basic research, including tissue mechanics, acoustics (in particular ultrasound), and EM-neuron interactions. As most commercially available simulation platforms are not yet capable of handling the complexity of ViP3.1, the IT'IS Foundation together with the FDA also developed the universally compatible Virtual Family VF2.0 consisting of 22 high resolution tissue groups and reduced geometrical features.

II. APPLICATION OF ViP3.1 IN THE REGULATORY SPACE

The Virtual Population models were first used for regulatory purposes to demonstrate the MR safety of active implantable medical devices, as defined in the Technical Specification of ISO/IEC TS 10974. The defined in silico (using ViP3.1) and experimental combined approach [5], however, must be further refined to meet the challenges of generating consistent compliance results as numerical tools and model capabilities are continually improved to better represent the actual physiological environment. The requirements, reliability, shortcomings, and impact on clinical trials of this approach will be discussed.

REFERENCES

[1] X. G. Xu, "An exponential growth of computational phantom research in radiation protection, imaging, and radiotherapy: A review of the fifty-year history," *Phys. Med. Biol.,* vol. 59(18), pp. R233-R302, 2014.

[2] A. Christ, W. Kainz, E. G. Hahn, K. Honegger, M. Zefferer, E. Neufeld, W. Rascher, R. Janka, W. Bautz, J. Chen, B. Kiefer, P. Schmitt, H.P. Hollenbach, J. Shen, M. Oberle, D. Szczerba, A. Kam, J.W. Guag, and N. Kuster, "The Virtual Family – development of surface-based anatomical models of thwo adults and two children for dosimetric simulations," *Phys. Med. Biol.,* vol. 55(2), pp. N23–38, 2010.

[3] M.C. Gosselin, E. Neufeld, H. Moser, E. Huber, S. Farcito, L. Gerber, M. Jedensjö, I. Hilber, F. Di Gennaro, B. Lloyd, E. Cherubini, D. Szczerba, W. Kainz, and N. Kuster, "Development of a new generation of high-resolution anatomical models for medical device evaluation: the Virtual Population 3.0," *Phys. Med. Biol.,* vol. 59(18), pp. 5287–5302, 2014.

[4] Hasgall PA, Di Gennaro F, Baumgartner C, Neufeld E, Gosselin MC, Payne D, Klingenböck A, Kuster N, "IT'IS Database for thermal and electromagnetic parameters of biological tissues," Version 2.6, January 13th, 2015.

[5] E. Cabot, T. Lloyd, A. Christ, W. Kainz, M. Doublas, G. Stenzel, S Wedan, and N. Kuster, "Evaluation of the RF heating of a generic deep brain stiumlator exposed in 1.5T magnetic resonance scanners," *Bioelectromagnetics*, vol. 34(2), pp.104–113, 2013.

Functionalized Anatomical Models for In Silico Investigation of EM-Neuronal Dynamics Interactions

Esra Neufeld[1,*] and Niels Kuster[1,2]

[1]IT'IS Foundation for Research on information Technologies in Society, Zurich, Switzerland
[2]Swiss Federal Institute of Technology (ETHZ), Zurich, Switzerland

*Corresponding author: neufeld@itis.ethz.ch

Abstract **-** A computational platform has been developed that is capable of simulating electromagnetic (EM) field interactions with neurons in complex tissue-structure environments, implementing the concept of functionalized anatomical phantoms. A high-resolution model of the head was developed for the analysis of EM-neuron interactions. Multimodal magnetic resonance imaging (MRI) and diffusion tensor imaging (DTI) data were acquired to guide neuron model placement and provide information on tissue anisotropy. The model features a large number of structures, particularly those (ears, eyes, and selected deep brain structures) relevant for applications such as DBS (Deep Brain Stimulation) and neuroprosthetics. Additionally a dedicated EM solver coupled with dynamic models of neuronal activity was also implemented. Functionalized models have been applied in three case studies, namely: a) transcranial alternating current brain stimulation; b) MRI gradient coil switching induced nerve stimulation; and c) muscle activation by a neuroprosthetic implant.

Index Terms **-** functionalized anatomical models, EM-neuron interactions, computational life sciences

I. INTRODUCTION

Implanted neuroprosthetic devices and brain stimulation represent beneficial applications of the interaction of EM fields with neurons. On the other hand, EM-neuron interaction can also be unintentional, as in the case of unintended neurostimulation caused by exposure to low frequency EM fields generated by MRI gradient coils. Numerical models are fundamental to assess MRI safety as well as general exposure safety. Accurate simulation tools are needed to support the investigation of EM-neuron interaction mechanisms towards development and optimization of novel stimulation devices and efficacious treatment protocols. As the human body is by nature inhomogeneous and anisotropic, simulations require representation of the human anatomy that capture these characteristics. Information regarding field distribution is not always sufficient to allow the impact on neuronal dynamics to be determined, and the modeling of EM fields needs to be coupled to that of neuronal behavior.

Image-based numerical anatomical models such as the Virtual Population (ViP) [1] are often employed to simulate physical and physiological processes in the human body. Anatomical model-based assessment of EM dosimetry represents a way to obtain detailed, realistic information about complex field distributions inside the human body under safe and controlled conditions, thus complementing or replacing experimental assessment. To enhance the value of the static models and extend their applicability, it is important to functionalize them by including dynamic models of tissue behavior, such as EM-tissue interactions, EM-induced heating accounting for biological thermoregulatory responses, and induced tissue damage. The goal of this study is to present specific examples of functionalization of the Multimodal Imaging-Based Detailed Anatomical Model of the Human Head and Neck (MIDA) [2] and ViP models to study the influence of EM fields on neuronal dynamics. Functionalized models can be used to evaluate EM-induced neuronal stimulation, inhibition, or synchronization, and the activation selectivity, e.g., to achieve improved understanding of how neurostimulation devices function.

II. METHODS

Simulation Platform: A high performance computing-enabled finite element method (FEM) quasi-static low frequency solver, customized to handle inhomogeneous and anisotropic electrical conductivity distributions inferred from the DTI data, was implemented. Neuron models with complex geometries, ion-channel distributions, and dynamics incorporated in different neuronal compartments, such as axons, soma, and dendritic tree can be coupled via an extracellular potential mechanism to the calculated EM potential. An embedded version of the NEURON code from Yale was used to perform the neuronal dynamics simulations. DTI data was used to guide the integration of selected neuron models in the anatomical head model. Existing neuron models, such as those available from the ModelDB repository, or specific mechanisms, e.g., channel dynamics, specified by the user, can also be integrated. Visualization of the transient variation of quantities, i.e., trans-membrane potentials, determination of stimulation thresholds, and detection of neuronal spiking, are available as post-processing functionality. Published neuronal dynamics simulations, e.g., of DBS-induced spiking, extracellular stimulation of rat hippocampus neurons, and the SENN model (a generic model of myelinated nerve fibers used for low-frequency EM-exposure safety assessments) were reproduced to provide validation of the new modeling platform.

Functional head model and tACS case study: The analysis in the first case-study was carried out through the development of a functionalized high-resolution anatomical model of the human head that includes embedded dynamic neuron models and is coupled to a dedicated EM simulation solver. For this purpose, a detailed head model was generated using multimodal MRI data acquired from a healthy female volunteer [2]. It features a $(0.5\ \text{mm})^3$ isotropic spatial resolution, more than 150 delineated anatomical structures and brain sub-structures, and Diffusion Tensor Imaging (DTI)-derived local tissue anisotropy. It was optimized to allow both structured and unstructured mesh generation to maximize usefulness for a wide range of simulation tools and methods [2]. The arteries and veins were separated using multiple angiographic datasets (time-of-flight and

phase-contrast). The head model includes a statistical shape model-based stereotactic atlas of the thalamus and mid-brain nuclei. Following segmentation, surfaces were extracted, simplified, and smoothed. For the case study of the tACS application, different montages including one featuring five small electrodes in a Cz-(Fz, C3, C4, Pz) montage [3] were modeled.

MRI gradient induced stimulation: A second case study was used to demonstrate the application of coupled EM-neuronal dynamics modeling. A local temperature dependent SENN model which considers the temperature dependence of the underlying Frankenhaeuser-Huxley model as well as a more realistic motor neuron model from [4] were used to study the safety-relevant impact of MRI gradient coil switching on neuronal dynamics while considering EM-induced tissue heating caused by the radiofrequency (RF) transmit coil. A quasi-static low-frequency solver was used to determine the gradient coil field, and the FDTD method was applied to simulate the RF energy deposition. The Pennes bioheat equation was used to simulate the temperature increase. Subsequently the thresholds for gradient coil switching inducing nerve activation were calculated using the coupled EM- neuronal dynamics solver. The roles of field inhomogeneity, heating, field- and nerve trajectory-smoothing, and various nerve activation mechanisms were also investigated.

Neuroprosthetic applications: The third case study involved the modeling of an implantable transverse intrafascicular multichannel electrode (TIME) for neuroprosthetic applications. This electrode applies multi-channel microstimulation to a rat sciatic nerve to selectively activate specific muscles [5]. A large number of neuron models, in which the position and neuron dynamical properties were randomly varied, were integrated in an anatomically detailed model of the rat sciatic nerve and associated to the activation of different muscles based on physiological and histological data [5].

III. RESULTS

For the **tACS** study various numerical methods (FEM and FVM), various discretization approaches involving conformal tetrahedral elements as well as rectilinear voxels, and different tissue property assignment approaches, e.g., tissue-specific scalar electrical conductivity and DTI-based anisotropic electrical conductivity, were applied. Different electrode montages could be compared with regard to the likelihood of visual phosphene induction. For the **MRI-induced stimulation** study, results of the simulations - contrary to the assumptions underlying current MR safety standards - suggest that, i) field foci occur *in vivo* and can result in neural stimulation, ii) end-node-type stimulation is not the only relevant mechanism and thus field-strength is not a sufficient safety criterion, iii) the SENN model is not always conservative at least when compared to other existing neuron models, iv) field smoothing is not always suitable but neuron trajectory smoothing is required, and v) thermal effects can strongly impact the neuronal dynamics. Finally, for the case of the **neuroprosthetics** application, the model was used to predict nerve recruitment and selectivity of muscle activation. Comparison with experimental findings showed satisfactory agreement.

IV. CONCLUSION

A computational platform was developed to realistically model both beneficial and safety-relevant EM-neuron interactions in a realistic anatomical context. A multimodal imaging-based high-resolution head model was developed for EM-neuron interaction investigations. The assignment of location-specific anisotropic brain tissue parameters was facilitated by integration of DTI tensor information. An application related to transcranial alternating current stimulation treatments was used to demonstrate the suitability of the models for a broad range of numerical methods and solvers. The simulation platform was validated against literature data, e.g., involving the SENN model. Experimental results, e.g., on the selectivity of muscle activation by implanted multi-channel neuroprosthetic electrodes, were also used for additional validation.

The newly developed simulation platform is uniquely suitable for simulations of EM-neuron interactions that reflect the complex, dynamic, inhomogeneous, and anisotropic nature of human physiology. The functionalized models and coupled EM-neuronal dynamics simulation environment described here are proposed as valuable tools for applications ranging from the design of novel neuro-prosthetic devices to optimization and personalization of patient treatment. Applications related to the safety assessment of, e.g., implantable devices, and interaction- mechanism studies are also facilitated.

ACKNOWLEDGMENT

The study was supported by the CTI (14930.1 PFLS-LS) and FDA's Critical Path Initiative.

REFERENCES

[1] M.-C. Gosselin, *et al.*, "The Virtual Population 3.0", *Phys. Med. Biol.*, vol. 59, 5287ff, 2014.
[2] M. I. Iacono, *et al.*, "A Multimodal Imaging-Based Detailed Anatomical Model of the Human Head and Neck", *PLoS One* 10 (4), 20152014.
[3] Laakso, I. and Hirata, A. Computational analysis shows why tACS induces retinal phosphenes. *J. Neur. Eng.* 10, 2013.
[4] McIntyre, C. C., *et al.*, Modeling the excitability of Mammalian nerve fibers: influence of afterpotentials on the recovery cycle. *J. Neurophysiol.* 87, 995ff, 2002.
[5] Raspopovic, Stanisa, *et al.* "Experimental validation of a hybrid computational model for selective stimulation using T." *Neural Systems and Rehab. Eng., IEEE Transactions on*, vol. 20(3) 395ff, 2012.

Evaluation of MRI Exposure of Patients with Deep Brain Stimulator with Virtual Population 3.0 and 1.0 Anatomical Phantoms

Aiping Yao[1,2,*], Earl Zastrow[1,2], Eugenia Cabot[1], Davnah Payne[1], and Niels Kuster[1,2]

[1]IT'IS Foundation, Zurich, Switzerland
[2]Department of Information Technology and Electrical Engineering, ETH-Zurich, Zurich, Switzerland

*Corresponding author: yao@itis.ethz.ch

Abstract **-** In this study, we aim to quantify the effect that the changes of anatomical features in the Virtual Population models version 1.0 (ViP 1.0) and version 3.0 (ViP 3.0) have on the estimation of the MRI exposure and the evaluation of implant safety. The differences were evaluated from both anatomical and dosimetrical point of view. A 1.5T RF birdcage coil positioned for head imaging was chosen as the MR exposure. The models show sufficiently similar averaged global and local SAR (< 0.5 dB). The differences in the integrated values used for implant safety evaluations were also smaller than the expected uncertainty. Nevertheless, the ViP 3.0 offers higher anatomical precision than the ViP 1.0 and therefore, more suitable for assessment of locally induced effects and should be used in any future evaluations.

Index Terms **-** MRI Exposure, implants, computable models

I. INTRODUCTION

The anatomical human phantoms have proven to be a useful tool in the dosimetric investigation of electromagnetic absorption in the human body. Most of the models available now were developed from the Computational Tomography (CT) or Magnetic Resonance (MR) images. The Virtual Population models (ViP) were developed from the MRI scans of healthy volunteers and reconstructed with 3D unstructured triangulated surfaces [1]. The ViP 1.0 have been released in 2007 and have been used a large number of studies, mainly in the field of electromagnetic (EM) dosimetry, e.g. from mobile phones and home appliances exposure assessment to the safety evaluation of medical implants [1-4]. The ViP 1.0 has several shortcomings: 1) the limited fidelity organ segmentation; 2) tissue surface quality; 3) inconsistent tissue assignment. All of which have been significantly improved in the ViP 3.0 [4].

This study aims to quantify the effect that the changes of anatomical entities have on the estimation of the MRI exposure and implant safety assessment. Four ViP models from the ViP 1.0 and ViP 3.0 are compared both from an anatomical and a dosimetrical point of view. A birdcage coil was chosen as an EM source, representing the RF radiation of an MRI scanner. The coil was driven under three different conditions to estimate the absorption dependence on the different excitation types.

II. METHODS

The ViP members – Ella (female, 26 y, 1.63 m and 59 kg), Duke (male, 34 y, 1.77 m and 72.4 kg), Billie (female, 11 y, 1.47 m, 35.4 kg) and Thelonious (male, 6 y, 1.17 and 19.3 kg) from versions 1.0 and 3.0 were selected for the evaluation of MRI exposure. A generic RF body coil with 75-cm coil diameter, 50-cm coil length, 150-cm shield length, and 64 MHz resonance frequency - similar to that of a 1.5T, 70-cm bore imaging system - was used as the RF source for MRI exposure during head imaging. Figure 1 shows the setup of the exposure scenario for all models.

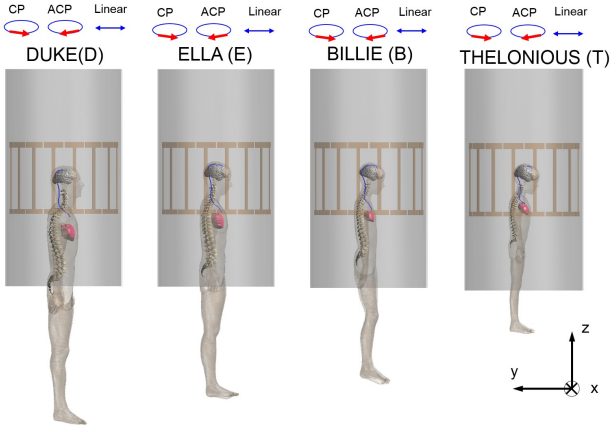

Figure 1. Locations of the models with respect to the generic RF coil. From left to right: Duke, Ella, Bilie and Thelonious.

For each model, three B1-field polarizations were considered: counter-clockwise (about the +z axis) circular (CP) and clockwise circular (about the +z axis) (ACP) and B1 parallel to the y-axis (LIN). The simulation platform SEMCAD X V14.8 (SPEAG, Zurich, Switzerland) and Sim4Life V1.2 (ZMT, Zurich, Switzerland) were used to run the simulation. The models were discretized with the resolution of $(2\ mm)^3$. The tissue dielectric properties at 64 MHz available from [5] were assigned to the models.

III. RESULTS

A. SAR Comparison

We investigated the whole-body SAR (wbSAR), head SAR (headSAR) and the peak spatial SAR averaged over 1 g mass in the head region (ps-headSAR1g). The absorption was evaluated at a fixed $B1_{RMS}$ field strength of 7 μT at the iso-center of the RF coil – which corresponds to the $B1_{RMS}$ limits of the commercial scanners [6]. The wbSAR, headSAR, and ps-headSAR1g show differences of up to 0.45 dB for all models and all exposure conditions – less than the estimated uncertainty of SAR evaluation of 1 dB.

B. Local Induced Power Deposition by a Generic DBS

In order to estimate the local effect caused by the different local tissue distributions, we extract and compare the tangential E-fields along two generic routing paths of a DBS: routing through left- (DBS-L) and right- (DBS-R) side of the cranium. The ViP 1.0 and ViP 3.0 show similar magnitude and phase of the tangential E-fields along the DBS clinical routings. Figure 3 illustrates the RMS magnitude and phase of the tangential E-fields at the $B1_{RMS}$ limit (7 µT) of CP exposure from the 'Ella' model.

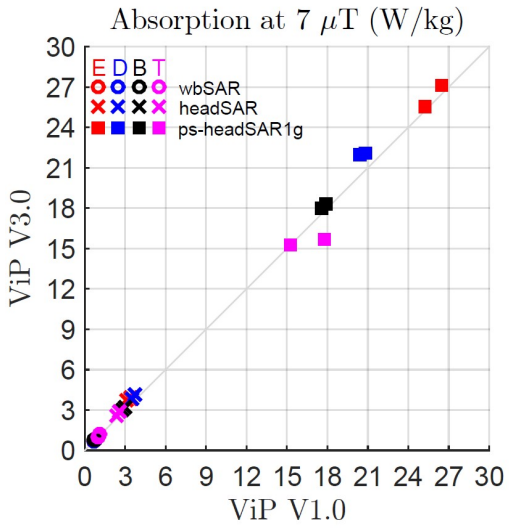

Figure 2. SAR comparison of Ella (E), Duke (D), Billie (B) and Thelonious (T). For each model, three B1-field polarizations are depicted.

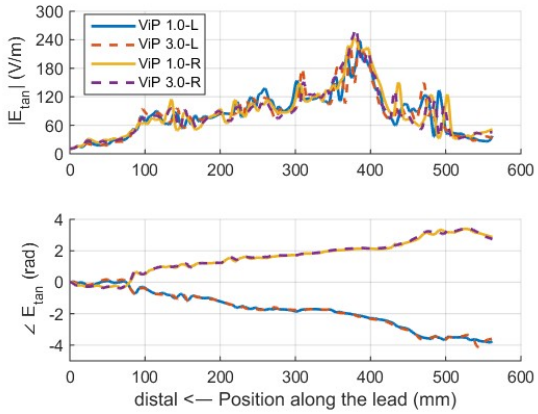

Figure 3. RMS magnitude and phase of the tangential E-fields along generic DBS clinical routings on left side (DBS-L) and right side (DBS-R)

We quantify the effect that the differences in the local E-fields distribution have on the potential RF-heating of medical implant, using a generic 40 cm-long DBS with similar construction to that described in [3]. The predictive model from [3] and the tangential E-fields obtained from ViP 1.0 and 3.0 were used to evaluate the Tier 3 [6] RF-induced heating of the considered implant. Figure 4 summarizes the results. The difference in the power deposition between ViP 1.0 and 3.0 are less than the estimated uncertainty of 1 dB, with the largest variation of 0.4 dB in the 'Duke' model.

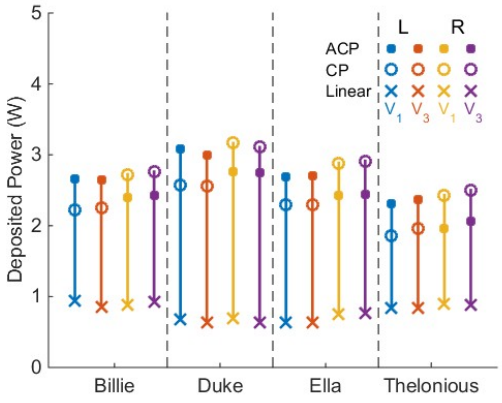

Figure 4. Predicted Tier 3 power deposited in brain tissue, evaluated for the four ViP models and for three B_1 polarizations.

IV. CONCLUSION

We evaluated the differences of ViP 1.0 and ViP 3.0 models for the application of RF exposure assessment during MRI. The local- and global- average SAR values are compared in four ViP models under three B1-polarizations at the head imaging position. The induced electric field distributions along generic DBS clinical routings for the same imaging position were used to estimate the power deposited inside the brain. No significant differences were found in the estimated power deposition by the generic implant or in the average SAR, for all considered exposure conditions. In summary, the differences in the integral results (average SAR and Tier 3 power deposition) for head-focused exposure and safety assessment applications obtained with the ViP 1.0 and 3.0 models are smaller than the associated uncertainty of these quantities. Nevertheless, the ViP 3.0 offers higher anatomical precision than the ViP 1.0 and thus, more suitable for assessment of locally induced effects and should be used in any future evaluations.

REFERENCES

[1] A. Christ, W. Kainz, G.E. Hahn, K. Honegger, M. Zefferer, *et al.*, "The Virtual Family—development of surface-based anatomical models of two adults and two children for dosimetric simulations," *Phys. Med. Biol.*, 59, pp. 5287–5303, 2014.

[2] A. Grässl, W. Renz, F. Hezel, M. Dieringer, L. Winter, *et al.*, "Modular 32-channel transceiver coil array for cardiac MRI at 7.0T," *Magnet. Reson. Med.*, 72(1), pp. 276-290, 2014.

[3] E. Zastrow, E. Cabot, and N. Kuster, "Assessment of local RF induced heating of AIMDs during MR exposure," General Assembly and Scientific Symposium (URSI GASS), 2014.

[4] M.C. Gosselin, E. Neufeld, H. Moser, E. Huber, S. Farcito, *et al.*, "Development of a new generation of high-resolution anatomical models for medical device evaluation: the Virtual Population 3.0," *Phys. Med. Biol.*, 59, pp. 5287–5303, 2014.

[5] P.A. Hasgall, F. Di Gennaro, C. Baumgartner, E. Neufeld, *et al.*, "IT'IS database for thermal and electromagnetic parameters of biological tissues" Version 2.6, IT'IS Foundation, 13 Jan. 2015. Web. 7 Mar. 2015. (www.itis.ethz.ch/database).

[6] ISO/IEC TS 10974:2012: Assessment of the safety of magnetic resonance imaging for patients with an active implantable medical device. International Organization for Standardization, Geneva, Switzerland.

Generating Useful Images for Medical Applications from the Visible Korean

Min Suk Chung*

Department of Anatomy, Ajou University School of Medicine, Suwon, Republic of Korea

*Corresponding author: dissect@ajou.ac.kr

Abstract **-** For the Visible Korean, a male cadaver was serially ground off to acquire the serially-sectioned images of a whole human body. Thereafter, more than 900 structures in the sectioned images were outlined to produce detailed segmented images; the sectioned images and segmented images were volume- and surface-reconstructed to create three-dimensional models. The Visible Korean data, distributed worldwide, encouraged researchers to develop the virtual dissection and computational phantom contributing to medical education and clinical practice.

Index Terms **-** medical applications, Visible Korean, sectioned images, segmented images, three-dimensional images

I. INTRODUCTION

In the United States, sectioned images of the whole human body, namely Visible Human Project data, were made with male and female cadavers [1]. The sectioned images with high resolution and real body color can be the source of realistic three-dimensional (3D) images, which cannot be made from alternative images such as CTs and MRIs. Techniques used for the Visible Human Project were upgraded in Korea for the Visible Korean (VK) [2]. The improved technology of the VK induced an increasingly good quality of the sectioned images, segmented images, and 3D models. The objective of this paper is to announce the availability of the sectioned images, segmented images, and 3D models from the VK, which might be the source of software for medical education and clinical training.

II. METHODS

A. Serial-sectioning to acquire a sectioned images; outlining to acquire segmented images

Before serial-sectioning, MRIs and CTs of a male cadaver were acquired, which would correspond to sectioned images. The whole body was serially-sectioned at 0.2 mm intervals. After serial-sectioning, the sectioned surfaces were photographed using digital camera to acquire sectioned images with 0.2 mm sized pixels [2].

More than 900 structures were outlined in the sectioned images (1 mm intervals) to prepare segmented images. The outlining was performed with Adobe Photoshop CS3 version 10 [3].

B. Volume reconstructing to create 3D models

In the case of the VK data, we could build a volume 3D image with 3,040 × 2,008 × 8,590 voxels, which would be too big to handle by current standard computers. Therefore, the voxel size of the sectioned images was increased from 0.2 mm to 1 mm. At the same time, the corresponding segmented images were prepared with 1 mm voxel size. Using the sectioned images and segmented images, isotropic volume 3D images were created using the computer language C++ [2].

C. Surface reconstructing to create 3D models

Surface reconstruction was achieved by using the commercial software including Alias Maya version 7.0 (Maya) and so on. For the surface reconstruction, only segmented images were necessary with the sectioned images excluded. Outlines of a structure from the neighboring segmented images were stacked; gaps between the outlines were filled with polygons to build a surface 3D model; the stacked outlines were deleted and the polygons were reduced in number to smooth the surface [4].

III. RESULTS

A. Acquiring sectioned images and segmented images

In 2001, a complete male cadaver was serially-sectioned to acquire 8,590 sectioned images with 3,040 × 2,008 resolution and 24 bit color, which took three months. More than 900 structures from the head to feet were outlined, which took eight years (Figure 1.). The VK data including all sectioned images and segmented images have been distributed worldwide free of charge.

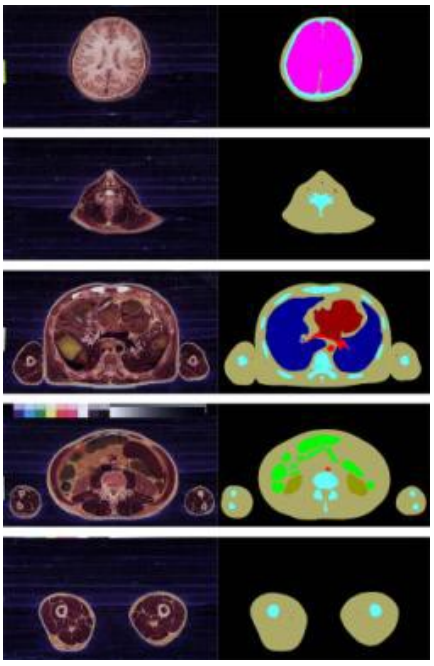

Figure 1. Corresponding serially-sectioned images and segmented images of the complete cadaver

We developed browsing software for the sectioned images, MRIs, CTs, and segmented images (1 mm intervals). In this software, the four kinds of images always corresponded to one another; they could be conveniently chosen with a graphic user interface (Figure 2) [5].

B. Creating volume models

In the composed software, the 3D models of selected structures were displayed and rotated with the real anatomical color shown. The 3D images were sectioned to display sectional surfaces (Figure 2) [2].

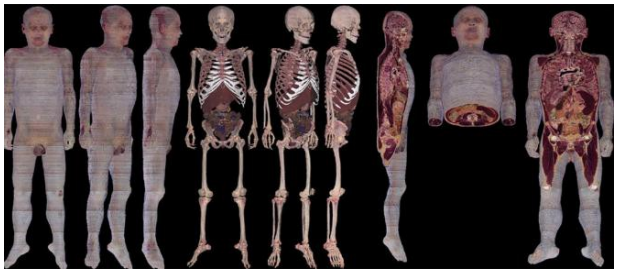

Figure 2. Volume models of complete cadaver, which are selected, rotated, and sectioned

C. Creating surface models

Three-dimensional surface models of various regions were created from the segmented images of VK. The models could be selected, rotated, and colored in a real time because of the small data size (Figure 3) [2]. They were inserted to a PDF file, where various organs of a whole body could be explored in varying manners. The PDF file is expected to be used as a satisfactory self-learning tool of anatomy [6].

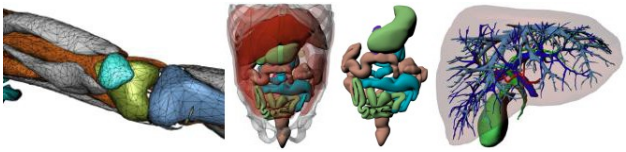

Figure 3. Surface models of lower limb, abdomen, gastrointestinal tract, and liver (left to right)

D. Applications

One application of the VK data was to make a polygon-surface phantom (PSRK-Man, polygon-surface reference Korean-Man), which was adjusted to the reference Korean data (Figure 4) [7].

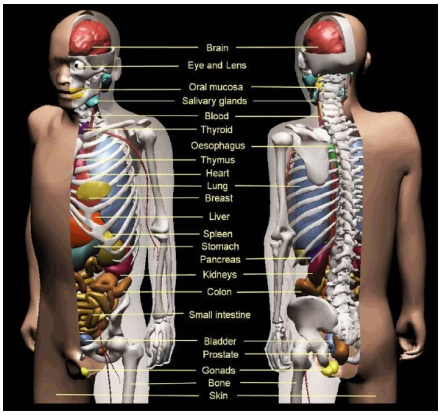

Figure 4. PSRK-Man tomographic polygon phantom

For more applications, other data from the female whole cadaver are being completed by the VK team.

IV. CONCLUSION

The VK data, which are being distributed worldwide, are expected to contribute to medical learning and clinical practice. Most information and data are downloadable freely from the homepage (http://anatomy.co.kr/).

REFERENCES

[1] V. M. Spitzer, M. J. Ackerman, A. L. Scherzinger, and D. G. Whitlock, "The Visible Human Male: A technical report," *J Am Med Inform Assoc*, vol. 3, pp. 118-130, 1996.

[2] J. S. Park, M. S. Chung, S. B. Hwang, Y. S. Lee, D. H. Har, *et al.*, "Visible Korean Human. Improved serially-sectioned images of the entire body," *IEEE Trans Med Imaging*, vol. 24, pp. 352-360, 2005.

[3] D. S. Shin, J. S. Park, H. S. Park, S. B. Hwang, and M. S. Chung, "Outlining of the detailed structures in sectioned images from Visible Korean," *Surg Radiol Anat*, vol. 34, pp. 235-247, 2012.

[4] J. S. Park, D. S. Shin, M. S. Chung, S. B. Hwang, and J. Chung, "Technique of semiautomatic surface reconstruction of the Visible Korean Human data using commercial software," *Clin Anat*, vol. 20, pp. 871-879, 2007.

[5] D. S. Shin, M. S. Chung, H. S. Park, J. S. Park, and S. B. Hwang, "Browsing software of the Visible Korean data used for teaching sectional anatomy," *Anat Sci Educ*, vol. 4, pp. 327-332, 2011.

[6] D. S. Shin, M. S. Chung, J. S. Park, H. S. Park, S. Lee, *et al.*, "Portable document format file showing the surface models of cadaver whole body," *J Korean Med Sci*, vol. 27, pp. 849-856, 2012.

[7] C. H. Kim, J. H. Jeong, W. E. Bolch, K. W. Cho, and S. B. Hwang, "A polygon-surface reference Korean male phantom (PSRK-Man) and its direct implementation in Geant4 Monte Carlo simulation," *Phys Med Biol*, vol. 56, pp. 3137-3161, 2011.

A Comprehensive Database of Physical Tissue Properties for Computational Simulations in Realistic Virtual Anatomies

Christian Baumgartner[1,*], Esra Neufeld[1], Davnah Payne[1], and Niels Kuster[1,2]

[1]IT'IS Foundation, Zurich, Switzerland
[2]ETH Zurich, Zurich, Switzerland

*Corresponding author: baumgartner@itis.ethz.ch

Abstract **-** Numerical simulations performed with computational anatomical models are only meaningful if realistic biological, physiological, and physical properties can be assigned to individual body tissues. Here we present a publicly available literature-based database of tissue properties for computational life sciences applications which includes averaged estimates and statistical information about the spread and standard deviation.

Index Terms **-** body tissues, physical properties, online database, computational life sciences

I. INTRODUCTION

Numerical modeling is rapidly becoming the preferred approach for designing new therapies, novel diagnostic methods, and next-generation medical devices. Yet the modeling of devices or diagnostic and therapeutic tools has until recently been performed only in simplified environments, which considerably compromises the transferability of results to systems consisting of living tissues and organs. Accordingly, the application of simulations for safety and efficacy evaluations in view of supporting regulatory submissions and extending or partially replacing experimental investigations and clinical studies has been limited. Overcoming this limitation has required significant progress in two areas: in the numerical tools themselves, which are now able to handle the full complexity of the human anatomy and are optimized for modeling living tissue, and in the computational phantoms used as a simulation environment, which have evolved from stylized models to extremely detailed models (reviewed in [1]).

Yet, powerful solvers and high-resolution anatomical models are not yet sufficient to achieve satisfactory levels of realism in computational simulations. Simulations of biological, physiological, or physical processes are only meaningful if appropriate properties are assigned to individual body tissues. Hence, recent progress in computational life sciences and in computational phantoms has emphasized the importance and the necessity for a reliable database of bio-physiological and bio-physical tissue properties, whereas the growing adoption of uncertainty budgets have generated the need for salient details on parameter variability.

Here we present a comprehensive, publicly available, and evolving database of tissue properties that includes dielectric properties and values of density, heat capacity, thermal conductivity, heat generation rate, transfer (perfusion) rate, low frequency electrical conductivity (including information about anisotropy in fibrous tissues), viscosity, and ultrasound propagation, absorption, and non-linearity for more than 100 biological tissues. This database represents to the best of our knowledge the only comprehensive resource available free of charge to the computational modeling community.

II. METHODS

A. General considerations and search strategy

The values are based on an extensive review of the literature but a few sources served as starting point for our search. These sources include the original SEMCAD X thermal properties database, which included values from sources such as Duck [2] and Williams and Leggett [3], the extensive dielectric tissue properties measurement from Gabriel [4], and McIntosh and Anderson's [5] review of thermal properties and blood perfusion. Williams and Leggett [3] also served as our main source of data on blood perfusion. The original SEMCAD X tissue properties database was compiled based on a dozen publications around 2004. The more systematic literature search started in 2011 and is ongoing. Besides rigorously screening all papers citing [2-5] for new values and relevant references, search is performed on PubMed and the ISI Web of Knowledge, using each individual property and tissue as keywords in combination with more generic ones such as "property", "biological", "human", with the name of the animal species used as a proxy for the human data, and with property-specific keywords such as "specific gravity" for density; "heat conduction", "thermal resistivity", and "thermal conduction" for thermal conductivity for example. Additional articles are selected from the bibliographies of all retrieved and retained publications. Other parameters are found by searching for specific applications, e.g., transcranial alternating current stimulation, in view of information about low frequency electrical properties.

B. Inclusion and exclusion criteria

To be retained as a possible source, scientific articles and books have to contain information about the species in which the measurements were performed, and the measurement methods and conditions. This information needs to be sufficient to determine whether any value can safely be used in humans and whether the methods are reliable. The absence of information about the direction of the low frequency conductivity measurement is not an exclusion criteria. Data collected during *in vivo* experiments, or on freshly excised tissue are preferred. Data collected on deceased individuals or on preserved tissues are excluded, unless strictly no other data are available and no substitution appears meaningful (see below). Human data are preferred over animal ones but they are limited. Experimental data collected at body temperature are preferred over those collected at room temperature. Data collected under arguably non-physiological temperature conditions are excluded.

C. Additional decision factors

When no reliable data is available for a given property and a given tissue, substitute values are chosen based on histological, physiological, and biological resemblances between tissues. Substitute values are either taken from one other tissue or in rare cases correspond to an average over multiple tissues. When a substitution is needed, the same substitute tissue is used for all the properties for which no raw data is available, whenever possible. When no sufficient resemblance exists with any tissue, a specific property can remain unavailable for a given tissue.

D. Quality assurance

Before including new data points, care is taken to assess by how much the new average value would change as compared to the previous database version. Any addition resulting in a change of 5% or more leads to a reevaluation of all the values currently used for a given property and tissue. Changes are also monitored over time by comparing averages across all releases. All modifications performed since the release of the first online database version are documented in a log file available online and justifications are formulated in an internal document available upon request.

E. Outreach

The public forum associated to the database offers the users the chance to ask questions, suggest improvements, or contribute with additional values. Any suggestion for additional values needs to be provided with a proper reference in view of quality control and citation.

III. RESULTS

The values we provide [6] consist of density, heat capacity, thermal conductivity, heat transfer (perfusion) rate, heat generation rate, dielectric properties, low frequency electrical conductivity, viscosity, and of ultrasound propagation, absorption, and non-linearity. Values are typically provided at body temperature. All values are available for online viewing and can be downloaded in various formats [7]. Additional documents available for download are a) a summary of all general considerations, remarks, and known issues regarding the database; b) the rational for each tissue substitution; c) previous versions of each database; d) a log file documenting the changes between versions; e) the list of all publications used to generate the database; and f) two tables including the specific references associated with each tissue and each property for which we provide a value. The database is automatically synchronized with our Virtual Population V1.x and V3.x models to maximize model usability and minimize human error when setting up simulations.

A unique feature of our database is that it provides averaged estimates and statistical information about the spread and standard deviation for the different thermal, density, perfusion, and rheological parameters. This information is crucial as the uncertainty and variability of material parameters contribute to the uncertainty and the variability associated with the simulated quantity of interest. For some material parameters, e.g., perfusion, the variation can be more than an order of magnitude, which can severely affect the simulation results. The number of data points from which the average for a given property and tissue is calculated varies between one and 88 and is provided for each tissue and property.

The IT'IS material parameter database is an evolving web resource. Accordingly we rely on input from database users and on contributions via our online forum. This forum is designed for users to suggest additional references, to question the assumptions behind the current values, and to discuss possible improvements.

IV. CONCLUSION

The IT'IS database is an open-access repository of electromagnetics, thermal, perfusion, density, fluid and acoustic properties of biological tissues. Additional data points are added as they become available but our priority is to include additional properties including, optical properties, and T1/T2 relaxation times. We strongly encourage users to contribute to this database and become members of a growing community.

REFERENCES

[1] X. G. Xu, "An exponential growth of computational phantom research in radiation protection, imaging, and radiotherapy: A review of the fifty-year history," *Phys. Med. Biol.*, vol. 59(18), pp. R233-R302, 2014.

[2] F. A. Duck, "Physical properties of tissue: a comprehensive reference book," *Medical Physics*, vol. 18, London, 1990

[3] L. R. Williams and R. W. Leggett, "Reference values for resting blood flow to organs of man," *Cl. Phys. Phys. Meas.*, vol. 10, pp.187–217, 1989

[4] C. Gabriel, "Compilation of the dielectric properties of body tissues at RF and microwave frequencies." *Report N.AL/OE-TR-1996-0004*, Brooks Air Force Base, 1996

[5] R. L. McIntosh and V. Anderson, "A comprehensive tissue properties database provided for the thermal assessment of a human at rest," *Bio-phys. Rev. Let*, vol. 5(3), pp.129–151, 2010.

[6] Hasgall PA, Di Gennaro F, Baumgartner C, Neufeld E, Gosselin MC, Payne D, Klingenböck A, Kuster N, "IT'IS Database for thermal and electromagnetic parameters of biological tissues," Version 2.6, January 13th, 2015.

[7] http://www.itis.ethz.ch/database

Poster Session

Counting Efficiency Calibration of Stand-up Type Whole-body Counter Using BOMAB and ICRP Phantoms

Jaeryong Yoo[1,2], Seyoung Park[1], Seokwon Yoon[1], Wi-Ho Ha[1], Seung-Sook Lee[1], and Kwang Pyo Kim[2,*]

[1]National Radiation Emergency Medical Center, Korea Institute of Radiological and Medical Sciences, Seoul, Republic of Korea
[2]Department of nuclear engineering, Kyung Hee University, Gyenggi-do, Republic of Korea

*Corresponding author: kpkim@khu.ac.kr

Abstract - A Whole-body counter is commonly used to measure radioactive materials in the human body. To improve efficiency calibration of a whole-body counting system, the counting efficiencies by phantom types were compared. Counting efficiencies of a whole-body counter were calculated by simulating the whole-body counter and calibration phantoms using MCNPX code. BOMAB and ICRP reference phantoms were used for the calculation. The counting efficiencies calculated by BOMAB male phantom and ICRP reference male were well agreed with relative bias less than 5%. However, there was about 10% difference in counting efficiencies for female. Although geometry and material composition of the BOMAB phantoms were simple, they could well represent real human body for the calibration purpose of a whole-body counter.

Index Terms - Whole-body counter, efficiency calibration, BOMAB phantom, ICRP reference phantom

I. INTRODUCTION

In the event of a radiation emergency, it is required to assess radionuclide intake and internal radiation dose for the internally contaminated victims. The internal radiation dose depends on type and amount of intake radionuclide. Direct or indirect measurement methods are available for the radionuclides in the human body. In vivo bioassays are commonly used to measure radioactive materials in the human body directly via whole-body. To use the whole-body counter, counting efficiency should be calibrated using anthropomorphic physical phantom in advance. The Bottle Manikin Absorber (BOMAB) phantoms have been widely used for efficiency calibration [1, 2].

The BOMAB phantoms are filled with radioactive material dissolved in acidic solution homogeneously. The BOMAB phantom can not reflect the anthropomorphic as there are no bones, internal organ, or tissue substitutes [3]. Therefore, it is expected that the uncertainty could be exist in the efficiency calibration using the BOMAB phantom. Several studies suggested the possibility of whole-body counter efficiency calibration using computational simulation methods [3]. However, the simulation methods could adjust only their own whole-body counting systems. The National Radiation Emergency Medical Center (NREMC) in Korea Institute of Radiological and Medical Sciences (KIRAMS) was constituted to prepare a countermeasure of medical preparedness and response involved in nuclear and radiological disaster. The NREMC performs intake and dose assessments for internally contaminated victims. The objectives of this study were to improve efficiency calibration of the whole-body counting system in KIRAMS using radiation transport code.

II. METHODS

A. Whole-body counting system

A stand-up type whole-body counter (model 2250, CANBERRA Ind., CT, USA) was used in this study. The system composed of two NaI(Tl) detectors (7.6 × 12.7 × 40.6 cm) and 10 cm-thick shield. The detection range of this system varies from 300 keV to 1,800 keV. For internal contamination monitoring, the subject stands in the whole-body counter facing the front direction. The subject leans against the rear surface of the whole-body counter.

B. BOMAB phantom

The BOMAB phantom is standard anthropomorphic physical phantom for whole-body counter efficiency calibration [4]. The BOMAB phantoms consist of cylinder or elliptical cylinder- shaped bottles representing, head, neck, chest, abdomen, arms, thighs, and calves. The material of bottle is polyethylene (PE). The side wall thickness of bottle is 0.5 cm and the top and bottom thickness are 2.5 and 1 cm, respectively. American National Standards Institute/Health Physics Society (ANSI/HPS) N13.30 standard provides the specifications for the each size of the BOMAB phantom such as reference male (BMP) and reference female (BFP). The BMP is 170 cm tall with a weight of 70 kg and BFP is 161 cm tall with a weight of 50 kg.

C. ICRP phantom

ICRP computational phantoms are described in ICRP publication 110 [5]. The ICRP reference phantoms were developed based on medical image data of real people. The ICRP reference phantoms consist of the skin, muscle tissue, soft tissue, adipose tissue, lungs, the wall organs (stomach, intestine etc.) and bones.

The ICRP reference male phantom (IMP) is 176 cm tall with a weight 73 kg and the reference female phantom (IFP) is 163 cm tall with a 60 kg. The IMP was segmented into 220, with a voxel resolution of 8 × 2.08 × 2.08 mm^3. The voxel volume of reference male is 34.6 mm^3. For IFP was segmented into 346 slices (had and trunk's width was 5-mm whereas, legs were sliced 20-mm and then intermediate slices of 5-mm width were obtained by interpolation) with a voxel resolution of 5 × 1.875 × 1.875 mm^3. The voxel volume of reference female is 17.6 mm^3. The total skin volume of the IMP is 3728.0 g and IFP is 2721.5 g. That is about 5% of total weight in both genders (3.728 kg of 73 kg in male and 2.721 kg of 60 kg in female)

POSTER

D. Simulations using Radiation Transport Code

The whole-body counter and phantoms were simulated using Monte Carlo N-Particle eXtended (MCNPX) code for efficiency calculation. The full energy peak efficiency of the NaI(Tl) detectors was determined from each simulation using the F8 tally. The history was 109 and simulated to achieve results with statistical uncertainties below 5% (k = 1). The following energies were simulated for both BOMAB and ICRP phantoms: 88 keV, 122 keV, 165 keV, 392 keV, 662 keV, 898 keV, 1,173 keV, 1,332 keV and 1,836 keV.

The radioactive materials inside the BOMAB phantoms were assumed to be distributed homogeneously. The ICRP reference phantoms were modified to make the same simulation conditions with the BOMAB phantoms: The material compositions of all internal organs (except skin) were assumed to be water [3].

III. RESULTS AND DISCUSSION

The counting efficiencies of a whole-body counter calculated by BOMAB and the ICRP phantoms are given in Figure 1. The efficiencies of the reference males using BOMAB phantom and ICRP phantom were very similar. Relative bias was less than 5%. Therefore, BOMAB phantom could well represent reference male from the aspect of counting efficiency of a whole-body counter.

The counting efficiency of a whole-body depended on phantom size and weight. The efficiency of the BFP was highest among the phantoms used in this study. It could be attributes to its smallest phantom size. The efficiencies of BMP, IMP and IFP were similar. Relative bias was less than 5%. However, the efficiency of BFP was higher than BMP by about 10% under photon energy of 600 keV. The BFP's weight was 50 kg that was about 70% of BMP's weight (70 kg).

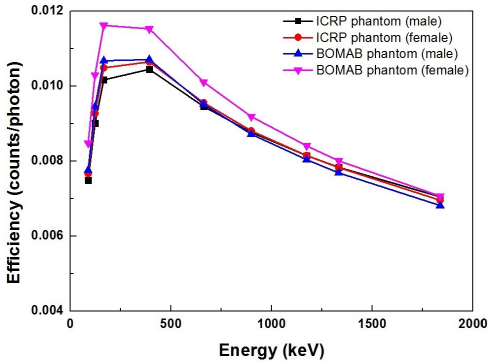

Figure 1. Counting efficiency for ICRP and BOMAB phantom (male and female reference phantom); the phantom filled with water

Figure 2 shows the counting efficiencies of the ICRP phantoms by material composition of internal organs and tissues. The first case assumed that all internal organs and tissues were water to make the similar situation with BOMAB phantom. The second case used ICRP material composition to make the similar situation with real human measurement. The efficiency curves of the two different cases were similar. The relative biases were less than 3% in both genders. Therefore, simple geometry and material composition (water-filling) of the BOMAB phantoms well represented real human body from the aspect of counting efficiency of a whole-body counter.

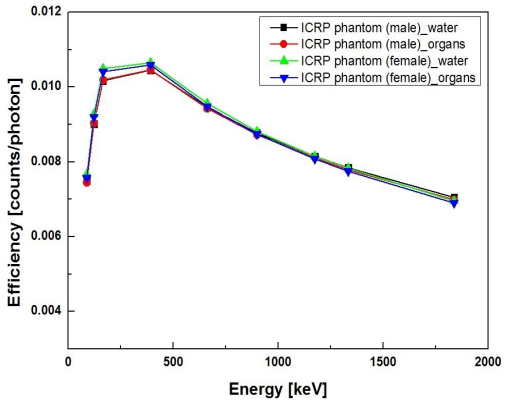

Figure 2. Counting efficiency of the ICRP phantoms in both genders; Material composition of all internal organs and tissues vs. water-filled

Distribution of intake radionuclide in human body depends on its biokinetics. Some radionuclides are selectively concentrated on a certain organ or some radionuclides are homogeneously distributed in human body. Therefore, radionuclide behavior in human body should be considered when calibrating counting efficiency of a whole-body counter.

IV. CONCLUSION

Counting efficiencies of a whole-body counter were calculated by simulating the whole-body counter and calibration phantoms using a radiation transport code. BOMAB male phantom could well represent male human body for calibration purpose. However, there was about 10% difference in counting efficiencies for female. In addition, simple geometry and material composition of the BOMAP phantoms could well represent real human body for the calibration purpose.

REFERENCES

[1] K. Capello, S Kedizior, and G. H. Kramer, "Voxel phantoms: The new ICRP computational phantoms: How do they compare?," *Health Physics Society*, Vol. 102 (6), pp. 626-630, 2012.

[2] J. Bento, S. Barros, P. Teles, P. Vaz, and M. Zankl, "Efficiency correction factors of an accuscan whole-body counter due to the biodistribution of 134Cs, 137Cs and 60Co," *Radiation Protection Dosimetry*, Vo. 155 (1), pp. 16-24, 2013.

[3] B. Zhang, M. Mille, and X. G. Xu, "An analysis of dependency of counting efficiency on worker anatomy for in vivo measurements: whole-body counting," *Physics in Medicine and Biology*, Vol. 53, pp. 3463-3475, 2008.

[4] American National Standards Institute/Health Physics Socoety, "Specifications for the Bottle Manikin Absorption Phantom," *McLean, VA: Health Physics Society*; ANSI/HPS N13.35 1999; 1999.

[5] International Commission on Radiological Protection. Adult reference computational phantoms, Oxford: Pergamon Press; *ICRP Publication 110*, 2009.

Anatomically Realistic Computer Phantom Modeling of Human Fetuses at Various Stages of Pregnancy for Dosimetry Study

Tomoaki Nagaoka[1,*], Tetsu Niwa[2], and Soichi Watanabe[1]

[1]Electromagnetic Compatibility Laboratory, National Institute of Information and Communications Technology, Koganei, Japan
[2]Department of Radiology, Tokai University School of Medicine Isehara, Japan

*Corresponding author: nagaoka@nict.go.jp

Abstract **-** The numerical dosimetry study on fetuses is one of the most important issues in electromagnetic field safety. In this study, we acquired fetal MRI images from pregnant women during the second and third trimesters of pregnancy and newly developed nine computational fetal models at various stages of pregnancy on the basis of the acquired images. The fetal models consist of about 20 different tissue types. These tissues were classified by medical staffs using both manual and semiautomatic segmentation techniques from fine-resolution images acquired by 3D-ture FISP (Fast Imaging with State Precession) sequence. The number of tissues and the spatial resolutions of the fetal models are better than those of models previously developed.

Index Terms **-** fetus, computational human model, EMF safety, specific absorption rate, magnetic resonance imaging

I. INTRODUCTION

Concerns regarding the adverse health effects of human exposure to radio-frequency (RF) electromagnetic fields (EMFs) have been increasing. The safety of RF-EMF is evaluated on the basis of specific absorption rate (SAR). Recently, we have carried out a detailed SAR estimation by numerical simulation using computational human models [1-3]. The SAR dosimetry on a fetus during pregnancy is one of the most important issues in EMF safety. For the dosimetry study, pregnant female models at various gestational ages are required, because the abdominal body types of pregnant females and the anatomical structures of gestational tissues including fetal tissue vary with fetal growth. There are a few reports on the development of pregnant female models at different gestational ages [4-7]. However, previous attempts have not realized anatomically correct fetal structures.

In this study, we newly acquired fetal images with fine resolution at various gestational ages by magnetic resonance imaging (MRI) scanner and developed high-fidelity anatomically realistic fetal models from acquired images.

II. DEVELOPMENT OF HIGH-FIDELITY FETAL MODELS

A. Fetal MRI acquisition

We have some problems in fetal MRI with fine resolution. One of the problems is motion artifact due to motions of the fetal and maternal organ (i.e. respiratory motion and bowel movement). The motion artifacts make it difficult to identify the fetal tissues. And also, it is difficult to acquire signals from very small regions and to scan a long time for pregnant woman. Therefore, the sequences of fetal MRI with fine resolution were decided after considering these problems and limitations.

In this study, fetal MRI acquisitions were performed by 3D-ture-FISP (Fast Imaging with State Precession) and BLADE sequences. Figure 1 shows the typical examples of the fetal MRI images. 3D-ture-FISP (Fast Imaging with State Precession) is easier to identify the continuity of the fetal tissues. Scan time is also short for the sequence. However, the sequence is lower contrast compared to the 2D-sequence. On the other hand, BLADE can be acquired the motion correction images without breath-holding, though difficult to assess the continuity of the tissues and organs. The tissue contrast of the images acquired by BLADE is higher than that by 3D- sequence (i.e. 3D-ture-FISP). Therefore, we can more clearly identify the fetal tissues. Fetal MRI images in the second and third trimesters of pregnancy were taken using a 1.5 T MRI scanner in the Kanagawa Children's Medical Center (KCMC). In this study, imaging plane is coronal to pregnant woman. Acquisition times of 3D-ture-FISP and BLADE are 13 seconds × 3 times and 4 minutes respectively.

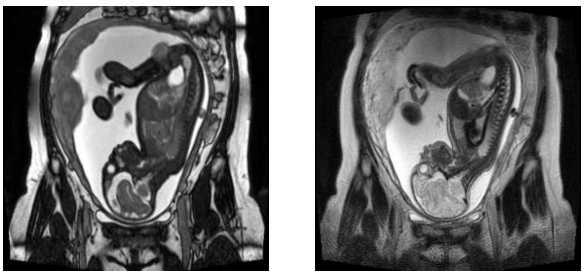

3D-ture-FISP image BLADE image

Figure 1. Fetal MRI images

B. Classification of fetal tissue

Figure 2 shows the process flow of tissue classification from acquired fetal MRI images. Classifications of the gestational tissues including fetal tissues were actually performed on the basis of 3D-ture-FISP images. BLADE images were used as reference images for identifying the gestational tissues from the 3D-ture-FISP images. The classification were also performed on the basis of acquired data under the supervision of a pediatric radiologist.

First, the image noise was removed by smoothing filter processing. Second, semiautomatic approximate classification was performed by identifying the parts that could be relatively easily classifiable by basic image segmentation methods. Finally, to obtain a detailed classification, the roughly classified image was

POSTER

manually edited by medical staff members using voxel editing software (Slice Omatic ver. 4.3).

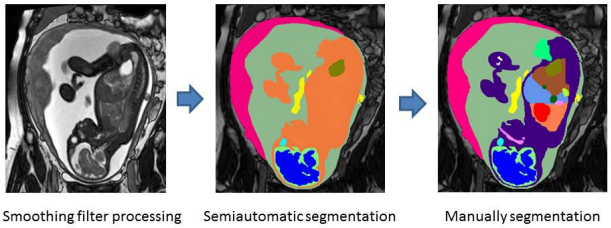

Figure 2. Process flow tissue classification

III. CHARACTERISTICS OF FETAL MODELS

We developed nine fetal models during second and third trimesters of pregnancy. As an example of volume-rendered display of the fetal model we developed, Figure 3 shows that at gestational ages of 33 weeks. Table 1 also shows the outlines of fetal models.

The developed fetal models are those at gestational ages of 20, 23, 26, 29, 32, 33, 36 and 37 weeks. The fetal models of No. 6 and 7 were constructed on the basis of the data from patients of the KCMC, and the other models were also constructed on the basis of fetal MRI data from health volunteers. The fetal models of No. 1, 3 and 4 were developed on the basis of the MRI data from the same volunteer. The models of No. 5 and 8 were also based on the MRI data from the same volunteer.

The fetal models consist of about 20 different tissue types including amniotic fluid, placenta, umbilical cord, brain, CSF (cerebrospinal fluid), eyeball, lens, lung, stomach, liver, heart, kidney and intestine. These models are composed of voxels of approximately 1.48 × 1.48 × 1.48 mm^3 or approximately 0.74 × 0.74 × 0.74 mm^3. The number of tissues and the spatial resolutions of the fetal models are better than those of the models previously developed [5-7].

Figure 3. An example of volume rendered display of fetal model

Table 1. Outlines of fetal models

No.	Fetal Model			
	Gastational age [weeks]	Resolution [mm]	Number of fetal tissue	Number of other gestational tissues
0	20	0.74	17	3
1	23	0.74	18	3
2	26	0.74	18	3
3	29	0.74	18	3
4	29	0.74	18	3
5	32	0.74	19	3
6	33	1.48	19	3
7	36	0.74	19	3
8	37	0.74	19	3

IV. CONCLUSION

We acquired fetal MRI images with fine-resolution from pregnant women during the second and third trimesters of pregnancy and classified the fetal tissues including gestational tissues from the acquired images by image processing technique and manual editing. Finally, we newly developed the nine fetal models at various stages of pregnancy. These models classified into about 20 different tissue types. The specifications of developed models are better than those of the models previously developed.

ACKNOWLEDGMENT

Parts of this research were supported by the Strategic International Cooperative Program (Joint Research Type), Japan Science and Technology Agency.

REFERENCES

[1] P.J. Dimbylow, "FDTD calculations of the whole-body averaged SAR in an anatomically realistic voxel model of the human body from 1 MHz to 1 GHz," *Phys. Med. Biol.*, vol. 42, pp. 479-490, 1997.

[2] A. Christ *et al.*, "The virtual family development of surface-based anatomical models of two adults and two children for dosimetric simulation," *Phys. Med. Biol.*, vol. 55, pp. N23-N38, 2010.

[3] T. Nagaoka *et al.*, "Development of realistic high-resolution whole-body voxel models of Japanese adult males and females of average height and weight, and application of models to radio-frequency electromagnetic-field dosimetry," *Phys. Med. Biol.*, vol. 49, pp. 1-15, 2004.

[4] P. Dimbylow, "SAR in the mother and foetus for RF plane wave irradiation," *Phys. Med. Biol.*, vol . 52, pp. 3791-3802, 2008

[5] T. Nagaoka *et al.*, "An anatomically realistic whole-body pregnant- woman model and specific absorption rates for pregnant-woman exposure to electromagnetic plane waves from 10 MHz to 2 GHz," *Phys. Med. Biol.*, vol. 52, pp. 6731-6745, 2007.

[6] T. Nagaoka *et al.*, "Anatomically realistic reference models of pregnant women for gestation ages of 13, 18, and 26 weeks," Proc. 30th Ann. Intl. Conf. IEEE EMBS, pp. 2817-2820, Vancouver, British Colombia, Canada, 2008.

[7] P. J. Dimbylow, T. Nagaoka, and X.G. Xu, "A comparison of foetal SAR in three sets of pregnant female models," *Phys. Med. Biol.*, vol. 54, pp. 2755-2767, 2009.

POSTER

RADAR Reference Adult and Pediatric Phantom Series - Nuclear Medicine and CT Dosimetry

Michael G Stabin[1], Diana E Carver[1], Susan D Kost[1], Nicholas D Fraser[1], David R Pickens[1], Ronald R Price[1], W Paul Segars[2]

[1]Vanderbilt University, Dept of Radiology and Radiological Sciences, Nashville, TN, USA
[2]Carl E. Ravin Advanced Imaging Laboratories, Duke University, Durham, NC, USA

*Corresponding author: michael.g.stabin@vanderbilt.edu

Abstract **-** The RAdiation Dose Assessment Resource (RADAR), a task group of the Society of Nuclear Medicine and Molecular Imaging (SNMMI), has developed a new generation of NURBS-based reference phantoms, based on the ICRP 89 reference masses for adults and five pediatric ages, of both genders (12 total) and pregnant women at three stages of gestation, to update photon and electron SAFs for internal emitters originally derived from stylized models. We further extended this phantom series to include pediatric subjects of age 3. 8, and 13 years, and using the 50th-percentile XCAT pediatric phantom models at each age, we developed models representing 10th, 25th, 75th, and 90th percentile models. We calculated SAFs for internal emitters and organ doses and effective doses for chest-abdomen-pelvis CT exams for all phantoms and 40 pediatric subjects previously imaged at our hospital. We then 'matched' a phantom to each of these patients, by gender and a subset of phantoms closest in age. Average torso diameter was used to select the most similar phantom and deemed the ultimate match candidate. The results of matching all 40 patients to the closest phantom in our database resulted in average patient-phantom match organ dose differences from 0.44 to 2.48 mGy and percent differences from 3.6 to 23.1%. For the entire set of patient-phantom matches, the overall average dose difference was 1.1 mGy, and the average overall percent difference was 8.9%.

Index Terms **-** radiation dose, anthropomorphic phantom

I. INTRODUCTION

Development of image-based anthropomorphic phantoms based on NonUniform Rational B-Spines (NURBS) surfaces was performed by Segars [1]. These models are easily deformed; we developed a phantom series based on the ICRP 89 reference masses [2] and generated specific absorbed fractions for internal sources of photons and electrons. We then extended the series to represent pediatric subjects of different age, and calculated organ doses and effective doses for simulate computed tomography (CT) imaging.

II. METHODS

A. Models

We developed a new generation of NURBS-based reference phantoms, based on the ICRP 89 reference masses for adults and five pediatric ages, of both genders (12 total) and pregnant women at three stages of gestation, to update photon and electron SAFs for internal emitters originally derived from stylized models. These are now incorporated in the OLINDA/EXM personal computer software for internal dose calculations. Models for three mouse and five rat models, also based on NURBS technology have been developed, and photon and electron SAFs generated (these are also incorporated in the OLINDA/EXM code). A compendium of dose estimates for many pharmaceuticals is in preparation and will be available soon. We further extended this phantom series to include pediatric subjects of age 3. 8, and 13 years, and using the 50th-percentile XCAT pediatric phantom models at each age, we developed models representing 10th, 25th, 75th, and 90th percentiles using height, weight, and BMI data from CDC growth charts, as well as anthropometric body measurements of children from the United States National Health and Nutrition Examination Survey (NHANES) (80 phantoms). Using this large phantom 'family' we calculated organ doses and effective doses from chest-abdomen-pelvis CT exams, using Monte Carlo methods.

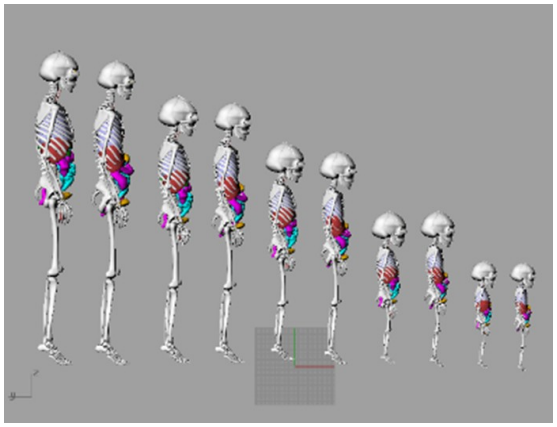

Figure 1. Several 50th percentile NURBS phantoms

B. Calculations

Pediatric patients who had undergone CAP CT scans as part of their routine care at Vanderbilt University Medical Center were chosen from our archives by pediatric radiologists. A total of 40 image sets were selected to represent pediatric patients spanning all ages, weights, and heights. Subjects varied in age from seven months to 17 years (mean 7.8 ± 4.7 years). There were 19 female patients (0-17 years, 9-84 kg) and 21 male patients (0-16 years, 7-100 kg). Simulations of helical CT examinations were performed using a Geant4-based Monte Carlo particle radiation transport code [3]. Specific scanner properties including the photon-energy spectrum, inherent and bowtie filtration, and geometry were incorporated into the simulation. An equivalent

POSTER

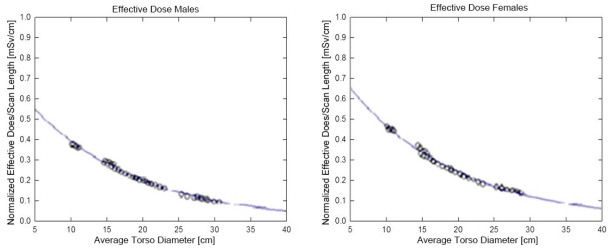

Figure 2. Effective doses for pediatric CAP exams, all ages

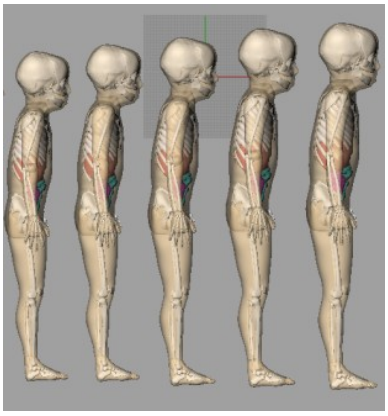

Figure 3. 10th, 25th, 50th, 75th and 90th percentile phantoms for the 5-year old male NURBS model

POSTER

energy-fluence source model for the simulated CT scanner (Philips Brilliance 64, 64 × 0.625 mm^2 collimation) was created following methods in Turner *et al*. This fluence model includes the effects of the body bowtie filter that provides x-ray filtration across the transverse direction of the patient. The simulation has a beam collimation of 42.1 mm based on physical measurements. We tested the 'matching' to 40 pediatric subjects previously imaged, for which we manually segmented many organ regions and performed dose calculations for as well. Patients were first matched by gender and a subset of phantoms closest in age. Because of the strong relationship between organ dose and patient diameter, average torso diameter was next used to select the most similar phantom and deemed the ultimate match candidate.

III. RESULTS

The NURBS models were deformed to represent adults and children of various ages, following the ICRP 89 recommended reference organ and body. The results were normalized to DLP and were well fit by exponential functions. The results of matching all 40 patients to the closest phantom in our database resulted in average patient-phantom match organ dose differences from 0.44 to 2.48 mGy and percent differences from 3.6 to 23.1%. For the entire set of patient-phantom matches, the overall average dose difference was 1.1 mGy, and the average overall percent difference was 8.9%.

ACKNOWLEDGMENT

This work was supported by grant NIH/NCI 1 R01 CA155400-01A1 awarded by the National Institutes of Health, United States Department of Health and Human Services.

REFERENCES

[1] Segars JP, "Development and Application of the New Dynamic NURBS-based Cardiac-Torso (NCAT) Phantom," *Ph.D. Dissertation, The University of North Carolina*, 2001.

[2] Stabin MG, Emmons MA, Segars WP, Fernald MJ, "Realistic reference adult and paediatric phantom series for internal and external dosimetry," *Radiation Protection Dosimetry* 2012:149(1):49-55.

[3] Carver DE, Kost SD, Fernald MJ, Lewis KJ, Fraser ND, Pickens DR, Price RR, Stabin MG, "Development and validation of a GEANT4 radiation transport code for CT dosimetry," *Health Phys*, in press

SPONSORS

(주)래드코어
RADCORE

(주)램텍
REMTECH

NEOSISKOREA Co., Ltd.

(주)핵광산업
NUCLEAR LIGHT INDUSTRY

jiYeoN
medical
(주)지연메디칼

RADCORE

MONTE CARLO RADIATION SAFETY ANALYSIS

- *Scope*
  - *Radiation Shielding Design and Analysis of Bio-Medical Laboratory of Heavy Ion Facility and Radiotherapy Facilities*
  - *Dose Assessment of RI Containers*
  - *Particle Transport Analysis in Nuclear Power Plant*
  - *Environmental Impact Assessment of Nuclear Power Plant*
  - *Criticality Analysis of Nuclear Fuel Storage and Transport Cask*

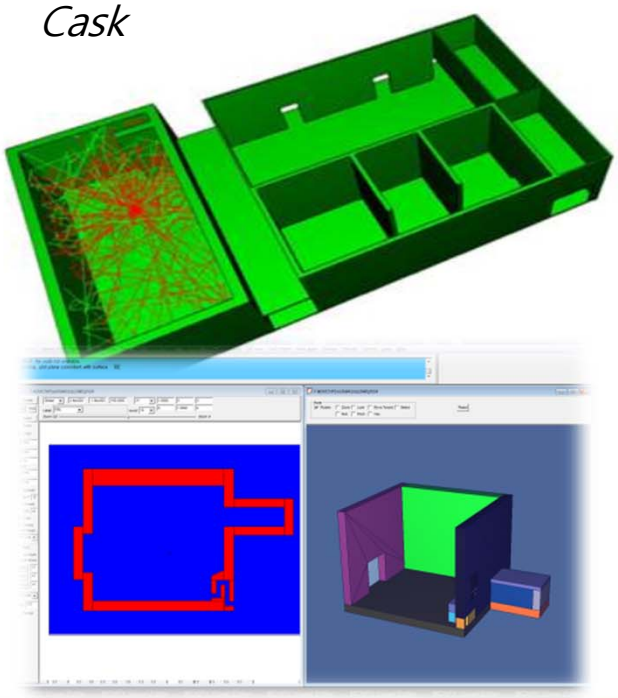

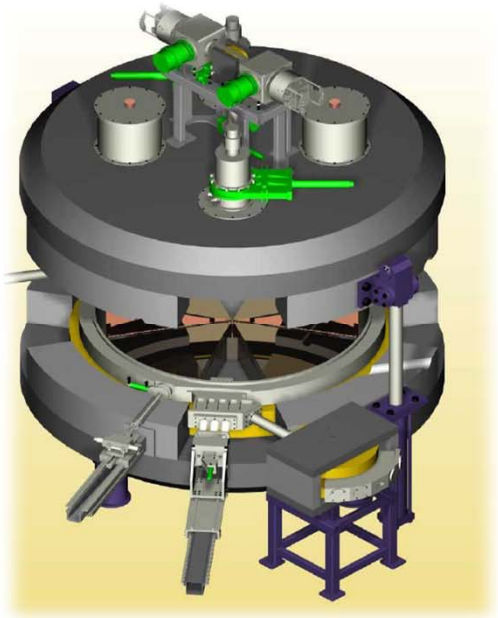

Radiation Core Techonolgies. Co., Ltd.
http://www.radcore.co.kr
E-mail: admin@radcore.co.kr
Tel: +82-42-934-4690
Fax: +82-42-367-0799

Part of ThermoFisher RM&SP

REMTECH

Radiation Environmental Measuring Technology

Since 1989

Introduce REMTECH

- Since 1989, our company has dedicated for customer's health and safe management in radiation field
- Provide a professional service to customers with last 25 years of experience and know-how .

Primary Markets

- Nuclear Power Plants (KHNP)
- Governmental organizations (KINS, KCCH, KAERI, KEPCO NF, etc.)
- Accelerator laboratories (Kyeong-ju, Pohang)
- Security market, Steel & Scrap industry

TLD Reader System

Radiation products

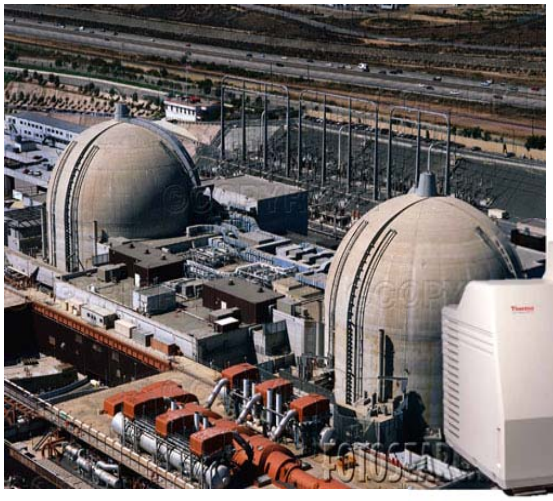

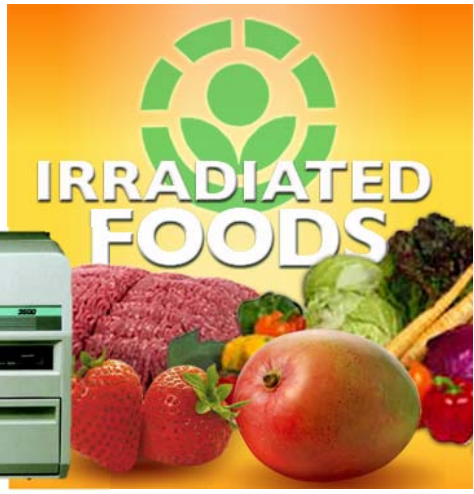

Portable Series

Security

contamination

Detection

Dosimeter

No.1003. JnK Digital tower 111, 26-gil, Digital-ro, Guro-gu, Seoul, Korea
Tel. (02)852-8205 Fax. (02)852-8206
www.remtech.co.kr

REMTECH

Thermo SCIENTIFIC

(주)네오시스코리아

NEOSISKOREA Co.,Ltd.

회사소개

㈜네오시스코리아는 **원자력산업 발전과 방사선 안전에 기여하는 국내 최고의 방사선 계측기기 전문기업**입니다.

세계 최대 방사능 측정장비 제조기업인 CANBERRA Industries Inc.와 가속기 이온원 전문기업인 PANTECHNIK S.A. 등을 포함한 해외 우수 기업들의 제품을 고객에게 공급하고 있습니다. 또한 국내 환경에 최적화된 방사선측정장비 및 가속기관련 장비를 개발하여 고객의 다양한 요구를 만족시키고 있습니다. 앞으로도 연구개발, 판매, 교육, A/S의 일원화된 시스템을 바탕으로 원자력산업 안전에 기여하는 최고의 제품과 서비스를 제공하도록 노력하겠습니다.

- **CANBERRA Industries Inc. 국내 독점 대리점**
- **PANTECHNIK S.A. 국내 독점 대리점**
- 방사선 측정장치 개발 및 분석연구, 컨설팅
- 식약처 지정 식품위생검사기관[제85호]
- 벤처기업인증[제20150400069호]
- ISO 9001:2008 품질경영시스템 인증
- OHSAS 18001:2007 안전보건경영시스템 인증
- ISO 14001:2004 환경경영시스템 인증

해외협력사

NUCLEAR LIGHT INDUSTRY

NUCLOCK Hot Cell series

The NUCLOCK hot cell series are all designed to accommodate dispensing systems or synthesis in safe, reliable, and sterile conditions. The NUCLOCK series with single or double either horizontally or vertically built is to have different configurations in regard to overall dimension, shielding requirement and various accessories.

The supportive material used for the structure of all the NUCLOCK is steel plate. The internal working area is made of stainless steel with well-polished surface, designed to allow for easy cleaning and decontamination.

The NUCLOCK series are all equipped with a touch screen that provides clear images, easy-to-use, and ergonomics, leading to accessing all the functions to be managed and controlled easily at a single point.

The NUCLOCK is also equipped with air tight system with acrylic glass panel held by inflatable gaskets mounted around the perimeter of each cells.

Vial extraction system for the NUCLOCK series is placed in a shielded container on the side of a cell where it can house a vial. It is therefore possible to extract the radiopharmaceuticals without opening the main door.

The ventilated pre-chambers for the introduction of materials are mounted on either side suitable for preparing dose of radio medicines.

NUCLEAR LIGHT INDUSTRY

Nuclear Light Ind. Co. Ltd. 40-19, Ori-ro 22da-gil, Guro-Gu, Seoul, South Korea
Tel. **82 2 2682 6571 Fax ** 82 2 2682 4929 email: info@nlik.com or hej@nlik.com www.nlik.com

Fast, Easy, Reliable Daily QA!!!

SUN NUCLEAR corporation

Jiyeon Medical Co.,Ltd.

#1117,40,63-ro,Yeongdeungpo-gu,Seoul,150-731,Korea

Tel: 02.784.7060 Fax: 02.784.7061 www.jymedical.kr / info@jymedical.kr

jiYeON medical

(주)지연메디칼